Effect of smectic and columnar short-range orders on the physical properties of nematic liquid crystals

A Thesis submitted for the award of the degree of

Doctor of Philosophy in Physics

by

Venkata Sai Dasari

11PHPH04

School of Physics

University of Hyderabad

Hyderabad, India 500 046

August 2016

.

To

My Parents

Declaration

I, **Venkata Sai Dasari**, hereby declare that this thesis entitled **"Effect of smectic and columnar short-range orders on the physical properties of nematic liquid crystals"** submitted by me under the supervision of **Dr. Surajit Dhara** is a bonafide research work which is also free from plagiarism. I also declare that it has not been submitted previously in part or in full in this university or any other University or Institution for the award of any degree or diploma. I hereby agree that my thesis can be deposited in Shodganga/INFLIBNET.

A report on plagiarism statistics from the University Librarian is enclosed at the end.

Venkata Sai Dasari
Reg. No: 11PHPH04.

Date:
Place: Hyderabad.

Certificate

This is to certify that the thesis entitled **"Effect of smectic and columnar short-range orders on the physical properties of nematic liquid crystals"** submitted by **Venkata Sai Dasari** bearing Reg. No. 11PHPH04 in fulfillment of the requirements for the award of Doctor of Philosophy in Physics is a bonafide work carried out by him under my supervision and is free of plagiarism.

The matter embodied in this report has not been submitted previously in part or in full to this University or any other University or Institution for the award of any degree or diploma.

Dr. Surajit Dhara
Thesis Supervisor.
School Of Physics,
University of Hyderabad.

Dean,
School Of Physics,
University of Hyderabad.

Acknowledgement

It is a great opportunity and pleasure to acknowledge all the well wishers without whom this doctoral thesis would not have been completed.

First, I express my gratitude to my supervisor Dr. Surajit Dhara for his valuable, continuous and inspiring guidance throughout my research work. His approach in selecting the problem, logical thinking in understanding and presenting the results greatly inspired me. I thank him for his patience and the help he given me.

I would like to thank my Ph.D Doctoral committee members Prof. V. S. S. Sastry, Prof. K. P. N. Murthy for their encouragement and thought provoking questions in the JRF period and Prof. Nirmal. K. Viswanathan, Dr. S. Srinath and Dr. G. Venkataiah for their insightful comments and fruitful discussions in the SRF period. I thank Prof. A. P. Pathak, Prof. D. Narayana Rao, Prof. M. Siva kumar, Prof. P. K. Suresh and Dr. Soma sanyal for the theoretical course work in the beginning of my research period. I thank Prof. Seshubhai, Prof. Vipin Srivastava, Prof. Sunandana and all the faculty members of School of Physics for their enlightening suggestions.

I thank Dr. Arun Roy, from RRI for providing the theoretical model for the anchoring transition. I also thank Prof. S. Mahapatra and research scholar Rudraditya for providing me the DFT calculations. I thank Dr. S. Krishna Prasad from CeNS for providing X-ray data and for the fruitful discussions. I thank all the collaborators for providing me the samples.

I thank my seniors Dr. T. Arun Kumar for his suggestions, Dr. P. Satyanarayana for introducing me to the experimental setup, LabVIEW and Mathematica programs and Dr. J. Ananthaiah for his help. I would extend my warm thanks to K. P. Zuhail, Rasmita Sahoo and M. V. Rasna for friendly atmosphere and their assistance. I wish all the best for young juniors Junaid Ahmad, Muhammed Rasi, and Subhransu.

I am happy to acknowledge Dr. M. Suman Kalyan, Dr. S. Siva Nasarayya Chari, Dr. Regina Jose, and Dr. Kamala Latha for their guidance.

I thank former Deans Prof. C. Bansal, Prof. S. P. Tiwari, and Prof. S. Chaturvedi and present Dean Prof. R. Singh, for providing needful facilities.

I want to express my gratitude to my close friend M. Uma Shankar (late) and his family for their support.

I thank my friends Phani, Manikanta, Narasimhappa, Ram Naik, Narasimha Rao, Sravan, M. Ramesh, Pavan naik, A. Ramesh, Ravi, Raju, Siva Nagi Reddy, Dhanunjay,

Naveen, Sriram, Kuladeep, Samlan, Devaraju, Alu and I.V. Shankar for various help. I thank Tirupathi, Bharat and Sanjeev for their help in computer programming. I thank my batch mates Siva, Anil, Uday, and Basha.

I thank T. Abraham, Shailaja, Prasad, Ravi Shankar and other non-teaching staff for their help and support. I thank K. Srinivas for introducing me to the Latex.

I greatly acknowledge UGC-India for providing financial support in the form of UGC-JRF and SRF. I also thank DST ITS Travel Grant and UPE Phase-II grant for giving me an opportunity to attend 13th European conference on Liquid Crystals, Manchester, UK.

I thank all my teachers from my schooling, faculty whom I spend during my job and UV coaching staff. I thank all friends from my schooling till today and students whom I worked.

I am fortunate to have Smt. Ammemma and Sri. Nageswara Rao as my parents. I thank them for their unconditional love, support and encouragement. For giving me the moral values, freedom in the life and made me whom I am today.

I thank my brother Rambabu and his family, for their affection and support. I thank my mama Venu for motivating me in the research direction. I thank my father-in-law, mother-in-law and their family members and all other relatives for their affection and support.

Finally, I thank my spouse Vanajakshi for understanding me and giving me love, support and encouragement and my daughter Hema Sai for making my life happy and complete.

Above all, I am indebted to the almighty God for giving me the life and moving me towards the research field.

I thank all those who have, directly or indirectly, helped me in completing this thesis.

Preface

Generally, matter exists in three common phases namely solid, liquid and vapour (gas). Some organic compounds exhibit a number of intermediate phases between ordered solid and isotropic liquid. In the intermediate phases, they can flow like fluids and have anisotropic properties similar to that of crystals. Organic compounds showing this behavior are called liquid crystals. They are composed of anisotropic molecules with variety of shapes, for example, rod-like, bent-like or disc-like etc. The mesophases exhibited by them can be identified by polarizing optical microscope (POM), calorimetric measurements and scattering techniques (X-ray, light scattering).
They have various applications, ranging from liquid crystal displays (LCD) to spacial light modulators (SLM), tunable lences, holographic devices etc. The electro-optic responses of the liquid crystal display depends upon the viscoelastic properties. The spacial responses of nematic LCs to electric or magnetic fields are determined by three curvature elastic constants namely, splay, bend and twist. The temporal response is determined by the rotational viscosity (γ_1), which is linearly proportional to the response time. The elastic constants and the rotational viscosity depends upon the shape of the constituent molecules, interactions and the orientational order.
In this thesis, we have studied optical, dielectric and viscoelastic properties of some calamitic and a discotic nematic liquid crystals. We find that the temperature dependence of the physical properties are strongly influenced by the short-range orders in the respective phases. The thesis is organized as follows.

Chapter I

Introduction

In this chapter, we have given a brief introduction to the various types of liquid crystals and the description of some of their physical properties, which are relevant for the later chapters.

Chapter II

Experimental techniques

In this chapter, we describe all the experimental techniques for measuring various physical properties of the liquid crystals. We describe experimental procedures for cell preparation, and measurement of birefringence, static dielectric constants, splay and bend elastic constants, and rotational viscosity.

Chapter III

Unusual temperature dependence of splay and bend elastic constants of a discotic nematic liquid crystal

Discotic nematic liquid crystals are very useful for wide and symmetrical viewing angle of LCDs and various applications in organic electronics. The physical studies on discotic nematic LCs are meager and more over in these compounds, the nematic phase mostly exists much above the ambient temperature. In 2000, Kumar *et al.* reported the first synthesis of room temperature discotic nematic LCs. However physical properties of these compounds have not been investigated.

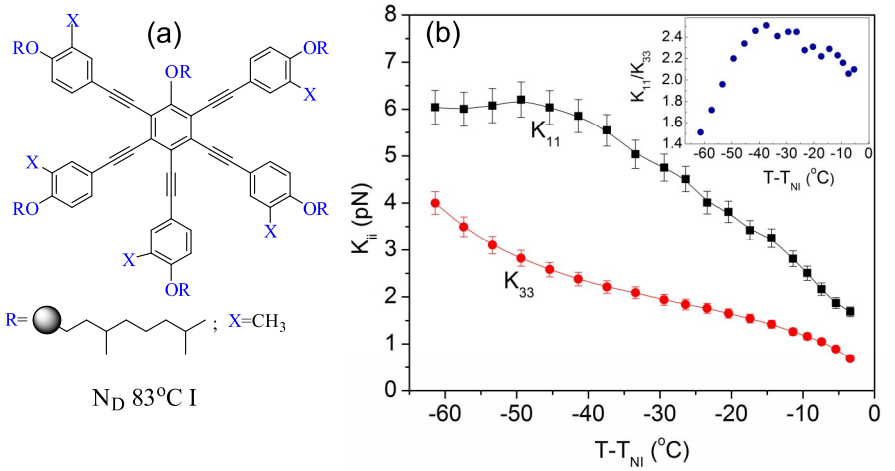

Figure 1: (a) Chemical structure and phase transition temperature of the discotic compound. (b) Variation of splay (K_{11}) and bend (K_{33}) elastic constants as a function of shifted temperature. (Inset) Variation of K_{11}/K_{33} as a function of shifted temperature.

In this chapter, we report studies on the birefringence, dielectric and viscoelastic properties of an ambient temperature discotic nematic liquid crystal. Chemical structure and phase transition temperature of the compound is shown in Fig.1(a). The birefringence is negative i.e., $(\Delta n = n_e - n_o) < 0$, and approximately equal to -0.2 at room temperature. The dielectric anisotropy ($\Delta\varepsilon$) is very small and negative. Fig.1(b) shows the temperature variation of splay and bend elastic constants. Interestingly we observe $K_{11} > K_{33}$ at all temperatures and they show very different temperature dependence. For example, as the temperature is reduced from the NI transition point, both the elastic constants increase but K_{11} increases more rapidly than K_{33}. Below $T - T_{NI} = -45°$C, K_{11} saturates whereas K_{33} shows a kind of diverging behavior. The temperature variation of K_{11}/K_{33} is also shown in the inset of Fig.1(a). It is observed that the ratio increases as the temperature decreases and reaches a maximum around $T - T_{NI} = -40°$C. Below this temperature it reduces rapidly as the ambient temperature is approached. The rotational viscosity (γ_1) is three orders of magnitude larger

than the convenctional calamitic nematic liquid crystals. The unusual behavior of the elastic constants and the high rotational viscosity suggests the presence of temperature dependent columnar short-range order in the discotic nematic phase. We proposed a simple model to explain the unusual temperature dependence of K_{11} and K_{33}.

Chapter IV

Experimental studies on the phase diagram and physical properties of mixture of calamitic and discotic nematic liquid crystals

In this chapter, we report phase diagram, and measurement of several physical properties of mixtures of calamitic (E18) and discotic molecules. The mixtures studied in this chapter are (E18), a multicomponent calamitic mixture and the discotic nematic LC that was studied in chapter-III. The calamitic mixture E18 and the disc like compound having the phase transition temperatures: Cr -10°C N 60°C I and Glass -35°C N 83°C I respectively. E18 was choosen because its birefringence of equal magnitude and opposite sign. Appropriate mixture of these compounds may shoe zero birefringence.

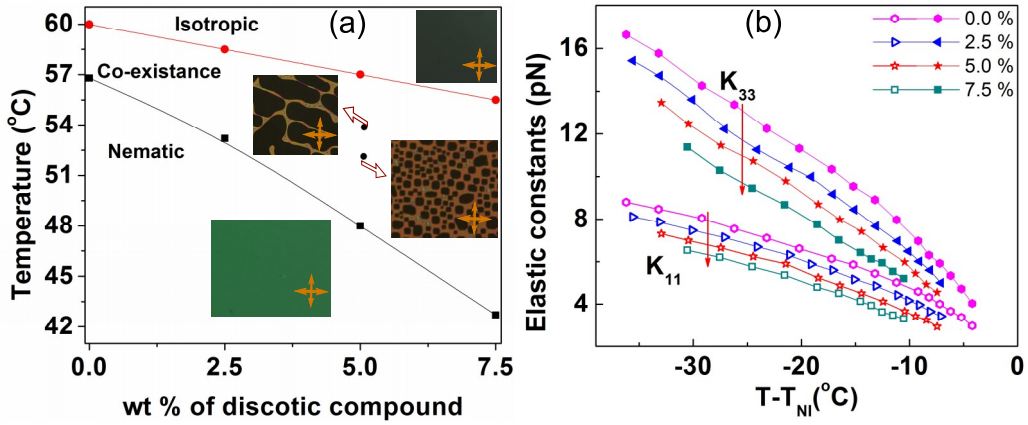

Figure 2: (a) Phase diagram of the mixtures with the variation of wt % of the discotic compound. (b) Variation of splay (K_{11}) and bend (K_{33}) elastic constants of the mixtures as a function of shifted temperature.

The E18 has a short isotropic nematic coexistence region, and the temperature width of the co-existence region increases with increase in wt % of discotic compound. Phase diagram of the mixtures with the variation of wt % of discotic compound and corresponding textures are shown in Fig.2(a). Both the birefringence and the dielectric anisotropy decreases with increasing wt% of the discotic compound. Both the elastic constants decreases with increasing wt % of discotic compounds (Fig.2(b)). For example K_{33} and K_{11} decreases approximately 22.4% and 20.0% respectively at room temperature. Rotational viscosity (γ_1) increases with the increase of wt% of discotic compound. For example, γ_1 of E18+7.5 wt % (disc-molecular) is approximately 74% larger than the value of E18 at room temperature. These results are discussed based

on the individual properties and their mutual alignment.

Chapter V

Effect of smectic short range order on the discontinuous anchoring transition in nematic liquid crystals

In the recent past, Dhara *et al.* observed a discontinuous anchoring transition of a liquid crystal, 4′-butyl-4-heptyl-bicyclohexyl-4-carbonitrile (CCN-47) from planar to homeotropic with a large thermal hysteresis on perfluoropolymer treated cells. They also demonstrated some new applications of this transition. However, the temperature dependent alignment and orientational properties of the homologous series on perfluoropolymer have not been investigated.

Figure 3: Chemical structure of CCN-mn compound.

Table 1: Phase transition temperatures, anchoring transition temperatures and thermal hysteresis of the compounds. K → Crystal, SmB → Smectic-B, SmA → Smectic-A, I → Isotropic, T_{ac} ⟶ anchoring transition temperature while cooling, T_{ah} ⟶ anchoring transition temperature while heating, thermal hysteresis, ΔT_h=T_{ah}-T_{ac}

Sample	Phase transition (°C)	nematic range (°C)	$T_{ac}(^\circ C)$	$T_{ah}(^\circ C)$	$\Delta T_h(^\circ C)$
CCN-35	K 38.4 N 49.3 I	10.9	No anchoring transition		0
CCN-38	K 41 SmA (23) N 49.5 I	26.5	41.4	43.7	2.3
CCN-46	K 30 SmB (26) N 54.7 I	28.7	44.7	47.8	3.1
CCN-47	K 25.6 SmA 28.2 N 57.3 I	29.1	44.5	49.8	5.3
CCN-55	K 25 SmB 30 N 66.4 I	30.4	27.3	36.8	9.5
CCN-73	K 38.6 SmB (38) N 50.2 I	12.2	No anchoring transition		0

In this chapter, we studied the temperature dependent alignment behavior of the homologous series of CCN-mn on perfluoropolymer treated cells. The chemical structure of the CCN-mn compound is shown in Fig.3. Among six compounds in the series, one (CCN-35) has only nematic phase and the remaining five have either smectic-A or smectic-B in addition to the nematic phase (see Table 1). We simultaneously performed temperature dependent dielectric measurements and optical polarizing microscope observations. It is found that except for CCN-35 and CCN-73, the remaining four compounds exhibit discontinuous anchoring transition from planar to homeotropic and vice versa with increasing thermal hysteresis. It suggested that smectic short range order is responsible for the anchoring transition. We developed a simple theory taking into account the effect of smectic short-range order at the substrates to explain the

experimental observation. The calculated anchoring transition temperatures in cooling (T_{ac}), heating (T_{ah}), and the thermal hysteresis (ΔT_h) from theoretically are given below. By considering the case of CCN-47, substituting the approximate values, the estimated parameters agree well with the experimental observations.

$$T_{ah} = T_{NA} + T_{NA}\frac{36D^2q^4\psi_0^2\xi_0^2}{[\beta_{11} + (\beta_{21} - 4|\beta_{22}|/3)S]^2} \tag{1}$$

$$T_{ac} = T_{NA} + T_{NA}\frac{36D^2q^4\psi_0^2\xi_0^2}{[\beta_{11} + (\beta_{21} + 2|\beta_{22}|/3)S]^2} \tag{2}$$

and the thermal hysteresis is given by

$$\Delta T_h = T_{ah} - T_{ac} \tag{3}$$

Chapter VI

Structure-property correlation of bicyclohexane nematic liquid crystals

To get more insight into the physical properties of these bicyclohexane liquid crystals, we measured birefringence, dielectric anisotropy, splay and bend elastic constants are reported in this chapter. The dielectric anisotropy is found to be large and negative ($\Delta\varepsilon < 0$) in all the compounds. The birefringence is very low in all the compounds, and near the room temperature, $\Delta n \approx 0.03$ (Fig.4(a)).

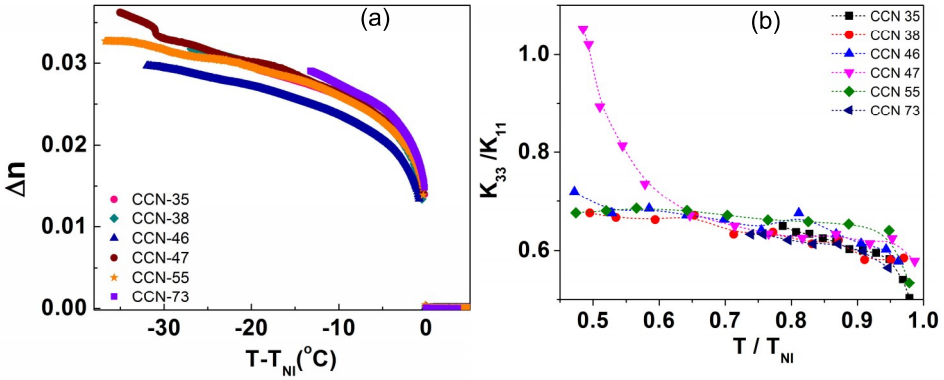

Figure 4: (a) Variation of birefringence as a function of shifted temperature. (b) Variation of K_{33}/K_{11} of the homologoes series as a function of temperature.

We find that in all the compounds $K_{33} < K_{11}$, which is in contrast to the conventional calamitic liquid crystals. Variation of K_{33}/K_{11} of the homologous series as a function of reduced temperature is shown in Fig.4(b). Interstingly, we observe that $K_{33}/K_{11} \simeq 0.7$, except very close to the SmA phase transition temperature (of CCN-47). The low birefringence, high negative dielectric anisotropy and the unexpected elastic constants ratio are discussed based on the optimized molecular structure obtained from density functional calculations.

Chapter VII

Birefringence, permittivity, curvature elasticity and rotational viscosity of ambient temperature, high birefringent nematic liquid crystal mixtures

Recently, J. Herman *et al.* synthesized novel high birefringent nematic liquid crystals containing quarterphenyl and phenylethynyltolane cores with isothiocyanate terminal group. These LCs have various applications ranging from display to non-display such as in the visible, ultraviolet regions and in long wave length radio frequency applications (GHz/THz frequencies). For the purpose of applications, we prepared some binary mixtures (Fig.5(a)) and measured the temperature variation of some physical properties such as birefringence, permittivity, curvature elasticity and rotational viscosity.

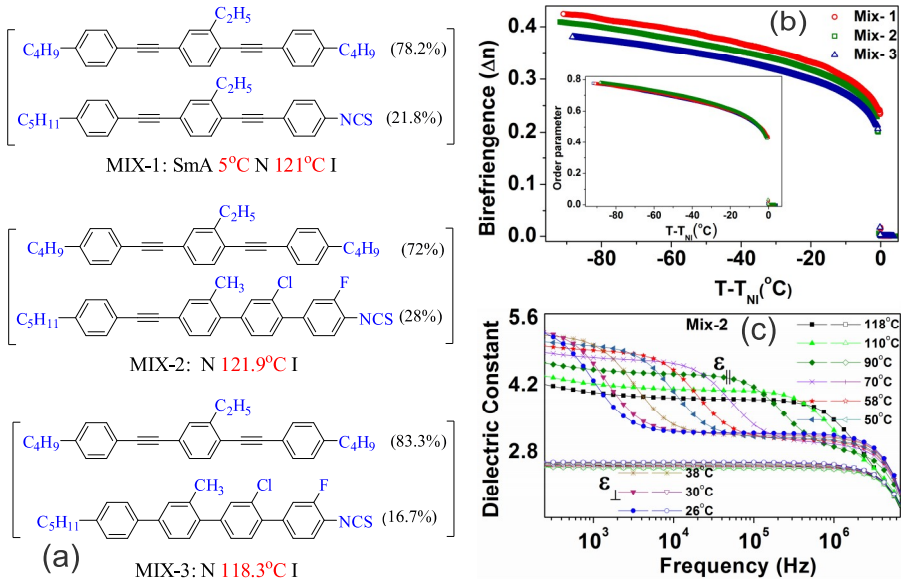

Figure 5: (a) Molecular structure, wt% of the individual compounds and the phase transition temperatures of the mixtures. (b) Variation of birefringence (Δn) and orientational order (S) of the mixtures as a function of shifted temperature. (c) The frequency dispersion of the real part of the dielectric constants, i.e., $\varepsilon_{||}(f)$ and $\varepsilon_{\perp}(f)$ at various temperatures of Mix-2.

The birefringence (Δn) jumps to $\simeq 0.22$ from zero at the nematic-isotropic (NI) transition and reaches to a high value ≈ 0.4 at room temperature and varies as $\Delta n_{Mix-1} > \Delta n_{Mix-2} > \Delta n_{Mix-3}$ (Fig.5(b)). Parallel component of dielectric constant ($\varepsilon_{||}$) measured at 4111 Hz shows unusual temperature dependence, i.e., it increases up to certain temperature and then decreases with decreasing temperature. To understand this we measured the frequency dispersion of the real parts of the dielectric constant, i.e., $\varepsilon_{||}(f)$ and $\varepsilon_{\perp}(f)$ at various temperatures (Fig.5(c)). The unusual behaviour is due to decrease of dielectric relaxation frequency with decreasing temperature. Both

splay (K_{11}) and bend (K_{33}) elastic constants increase with decreasing temperature and these values are comparatively larger than many common nematic liquid crystals. The rotational viscosity (γ_1) increases very rapidly with decreasing temperature. At room temperature $\gamma_1 \simeq 1$ Pa s, which is about two orders of magnitude larger than conventional nematic liquid crystal such as 4-n-pentyl-4$'$-cyanobiphenyl (5CB). The figure of merit (FoM), (which characterizes the performance of liquid crystal) of the mixtures at high temperature is reasonably large but reduces at room temperature.

Contents

List of Abbreviations and Symbols

LC	:	Liquid crystal
1D	:	One dimentional
2D	:	Two dimentional
3D	:	Three dimentional
I	:	Isotropic phase
Cr or K	:	Crystalline phase
N	:	Nematic phase
N^*	:	Chiral nematic phase
SmA	:	Smectic-A phase
SmC	:	Smectic-C phase
SmB	:	Smectic-B phase
NLC	:	Nematic liquid crystal
LCD	:	Liquid crystal display
N_{Col}	:	Columnar discotic nematic phase
Col_h	:	Columnar hexagonal phase
Col_r	:	Columnar rectangular phase
Col_L	:	Columnar lamellar phase
N_D	:	Discotic nematic phase
$\hat{n}$	:	Liquid crystal director
S	:	Scalar order parameter
Q_{ij}	:	Tensor order parameter
ITO	:	Indium tin oxide
OPM	:	Optical polarising microscope
n	:	Refractive index
n_o	:	Ordinary refractive index
n_e	:	Extraordinary refractive index
$n_{\|\|}$	:	Refractive index parallel to $\hat{n}$
$n_\perp$	:	Refractive index perpendicular to $\hat{n}$
$\Delta n = n_e - n_o$	:	Birefringence
$\Delta\Phi$	:	Optical phase difference
$\varepsilon_{\|\|}$	:	Dielectric constant parallel to $\hat{n}$
$\varepsilon_\perp$	:	Dielectric constant perpendicular to $\hat{n}$
$\Delta\varepsilon = \varepsilon_{\|\|} - \varepsilon_\perp$	:	Dielectric anisotropy
$\overline{\varepsilon} = \langle\varepsilon\rangle = (\varepsilon_{\|\|} + 2\varepsilon_\perp)/3$	:	Average dielectric constant
$\varepsilon_\circ$	:	Vacuum permittivity

...contd.

ε'	:	Real part of complex permittivity
ε''	:	Imaginary part of complex permittivity
$\varepsilon^* = \varepsilon' + i\varepsilon''$	:	Complex permittivity
$\varepsilon'_{\|\|}$	:	Real part of complex permittivity parallel to $\hat{n}$
$\varepsilon''_{\|\|}$	:	Imaginary part of complex permittivity parallel to $\hat{n}$
K_{ii}	:	Arbitary elastic constants
K_{11}, K_{22}, K_{33}	:	Splay, Twist and Bend elastic constants
$\tau_\circ$	:	Relaxation time
γ_1	:	Rotational viscosity coefficient
NI	:	Nematic-isotropic phase transition
NA	:	Nematic-smectic-A phase transition
T	:	Absolute temperature
T_{NI}	:	Nematic-isotropic phase transition temperature
T_{NA}	:	Nematic-smectic-A phase transition temperature
T_{ac}	:	Anchoring transition temperature while cooling
T_{ah}	:	Anchoring transition temperature while heating
ΔT_h	:	Temperature range of thermal hysteresis
θ	:	Tilt angle (polar)
ϕ	:	Twist angle (azimuthal)
γ^E	:	Molecular polarizability
$\gamma^E_{\|\|}$	:	Molecular polarizability parallel to $\hat{n}$
$\gamma^E_\perp$	:	Molecular polarizability perpendicular to $\hat{n}$
$\Delta\gamma^E = \gamma^E_{\|\|} - \gamma^E_\perp$	:	Molecular polarizability anisotropy
$\langle\gamma^E\rangle = (\gamma^E_{\|\|} + 2\gamma^E_\perp)/3$	:	Average molecular polarizability
$\vec{E}$	:	Electric field vector
$\vec{D}$	:	Electric displacement vector
λ	:	Wavelength
ω	:	Angular frequency
f_s	:	Surface energy density
f_{el}	:	Elastic distortion energy density
V	:	Voltage
V_{th}	:	Freedericksz threshold voltage
β	:	Exponent in Haller extrapolation
k_B	:	Boltzsmann constant
θ_m	:	tilt angle at the middle of the cell
γ	:	$\frac{\varepsilon_{\|\|}}{\varepsilon_\perp} - 1$
ν	:	$\frac{n_e^2}{n_o^2} - 1$
κ	:	$\frac{K_{33}}{K_{11}} - 1$

List of Figures

List of Tables

1

Introduction

In general, with variation of temperature, matter transforms from ordered solid phase to isotropic liquid phase at some characteristic temperature (melting point). In the solid phase, there exists long-range three dimensional positional (center of mass) and orientational order, whereas in liquids both orders disappear and possess only short-range order among the molecules. In 1888, an Austrian botanist Fredrich Reinitzer observed two transition temperatures in some organic materials. At the first transition temperature it transforms to a turbid liquid and in the next transition it transforms to a clear liquid. The class of compounds exhibiting these intermediate phases were named as liquid crystals by Lehman, in 1889. In the intermediate phases they have zero or one or two dimensional positional order in addition to orientational order. In these phases they exhibit liquid-like behavior such as surface tension and viscosity and solid-like properties such as optical anisotropy (birefringence), conductivity anisotropy, dielectric and diamagnetic susceptibility anisotropy [1, 2]. Due to a lack of 3-D positional order and large response to electric and magnetic fields, they are quite useful in display and non-display applications. Mainly liquid crystals are classified as thermotropic and lyotropic liquid crystals. Thermotropic LC exhibits various phases with the variation of temperature where as in lyotropic, they appear with variation of concentration in the solvent [3, 4]. In this thesis, we measure various physical properties of some nematic liquid crystals and investigate effect of short range order. In this chapter, we discuss various LC phases and physical properties which are relevant to the later chapters.

1.1 Classification of liquid crystals

Thermotropic liquid crystals can be classified based on the shape of the molecules, namely [5, 6]
(i) **calamitic** made up of rod like molecules,
(ii) **bent-like** made up of bend core molecules,
(iii) **discotic** made up of disc shaped molecules.

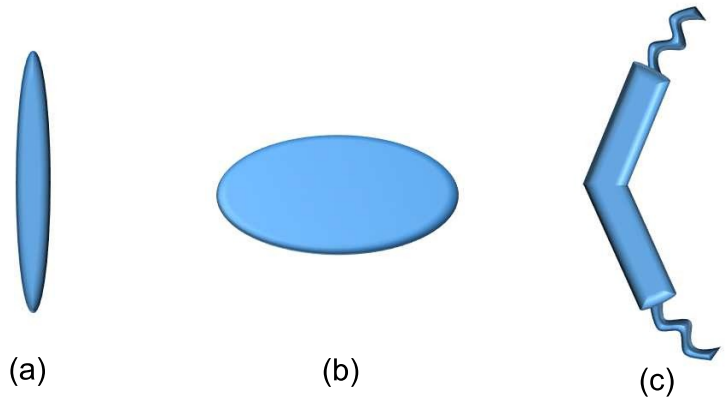

Figure 1.1: Schematic representation of (a) calamitic, (b) discotic and (c) bent-core molecules.

1.1.1 Calamitic

Calamitic liquid crystals are made up of rod-shaped molecules with rigid core and flexible side chains. The physical properties are influenced by the nature of both rigid core and flexible chains. They exhibit various phases. Some of the phases relevant to the present thesis are discussed here.

Nematic (N)

Nematic phase is the simplest and common phase among all the liquid crystalline phases. In this phase, center of mass of the molecules are randomly distributed (fluid like, no positional order) and long axes of the molecules are aligned on an average along a direction. It is represented by a unit vector, called director $\hat{n}$ which is apolar in nature, i.e., $\hat{n}$ and $-\hat{n}$ are equivalent (indistinguishable) hence it does not lead to any macroscopic polarity. Rotational symmetry exists along the director, so usually they are uniaxial in nature.

Order Parameter (S)

When phase changes from disorder to order, the symmetry is reduced and orderness appears. To put it in quantitatively, a parameter is defined which is zero in disorder

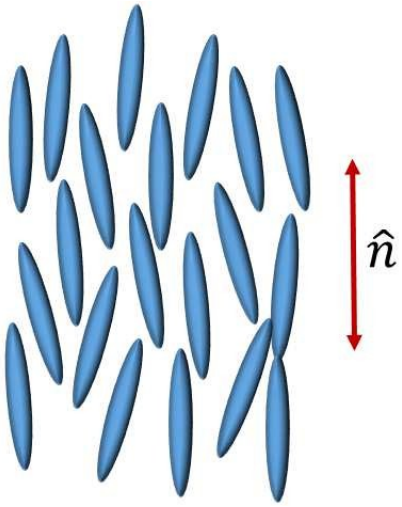

Figure 1.2: Schematic representation of nematic phase of rod like molecules. The arrow (↕) represents the director ($\hat{n}$).

phase and non zero in ordered phase called order parameter. In the nematic phase, the average orientation of the long axes of the molecules is along the director. To define the local orientation of the director at a point $\overrightarrow{r}(x,y,z)$, consider the unit vector $\hat{a}$ along the long axis of the molecule [4]. The thermal average of $\hat{a}$ over a microscopic volume around $\overrightarrow{r}$. The average $\langle \hat{a}.\hat{a} \rangle$ is a scalar constant and is not useful. This average is ensemble average. The value of $\langle \hat{a} \rangle$ is zero since nematic director is apolar in nature. The next choice of order parameter is second rank tensor S, and the elements are given by

$$S_{\alpha\beta} = \langle a_\alpha a_\beta \rangle - \frac{1}{3}\delta_{\alpha\beta}, \alpha, \beta = x, y, z, \tag{1.1}$$

where x, y and z are the laboratory fixed coordinate system. The addition of Kronecker delta term ensures zero value of order parameter since $\langle a_\alpha^2 \rangle = 1/3$. This is symmetric and traceless and contains five independent elements. In the principal coordinate system, this tensor can be diagonalised. The distinct diagonal elements represent biaxial phase, where as two equal diagonal elements lead uniaxial phase. In the uniaxial nematic phase, the general form of order parameter field is given by

$$S_{\alpha\beta}(\overrightarrow{r}) = S\left(n_\alpha(\overrightarrow{r})n_\beta(\overrightarrow{r}) - \frac{1}{3}\delta_{\alpha\beta}\right), \tag{1.2}$$

where S is a measure of the degree of alignment of long axes of the molecules along $\hat{n}(\overrightarrow{r})$ and the expression in the parenthesis defines the spacial variation of $\hat{n}(\overrightarrow{r})$ from point to point. In the well aligned nematic phase, $\hat{n}$ is independent of $\overrightarrow{r}$. For the cylindrically symmetric molecules, the scalar order parameter is given by

$$S = \frac{3\langle cos^2\theta\rangle - 1}{2}, \tag{1.3}$$

where the angular brackets represent ensemble average, and θ is the angle made by the long axis of the molecule $\hat{a}$ with the director $\hat{n}$. For a perfectly aligned sample, $\theta = 0$ or π, then $\langle cos^2\theta\rangle$ =1, thus $S = 1$. In isotropic phase, θ varies from 0 to π, then $\langle cos^2\theta\rangle$ =1/3, thus $S = 0$. Usually it varies from 0.3 to 0.8 in the nematic phase with variation of temperature. The order parameter is related to the physical properties such as diamagnetic and dielectric anisotropy, birefringence etc [3].

Cholesteric

Cholesteric phase is formed when the molecules are chiral or chiral dopants are added to the nematic phase. If the orientational order rotates in space then it leads to helical structure. By moving along the helix axis, the director rotates. Hence helix axis is perpendicular to the local director. A full rotation of director completes through a distance p called pitch. Since $\hat{n}$ and $-\hat{n}$ are equivalent, the pitch repeats through a distance $p/2$. Nematic phase can be assumed as cholesteric phase having pitch infinity. Here uniaxial optic axis is the helix axis. A schematic representation of cholesteric phase is shown in Fig.1.3.

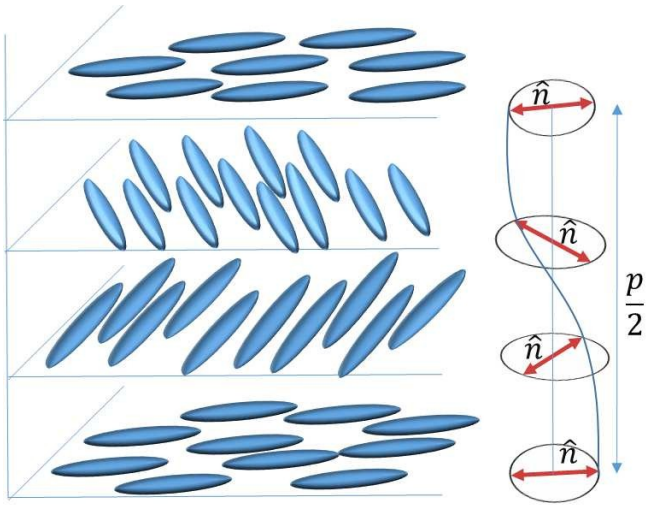

Figure 1.3: Schematic representation of arrangement of rod like molecules in the cholesteric phase. The red arrow indicates director ($\hat{n}$) in respective layers. Half-pitch is denoted by $p/2$.

Smectic

In smectics, in addition to the orientational order it shows layered structure of the molecules [1]. So, it exhibits 1-dimentional translational order and 1-D density wave

along the layer normal. Within the layers, the center of mass of the molecules are random (fluid-like). The layered structure (periodic) is described by a density wave and is given by

$$\rho = \rho_o[1 + Re\{|\Psi|e^{i(q_0 z+\phi)}\}], \tag{1.4}$$

where ρ_o is the back ground density, $|\psi|$ complex amplitude of the density wave, $q_o(= 2\pi/d)$, d is the layer thickness, ϕ is an arbitrary phase. The layers in the xy-plane and layer normal $\hat{n}$ along z-axis. Based on the orientation and arrangement of the molecules in the layers, smectics are classified as Smectic-A, Smectic-B, Smectic-C etc.

Smectic-A (SmA)

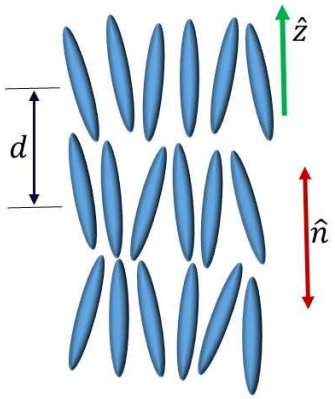

Figure 1.4: Schematic representation of layer structure of the molecules in the smectic-A phase. The director ($\hat{n}$) is along the layer normal.

In the smectic-A phase, the long axes of the molecules are parallel to the layer normal. Each layer is like a two dimensional fluid. The interaction among the layers are relatively weak. Even though smectic phase is more turbid than nematic, due to weak interactions among the layers, they can slide relatively easy one over the other. This SmA phase shows uniaxial symmetry. If the molecules are composed of symmetric and non polar then layer spacing (d) in smectic phase is approximately equal to molecular length (l). Otherwise, if the molecules consist of longitudinal dipole moment then near neighbour anti-parallel correlations can affect the structure [7].

Smectic-C (SmC)

In the smectic-C, the molecules form layers and the center of mass are random within the layer similar to SmA arrangement, but the molecules are tilted at an angle θ with the layer normal. Due to the tilt angle θ, the layer thickness is less than the molecular length.

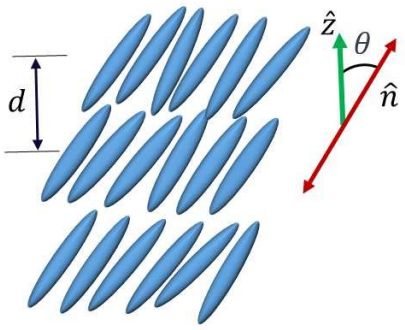

Figure 1.5: Schematic representation of layer arrangement of rod like molecules in the smectic-C (SmC) phase. The director $\hat{n}$ makes an angle θ with the layer normal.

Smectic-B (SmB)

In the smectic-B phase, the molecules form layers and the long axes of the molecules are parallel to the layer normal. SmB phase is more ordered than SmA and SmC. In SmB, the molecules form hexagonal order within the layer. There is a small correlation among the hexagonal networks and the hexagonal lattices repeat positional order over a large length scale around 150-600 Å [8]. The side view and top view of the molecular arrangement in the SmB phase is shown in Fig.1.6.

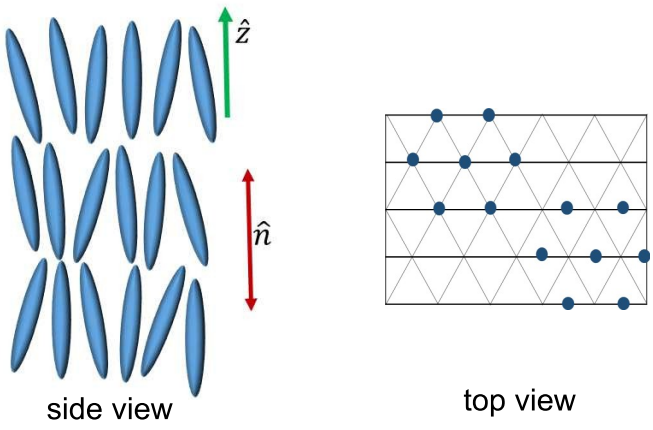

Figure 1.6: Schematic representation of the arrangement of the molecules in the side and topview in the smectic-B (SmB) phase.

1.1.2 Discotic

About forty years ago, S. Chandrashekhar and his colleagues from Raman Research Institute, India reported the discovery of discotic liquid crystal. In discotic liquid crystals the disc-shaped molecules are composed of flat rigid core and is surrounded

by flexible chains [9]. Due to van der Waals interaction and overlapping of π electrons of the neighbouring aromatic cores they tend to self-organize into 1D column and then organize into various 2D lattices. The motion of the side chains give the fluidity of the disc in 3D and is one of the reason for the mesomorphic behavior [10]. The discotic LCs exhibit various sub-phases [11]. Some of the common phases are nematic, columnar etc.

1.1.3 Nematic phases of discotic NLCs

Discotic NLCs exhibit various nematic phases. They are discotic nematic (N_D), columnar nematic (N_{Col}), chiral nematic (N_D^*) etc. A schematic representation of some of the discotic nematic phases are shown in Fig.1.7.

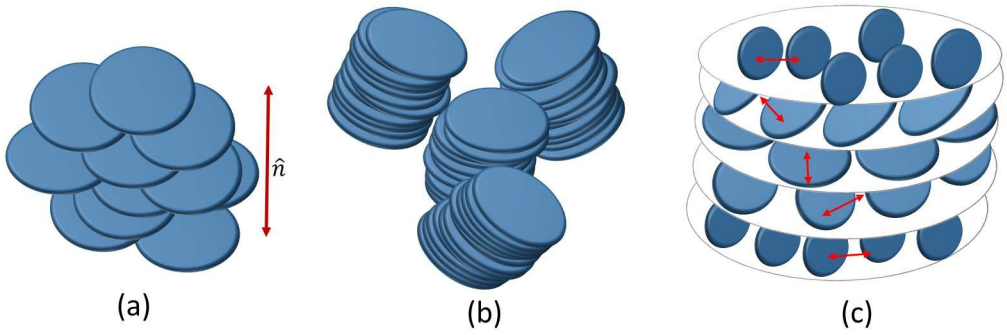

Figure 1.7: Schematic representation of arrangement of discotic molecules in the (a) discotic nematic (N_D), (b) columnar nematic (N_{Col}) and (c) chiral nematic (N_D^*) phases. The red arrows indicates the director $\hat{n}$.

Discotic nematic is the simplest phase formed by the discotic liquid crystals. The center of mass of the discs are random and the short axis (disc normal) of the discs on an average points in direction known as a director. So, in this phase it has net orientational order but no positional order. Due to interactions among the discs, they tend to form columnar stacks. These columnar rods as building blocks and show columnar nematic phase (N_{Col}). In this phase, it exhibit short range positional order and long range orientational order. Similar to chiral calamitic (N^*), it forms chiral discotic nematic phase (N_D^*). Similarly, due to strong interactions they form aggregates. If these aggregate superstructures act as building block then it forms nematic lateral phase (N_L).

1.1.4 Columnar phases of discotic LCs

Columnar phase is the most common phase exhibited by the discotic LCs. The disc molecules are self assembled into columns. These columns self-organise into various 2D lattices and form columnar phase. In the columns, the disc molecules may be

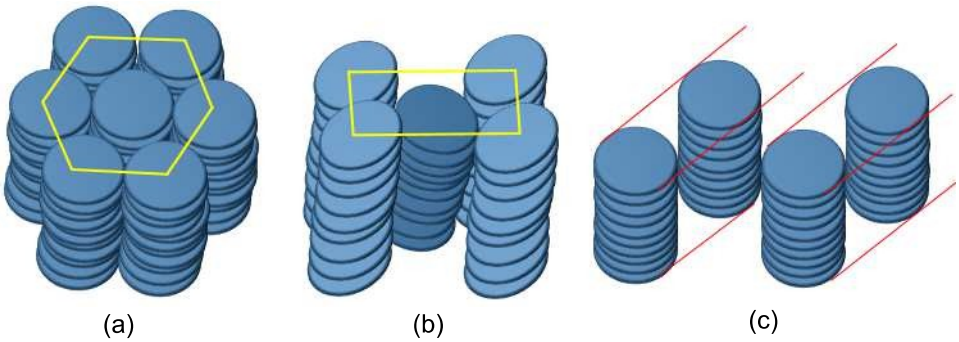

Figure 1.8: Schematic representation of arrangement of discotic molecules in (a) hexagonal columnar (Col_h), (b) rectangular columnar (Col_r) and (c) columnar lamellar (Col_L) phases.

arranged in periodic or aperiodic manner. Based on the order, orientation of the disc molecules and symmetry of the columns, various columnar phases are formed. They are columnar hexagonal phase (Col_h), columnar rectangular phase (Col_r), columnar lamellar phase (Col_L) etc. The schematic representation of some of the columnar phases is shown in Fig.1.8.

1.2 Optical properties

1.2.1 Refractive index (n)

Refractive index is the property of the medium, which is determined by the relative speed of light in the medium. In the nematic liquid crystals, the optic axis is along the liquid crystal director $\hat{n}$. In the uniaxial nematic liquid crystals, if the polarization of the electric field vector of light is along and perpendicular to the director then corresponding refractive indices are $n_{||}$ and $n_{\perp}$ respectively, where $||$ and $\perp$ represent direction in relation to the director $\hat{n}$. The average value of refractive index of the nematic phase is given by

$$\langle n^2 \rangle = \frac{1}{3}(n_{||}^2 + 2n_{\perp}^2).$$

1.2.2 Birefringence (Δn)

Optical anisotropy or birefringence (Δn) is given by

$$\Delta n = n_e - n_o = n_{||} - n_{\perp}.$$

It is positive and the value varies from 0.01 to 0.8 for calamitic liquid crystals [4, 12], and negative for discotic liquid crystals. The birefringence of the liquid crystal can be

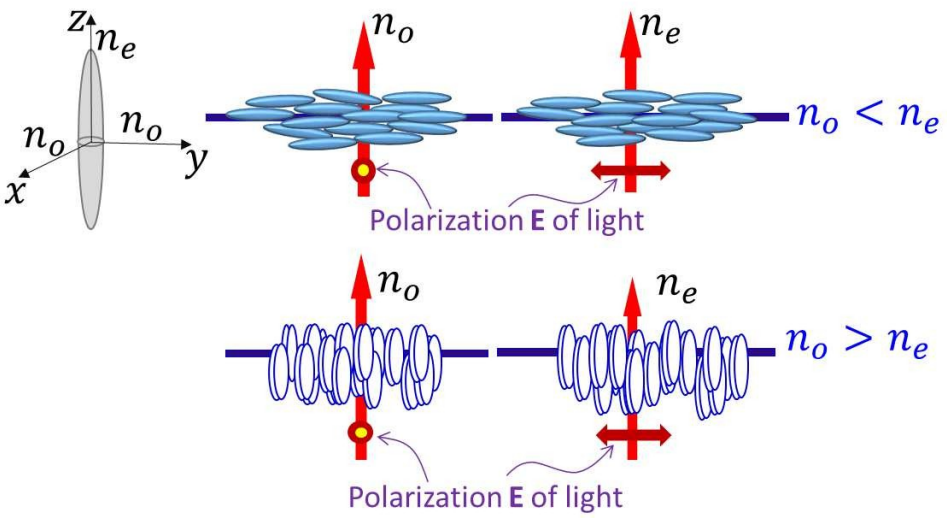

Figure 1.9: Schematic representation of arrangement of calamitic and discotic molecules along the director and representation of polarization of electric field of light $\overrightarrow{E}$ perpendicular and along the optic axis.

used to estimate order parameter (S) by using the Haller extrapolation [13].

$$S \approx \frac{\Delta n}{\Delta n_o},$$

where Δn_o is the birefringence of the perfectly aligned state of the LC.

1.3 Dielectric constants ($\varepsilon_{||}$ and $\varepsilon_{\perp}$)

Dielecric properties are related to the response of the given material to the external electric field. Dielectric constants depend upon the charge distribution in the molecules and intermolecular interactions. The value of dielectric constants will vary with the variation of both temperature and the frequency of the electric field. In liquid crystals, parallel ($\varepsilon_{||}$) and perpendicular ($\varepsilon_{\perp}$) components of the dielectric constants are measured when the electric field is along and perpendicular to the director respectively. The dielectric anisotropy is defined as $\Delta\varepsilon = \varepsilon_{||} - \varepsilon_{\perp}$.
According to the Maier and Meier's theory, the dielectric constants are given by [14]

$$\varepsilon_{||} = 1 + 4\pi\frac{\rho N_A h F}{M}\left[\langle\gamma^E\rangle + \frac{2}{3}\Delta\gamma^E S + F\frac{\mu^2}{3k_BT}\left\{1 - (1 - 3cos^2\beta)S\right\}\right], \quad (1.5)$$

$$\varepsilon_{\perp} = 1 + 4\pi\frac{\rho N_A h F}{M}\left[\langle\gamma^E\rangle - \frac{1}{3}\Delta\gamma^E S + F\frac{\mu^2}{3k_BT}\left\{1 + \frac{1}{2}(1 - 3cos^2\beta)S\right\}\right], \quad (1.6)$$

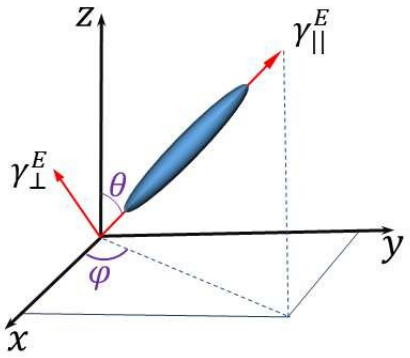

Figure 1.10: Schematic representation of principal components of the polarizabilities of the molecule.

where M is the molecular weight, N_A is the Avogadro number, ρ the density, k_B is the Boltzmann constant, $\langle\gamma^E\rangle = (\gamma_{||}^E + 2\gamma_{\perp}^E)/3$ is the average molecular polarizability, $\Delta\gamma^E = \gamma_{||}^E - \gamma_{\perp}^E$ is the polarizability anisotropy, $h = 3\langle\varepsilon\rangle/(2\langle\varepsilon\rangle + 1)$ is the cavity field factor, $F = 1/(1 - f\langle\gamma^E\rangle)$ where $f = (\langle\varepsilon\rangle - 1)/[2\pi a^3(2\langle\varepsilon\rangle - 1)]$ is the reaction field factor for spherical cavity and $a^3 = 3(\mu/4\pi)N_{A\rho}$ is the cavity volume and β is the angle between the molecular dipole moment and the axis of the maximum polarizability of the molecule and S is the order parameter. From the Eq.(1.5) and Eq.(1.6), the parallel ($\varepsilon_{||}$) and perpendicular ($\varepsilon_{\perp}$) component of the dielectric constants depends upon the order parameter (S).

The average dielectric constant $\langle\varepsilon\rangle$ is given by

$$\langle\varepsilon\rangle = \frac{(\varepsilon_{||} + 2\varepsilon_{\perp})}{3} = 1 + 4\pi\frac{\rho N_A h F}{M}\left[\langle\gamma^E\rangle + F\frac{\mu^2}{3k_B T}\right]. \tag{1.7}$$

The average dielectric constant $\langle\varepsilon\rangle$, is independent of both order parameter (S) and the angle β between the polarizability anisotropy and dipolemoment.
The dielectric anisotropy ($\Delta\varepsilon$) is given by

$$\Delta\varepsilon = \varepsilon_{||} - \varepsilon_{\perp} = 4\pi\frac{\rho N_A h F}{M}\left[\Delta\gamma^E - F\frac{\mu^2}{2k_B T}(1 - 3cos^2\beta)\right]S. \tag{1.8}$$

From the Eq.(1.8), the dielectric anisotropy ($\Delta\varepsilon$), is proportional to order parameter (S). The sign of the dielectric anisotropy ($\Delta\varepsilon$) is determined by the relative magnitude of the two terms in the square bracket of the Eq.(1.8). When the angle $\beta < 55°$, then the two terms in the bracket will be added up and give positive dielectric anisotropy. For $\beta \backsim 55°$, the second term will be zero and left with polarisability anisotropy ($\Delta\gamma^E$). For $\beta > 55°$, the sign of the dielectric anisotropy ($\Delta\varepsilon < 0$ or > 0), is determined by the relative strength of the polarisability anisotropy ($\Delta\gamma^E$) and dipolar contribution.

1.3.1 Response of LC to an electric field

The electric displacement $\overrightarrow{D}$ induced in the nematic liquid crystal by an external electric field $\overrightarrow{E}$ is given by [15, 16],

$$\overrightarrow{D} = \varepsilon_o \varepsilon_\perp \overrightarrow{E} + \varepsilon_o \Delta\varepsilon (\hat{n}.\overrightarrow{E})\hat{n}. \tag{1.9}$$

The total electric energy of the nematic liquid crystal medium can be written as

$$\omega_{ele} = \int_0^E \overrightarrow{D}.d\overrightarrow{E}, \tag{1.10}$$

and it is given by

$$\omega_{ele} = -\frac{1}{2}\overrightarrow{D}.\overrightarrow{E} = -\frac{1}{2}\varepsilon_o\varepsilon_\perp E^2 - \frac{1}{2}\varepsilon_o \Delta\varepsilon E^2 (\hat{n}.\overrightarrow{E})^2. \tag{1.11}$$

In Eq.(1.11), the first term is independent of liquid crystal orientation and dielectric anisotropy of the medium. So, from the second term, the minimization of the electric energy depends upon the dielectric anisotropy $\Delta\varepsilon$ of the medium and relative orientation of the director $(\hat{n})$ in relative to the electric field $\overrightarrow{E}$. For positive dielectric anisotropy $(\Delta\varepsilon > 0)$, energy will be minimized if $\hat{n} || \overrightarrow{E}$ and for negative dielectric anisotropy $(\Delta\varepsilon < 0)$, then energy will be minimized if $\hat{n} \perp \overrightarrow{E}$.

1.4 Curvature elastic constants

Nematic liquid crystals have orientational order, they exhibit curvature elasticity. In a single-domain and uniformly oriented nematic liquid crystal, the director $\hat{n}$ is independent of position $\overrightarrow{r}$. When the distortion is induced by means of electric or magnetic field in the director $\hat{n}(\overrightarrow{r})$, then the derivative of $\hat{n}(\overrightarrow{r})$ exists. The liquid crystal medium opposes such deformation since one needs to do work against the inter-molecular forces. So an elastic restoring torque comes in to play that tends to bring back $\hat{n}(\overrightarrow{r})$ to the undisturbed state. Any deformation can be constructed as the combination of three basic independent curvature deformations, namely splay, twist and bend distortions. A schematic representation of elastic deformations are shown in Fig.1.11.

The elastic free energy per unit volume is given by [1, 2, 17],

$$f_N = \frac{1}{2}\left[K_{11}(\nabla.\hat{n})^2 + K_{22}(\hat{n}.\nabla\times\hat{n})^2 + K_{33}(\hat{n}\times\nabla\times\hat{n})^2\right], \tag{1.12}$$

where K_{11}, K_{22}, and K_{33} represents the splay, bend, and twist elastic constants respectively. These are positive and generally $K_{33} > K_{11} > K_{22}$ for rod-like molecules, and $K_{22} > K_{11} > K_{33}$ for disc-like molecules [18]. Energy density f_N has the units of energy/vol, and $\hat{n}$ is dimensionless so elastic constants have units of force, i.e, newton (N). The typical value of the elastic constants are approximately equal to the order of

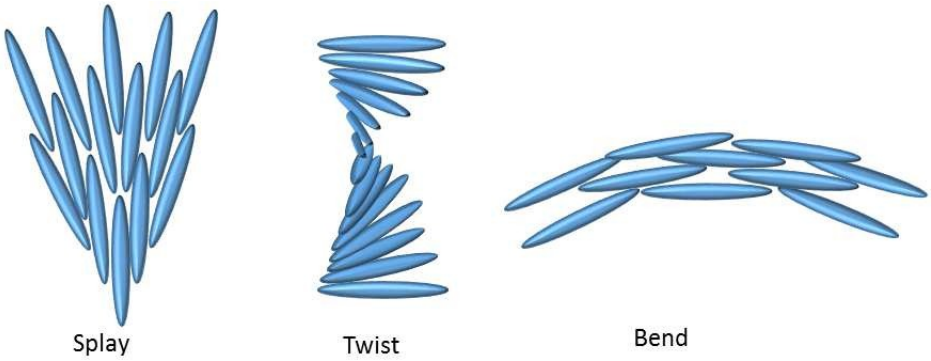

Figure 1.11: Schematic representation of splay, twist, and bend distortions.

nematic interaction energy per unit molecular length. At the isotropic-nematic transition, thermal energy ($k_B T_{NI}$) per molecule is comparable to the interaction energy of the molecule in the nematic phase. For eg. $T_{NI} \approx 330$ K, molecular length $a \approx 10$Å, $k_B \approx 10^{-24}$ JK^{-1}, then elastic constant, $K_{ii} \backsim K_B T_{NI}/a \backsim 10^{-12}$N.

1.5 Rotational viscosity (γ_1)

Rotational viscosity (γ_1) is one of the important parameter for electro-optical applications in the liquid crystal devices. The response time of the device is proportional to the rotational viscosity. It is an internal friction experienced by the liquid crystal directors while rotating. The magnitude of (γ_1) depends on the constituents, structure of the molecules, inter-molecular interactions, and temperature. For a positive dielectric anisotropy NLCs in a planar cell of thickness d, the value of γ_1 is given by [19, 20]

$$\gamma_1 = \frac{\tau_o K_{11} \pi^2}{d^2}, \tag{1.13}$$

where τ_o is the relaxation time and K_{11} is the splay elastic constant.

1.6 Types of alignment

In an unaligned liquid crystal sample, the director ($\hat{n}$) is oriented randomly, i.e., it varies from point to point in the medium. In order to measure the physical properties and also for the application [21, 22], the director $\hat{n}$, needs to be aligned with respect to the boundary surfaces. The uniform alignment of the director enables us to measure the physical properties such as birefringence, static dielectric constants, curvature elastic constants etc. Commonly two types of alignments are used namely homogeneous or planar and homeotropic or perpendicular directions for physical measurements.

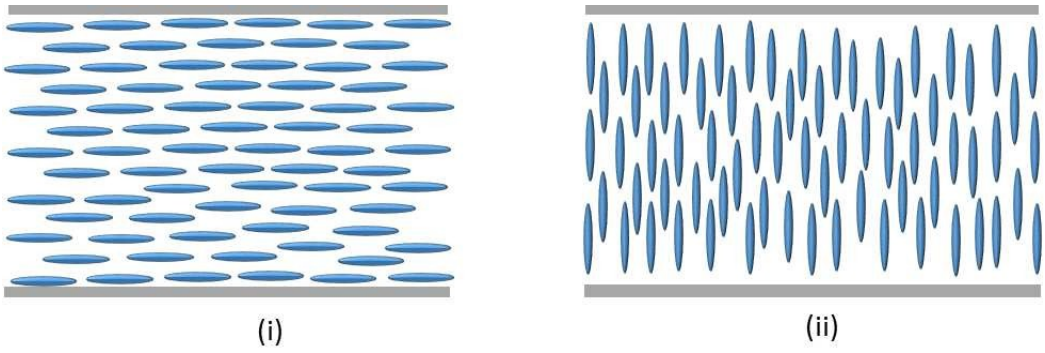

Figure 1.12: Schematic representation of (i) homogeneous and (ii) homeotropic alignment of the rod-like molecules on the substrates.

1.6.1 Homogeneous alignment

If the molecules of the liquid crystals are aligned along one direction in the plane of the substrate then it is called homogeneous or planar alignment. Here we coat the glass substrate with a thin layer of polyimide. The interactions among the polyimide and liquid crystal molecules are such that they give in-plane orientation of the liquid crystal molecules. To make them align in a particular direction to the surface we rub the surfaces. The process of rubbing makes micro grooves over the substrate and the long axis of the molecules are aligned parallel to the grooves (rubbing direction). In case of uniaxial nematic liquid crystals, the optic axis is along the rubbing direction. A schematic representation of homogeneous alignment is shown in Fig.1.12(i).

1.6.2 Homeotropic alignment

If the molecules are aligned perpendicular to the plane of the substrate then it is called homeotropic or vertical alignment. Usually surfactant molecules are used for this alignment, which have amphiphilic polar groups and aliphatic alkyl chains. When the surfactant is coated on a glass substrate, the polar groups get attracted and sticks to the surface and alkyl chains stay perpendicular to the surface. The alkyl chains interact with liquid crystal molecules and provide vertical alignment of the director on the surface. A schematic representation of homeotropic alignment is shown in in Fig.1.12(ii).

1.7 Anchoring transition

When the nematic phase is in contact with another material (solid, liquid, gas), LC adopts a particular orientation on the contact area of another material. The phe-

nomenon of orientation of LC by the surface is called anchoring. A particular orientation of the director is due to the balance among various interactions. Generally, surface imposes a particular direction called anchoring direction or easy direction. So, anchoring direction is the spontaneous orientation of the LC director. If the anchoring direction changes from one direction to another direction then the phenomenon is called anchoring transition. In chapter-5, we have studied anchoring transition of some LCs.

1.8 Freedericksz transition

The transition from an uniformly aligned state to distorted state by the application of electric or magnetic field is called Freedericksz transition. Consider, the positive dielectric anisotropy ($\Delta\varepsilon > 0$) liquid crystal is homogeneously aligned on the surface.

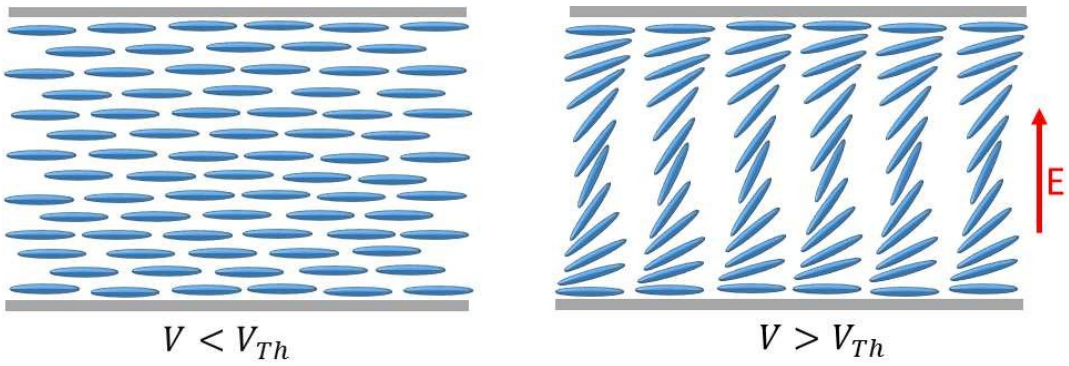

Figure 1.13: Schematic representation of director configuration below ($V < V_{Th}$) and above ($V > V_{Th}$) the threshold field respectively.

By applying the field the corresponding electric energy is given by

$$\omega_{ele} = -\frac{1}{2}\overrightarrow{D}.\overrightarrow{E} = -\frac{1}{2}\varepsilon_o\varepsilon_\perp E^2 - \frac{1}{2}\varepsilon_o\Delta\varepsilon E^2(\hat{n}.\overrightarrow{E})^2. \tag{1.14}$$

From the Eq.(1.14), the electric energy will be minimized when the director $\hat{n}$ is along the field direction. When the external field is applied, there exist a competition between the surface field and the electric energy. At zero and small voltages the director is uniformly aligned along the surface. By increasing the voltage, at certain value the director begins to deform i.e., electric energy overcomes the surface energy. At higher voltage, the director is aligned along the field direction except a very thin regions near the surface. The corresponding voltage at which the director begins to deform is called Freedericksz threshold voltage and the phenomenon is called Freedericksz transition [23]. This transition is field induced second order transition. A schematic representation of Freedericksz transition is shown in Fig.1.13.

The threshold voltage is given by

$$V_{Th} = \pi \sqrt{\frac{K_{11}}{\varepsilon_o \Delta\varepsilon}}, \tag{1.15}$$

where K_{11} is the splay elastic constant. Threshold voltage is independent of cell thickness. In case of negative dielectric material ($\Delta\varepsilon < 0$), we take homeotropic alignment of the molecules and the corresponding threshold voltage is given by

$$V_{Th} = \pi \sqrt{\frac{K_{33}}{\varepsilon_o \Delta\varepsilon}}, \tag{1.16}$$

where K_{33} is the bend elastic constant.

References

[1] S. Chandrasekhar, *Liquid Crystals*. Cambridge University Press, 1992.

[2] P. de Gennes and J. Prost, *The Physics of Liquid Crystals*. International series of monographs on physics, Clarendon Press, 1993.

[3] P. J. Collings and M. Hird, *Introduction to liquid crystals: chemistry and physics*. CRC Press, 1997.

[4] W. H. Jeu, *Physical properties of liquid crystalline materials*, vol. 1. CRC Press, 1980.

[5] G. Friedel, "The mesomorphic states of matter," in *Annales de Physique*, vol. 18, p. 5, 1922.

[6] M. J. Stephen and J. P. Straley, "Physics of liquid crystals," *Reviews of Modern Physics*, vol. 46, no. 4, p. 617, 1974.

[7] S. K. Pal, V. Raghunathan, and S. Kumar, "Phase transitions in novel disulphide-bridged alkoxycyanobiphenyl dimers," *Liquid Crystals*, vol. 34, no. 2, pp. 135–141, 2007.

[8] P. J. Collings and M. Hird, *Introduction to liquid crystals: chemistry and physics*. CRC Press, 1997.

[9] S. Chandrasekhar, B. Sadashiva, and K. Suresh, "Liquid crystals of disc-like molecules," *pramana*, vol. 9, no. 5, pp. 471–480, 1977.

[10] J. K. Vij, A. Kocot, and T. S. Perova, "Order parameter, alignment and anchoring transition in discotic liquid crystals," *Molecular Crystals and Liquid Crystals*, vol. 397, no. 1, pp. 231–244, 2003.

[11] S. Kumar, *Chemistry of discotic liquid crystals: from monomers to polymers*. CRC press, 2016.

[12] S. Gauza, C.-H. Wen, S.-T. Wu, N. Janarthanan, and C.-S. Hsu, "Super high birefringence isothiocyanato biphenyl-bistolane liquid crystals," *Japanese journal of applied physics*, vol. 43, no. 11R, p. 7634, 2004.

[13] I. Haller, "Thermodynamic and static properties of liquid crystals," *Progress in solid state chemistry*, vol. 10, pp. 103–118, 1975.

[14] W. Maier and G. Meier, "Anisotrope dk-dispersion im radiofrequenzgebiet bei homogen geordneten kristallinen flüssigkeiten," *Zeitschrift für Naturforschung A*, vol. 16, no. 11, pp. 1200–1205, 1961.

[15] H. J. Deuling, "Deformation of nematic liquid crystals in an electric field," *Molecular Crystals and Liquid Crystals*, vol. 19, no. 2, pp. 123–131, 1972.

[16] H. Gruler and G. Meier, "Electric field-induced deformations in oriented liquid crystals of the nematic type," *Molecular Crystals and Liquid Crystals*, vol. 16, no. 4, pp. 299–310, 1972.

[17] F. C. Frank, "I. liquid crystals. on the theory of liquid crystals," *Discussions of the Faraday Society*, vol. 25, pp. 19–28, 1958.

[18] K. Sokalski and T. W. Ruijgrok, "Elastic constants for liquid crystals of disc-like molecules," *Physica A: Statistical Mechanics and its Applications*, vol. 113, no. 1, pp. 126–132, 1982.

[19] S.-T. Wu and C.-S. Wu, "Experimental confirmation of the osipov-terentjev theory on the viscosity of nematic liquid crystals," *Physical Review A*, vol. 42, no. 4, p. 2219, 1990.

[20] M. Dark, M. Moore, D. Shenoy, and R. Shashidhar, "Rotational viscosity and molecular structure of nematic liquid crystals," *Liquid crystals*, vol. 33, no. 1, pp. 67–73, 2006.

[21] A. A. Sonin, *The surface physics of liquid crystals*. Taylor & Francis, 1995.

[22] K. Takatoh, M. Sakamoto, R. Hasegawa, M. Koden, N. Itoh, and M. Hasegawa, *Alignment technology and applications of liquid crystal devices*. CRC Press, 2005.

[23] L. M. Blinov, "Electro-optical effects in liquid crystals," *Soviet Physics Uspekhi*, vol. 17, no. 5, p. 658, 1975.

2

Experimental

2.1 Introduction

In this chapter, first we describe experimental procedure for cell preparation. We also describe all the experimental techniques for measuring various physical properties of the liquid crystals such as birefringence, static dielectric constants, splay and bend elastic constants and rotational viscosity.

2.2 Preparation of experimental cell

The experimental cell is made of two glass plate of thinkness around 1mm and have the dimension 1 cm x 1.5 cm. The glass slides are coated with transparent indium-tin-oxide (ITO) layer of thickness 1500 Å and have the resistivity 15-20 Ω/sq. The required pattern of ITO can be achieved by chemical etching with hydrochloric acid (HCl) and Zinc powder (see Fig.2.1(a) and Fig.2.1(b)). These glass plates are cleaned thoroughly with hexane, acetone and distilled water in ultrasonicator waterbath. Based on the requirement, appropriate polyimide is spin coated on the glass slides. For homogeneous or planar alignment, we used polyimide AL-1254, whereas for homeotropic or vertical alignment, polyimide JALS-204 were used. They were cured in an oven at 180 °C and 200 °C for one hour respectively. The cured glass plates are rubbed unidirectionally by using a homemade rubbing machine. The rubbed glass plates are arranged such that their active areas facing each other and rubbing directions are anti parallel. The glass slides are stuck each other by using UV-curable adhesive glue. The thickness

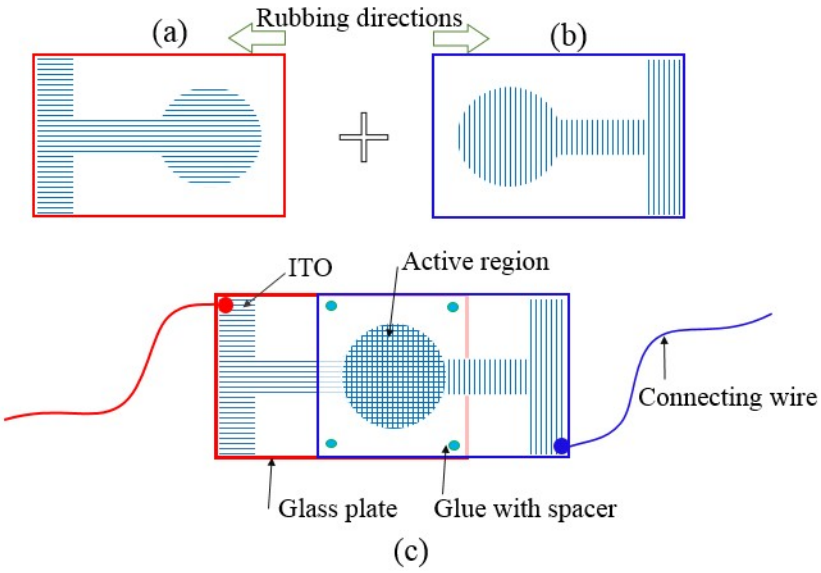

Figure 2.1: (a) and (b) Schmatic representation of top view of the two glass plates. (c) Experimental cell.

of the cells is controlled by appropriate size of silica beads of 5-10μm size. Electrical connections are given to the cell by soldering the copper wire by using ultrasonic soldering machine (sunbounder USM-IV). The schematic top view of the glass slides and the experimental cell is shown in Fig.2.1.

2.2.1 Measurement of cell thinkness

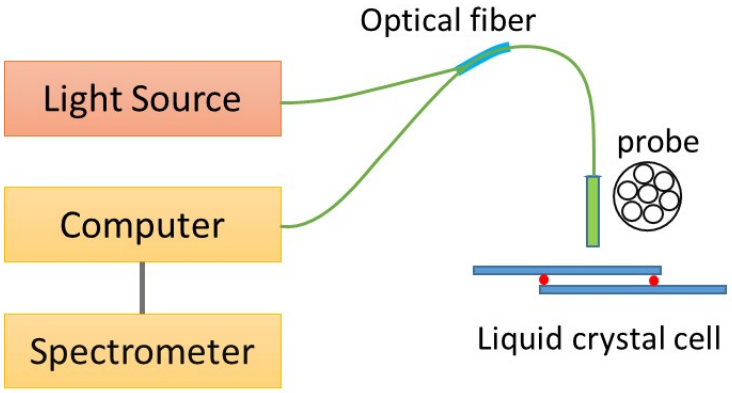

Figure 2.2: Schematic setup for measurement of cell thickness.

The accurate thickness of the cell is very important for the physical measurements. The thickness of the cell is measured with Ocean optics spectrometer using interferometric method [1]. The experimental setup for the measurement of thickness of the cell is

shown in Fig.2.2. The empty cell is kept under spectrometer probe, consists of optical fibers. The light emitted by the source is illuminated over the cell through outer fibers. The reflected light from the cell is fedback to the spectrometer through central fibre. The corresponding spectrum is analysed by computer using spectrasuite software. The spectrum consists of alternative bright and dark fringes. The thickness (d) of the cell is measured by using the formula,

$$d = \frac{\lambda_m \lambda_n}{\lambda_n - \lambda_m} \times \frac{n-m}{2} \tag{2.1}$$

where λ_m, λ_n are corresponding wavelengths of m^{th} and n^{th} maxima or minima.

2.3 Dielectric measurements ($\varepsilon_{||}$ and $\varepsilon_{\perp}$)

The plates with an active area (ITO) of A and are separated by a distance d and forms a parallel plate capacitor. The empty capacitance is given by $c_o = \varepsilon_o A/d$ and also can be measured by using LCR meter (Agilent E4980A) or Impedance analyzer. The ratio of capacitance of the cell with liquid crystal to the capacitance of empty cell gives dielectric constant.

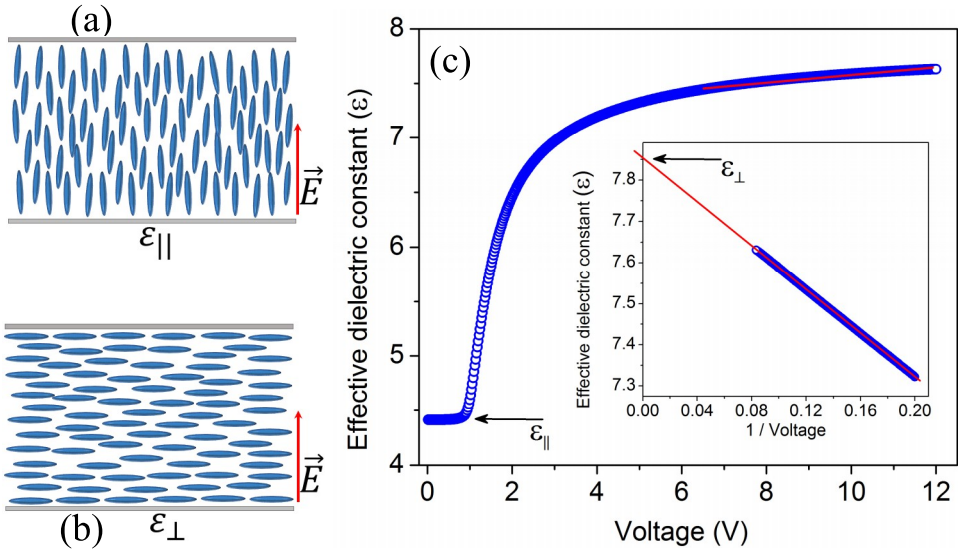

Figure 2.3: Schematic representation of director ($\hat{n}$) configuration in the measurement of (a) parallel and (b) perpendicular component of dielectric constants respectively. (c) Variation of effective dielectric constant as a function of voltage for a material with negative dielectric anisotropy. (Inset) Extrapolation of dielectric constant at higher voltages to 1/V = 0 to get $\varepsilon_{\perp}$.

Usually we measure $\varepsilon_{||}$ in homeotropic cell and $\varepsilon_{\perp}$ in planar cell. Although occasionally we have used extrapolation method. In case of positive dielectric anisotropy material, below the Freedericksz threshold voltage, the dielectric constant is almost constant

and the liquid crystal director is along the plane of the surface and perpendicular the applied field. This gives the perpendicular component of dielectric constant $\varepsilon_{\perp}$. By increasing the voltage above the Freedericksz threshold voltage, dielectric constant increases rapidly then saturate. The dielectric constant at higher voltages is plotted against $1/V$ and by the extrapolation $1/V = 0$, the director is aligned along the electric field direction. This gives the parallel component of the dielectric constant ($\varepsilon_{||}$). This value is almost equal to that measurement in homeotropic cell. In case of negative dielectric anisotropy materials, we used the homeotropic cell. Below the Freedericksz threshold voltage, it gives the parallel component ($\varepsilon_{||}$) and by extrapolating the dielectric constant at higher voltages to $1/V = 0$ gives the perpendicular ($\varepsilon_{\perp}$) component of dielectric constant. From the above values, the average dielectric constant ($\overline{\varepsilon} = (\varepsilon_{||} + \varepsilon_{\perp})/2$) and the dielectric ansiotropy ($\Delta\varepsilon = (\varepsilon_{||} - \varepsilon_{\perp})$) values are calculated.

2.4 Experimental setup

The experimental set up for measurement of physical properties is shown below.

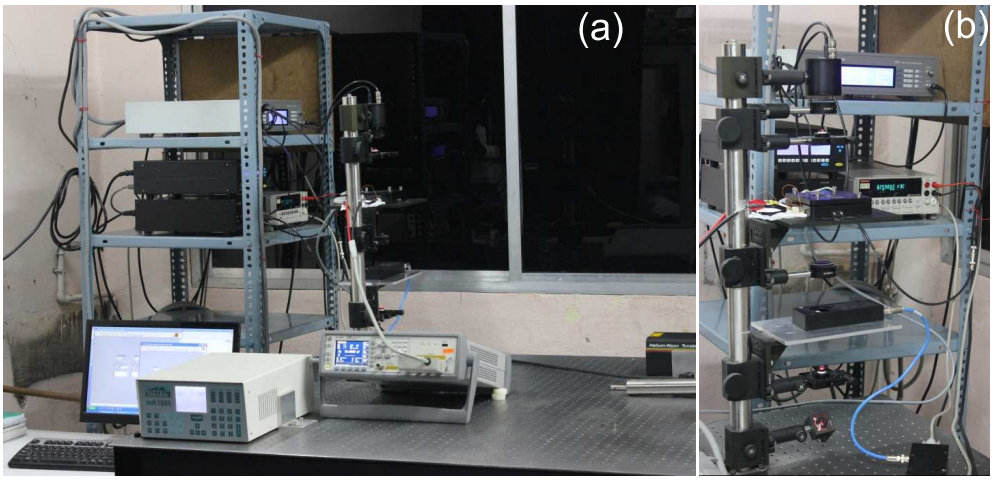

Figure 2.4: Various instructments and their assembly in (a) front and (b) side view of the experimental setup used for the measurement of various physical properties.

2.5 Birefringence (Δn)

The birefringence in an uniaxial system is defined as $\Delta n = n_e - n_o$, where n_e and n_o are the extraordinay and ordinary refractive indices respectively. Here, we measured by two techniques (i) intensity measurement technique and (ii) phase modulation technique. We briefly mention here both the techniques.

2.5.1 Intensity measurement technique

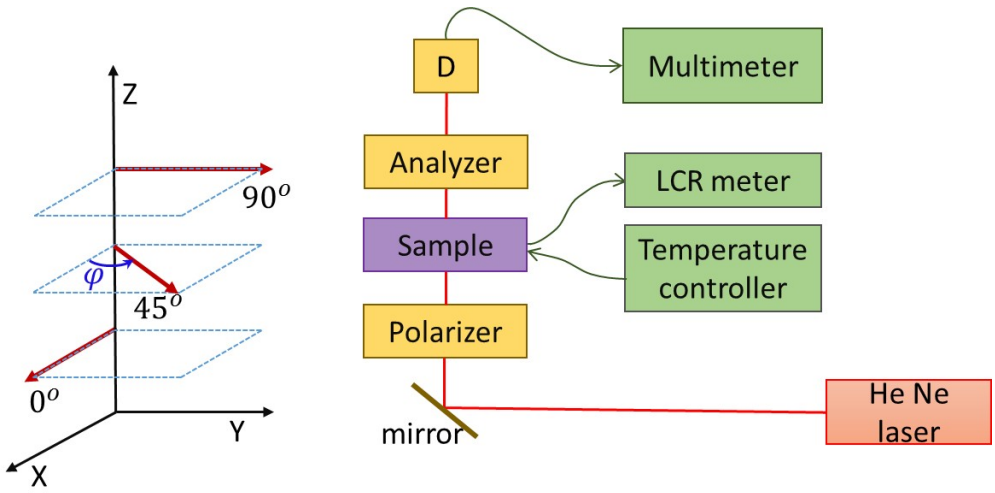

Figure 2.5: Experimental setup to measure birefringence using intensity measurement.

In this technique, the birefringence of the sample can be measured by measuring the d.c. intensity at the detector. The optical setup for measuring the birefringence of the sample in the intensity measurement technique is shown in Fig.2.5. The setup consists of two Glan-Thampson polarizers, a He-Ne laser source and a detector. In the set up, polariser and analyser are in the crossed position. All the instruments are arranged in the vertical bench setup, and the sample is kept on a plate with a hole through which light can pass. The light first passes through the Glan-Thampson polarizer, then pass through the liquid crystal sample. Here the liquid crystal director making an angle 45° with the polariser. The transmitted light passes through the second Glan-Thampson polariser and then to the detector. The detector output given to a Keithley DC voltmeter to measure the output intensity. Let us assume the polariser and the analyser are along the x and y directions and the light propagates along the z direction. Liquid crystal director $\hat{n}$ makes an angle ϕ with polariser. The electric field of the transmitted light intensity at the detector can be represented by Jones matrix and given by [2]

$$E_{out} = P_{vertical} R(-\phi) J_{lc} R(\phi) P_{horizontal} E_{in}, \tag{2.2}$$

where, $R(\phi)$ rotation matrix about an angle ϕ, J_{lc} is the Jones matrix of the liquid crystal. By substituting the Jones matrix for each optical element, we get

$$\begin{pmatrix} E_x^{out} \\ E_y^{out} \end{pmatrix} = \begin{pmatrix} 0 & 0 \\ 0 & 1 \end{pmatrix} \begin{pmatrix} \cos\varphi & -\sin\varphi \\ \sin\varphi & \cos\varphi \end{pmatrix} \begin{pmatrix} e^{-\frac{2\pi}{\lambda} i n_e d} & 0 \\ 0 & e^{-\frac{2\pi}{\lambda} i n_o d} \end{pmatrix} \times \begin{pmatrix} \cos\varphi & \sin\varphi \\ -\sin\varphi & \cos\varphi \end{pmatrix} \begin{pmatrix} 1 & 0 \\ 0 & 0 \end{pmatrix} \begin{pmatrix} E_x^{in} \\ E_y^{in} \end{pmatrix}. \tag{2.3}$$

On simplification,

$$\begin{pmatrix} E_x^{out} \\ E_y^{out} \end{pmatrix} = \begin{pmatrix} 0 \\ iE_x^{in} e^{\frac{-\pi i}{\lambda}(n_e+n_o)d} \sin^2(2\varphi) \sin^2\left(\frac{\pi(n_e-n_o)d}{\lambda}\right) \end{pmatrix}. \tag{2.4}$$

The intensity at the detector is given by

$$I_{mea} = |E_x|^2 + |E_x|^2 = (E_x^{in})^2 sin^2(2\varphi) sin^2\left(\frac{\pi\Delta n(\lambda)d}{\lambda}\right). \tag{2.5}$$

In the setup the rubbing direction makes an angle $\varphi = 45°$ with the polarizer, and the intensity is given by

$$I_{mea} = I_o sin^2\left(\frac{\pi\Delta n(\lambda)d}{\lambda}\right). \tag{2.6}$$

Then when Δn changes, the I_{mea} goes through several maxima and minima. The birefringence is given by

$$\Delta n(\lambda) = \frac{\lambda}{\pi d} arcsin\left(\sqrt{\frac{I_{mea}}{I_o}}\right). \tag{2.7}$$

If the minimum intensity is not zero, the birefringence can be obtained from the relation:

$$\Delta n(\lambda) = \frac{\lambda}{\pi d} arcsin\left(\sqrt{\frac{I_{mea} - I_{min}}{I_{max} - I_{min}}}\right). \tag{2.8}$$

.

The temperature of the liquid crystal sample is controlled by the temperature controller (Instec mk 1000) with an accuracy of 10 mk. To apply field and to get the capacitance values, liquid crystal cell is connected through LCR meter (Agilent E4980A). To measure the voltage dependent birefringence, temperature is kept constant and voltage varied with finite steps and at each step corresponding intensity is measured at the detector. To measure the temperature dependent birefringence, voltage is kept fixed and the temperature is varied in discrete steps and at each step corresponding intensity at the detector and capacitance are measured. All the instruments are interfaced to the computer through the LabVIEW software.

2.5.2 Phase modulation technique

The optical setup for measuring the birefringence of the sample using phase modulation technique [3] is shown in Fig.2.6. The setup consists of two Glan-Thampson polarizers, a He-Ne laser source, a photoelastic modulator (PEM) and a detector. Photoelastic modulator (PEM) is an optical device used to modulate the polarisation state of light beam at a certain frequency. A rectangular fused silica bar present in the PEM is made to vibrate with a natural resonant frequency and these vibrations are maintained

by quartz piezoelectric transducer attached to the end of the bar. An oscillating birefringence occurs at the center of an optical element at a frequency about 50 kHz. The magnitude of the birefringence is electronically controlled by the PEM controller. The polariser and the analyser are mounted at an angle 90^o. The PEM head and the liquid crystal cell are placed in sucession to the polariser at an angle 45^o with the polariser. All the optical elements are placed in the vertical setup. The light first passes through the Glan-Thampson polarizer then the PEM and the liquid crystal sample. The modulated transmitted light passes through the second Glan-Thampson polariser and reaches to the detector. The detector output given to a lock-in amplifier for the detection of the first and the second harmonics of the output AC signal in reference to the frequency of the PEM controller. The temperature of the liquid crystal sample is controlled by the temperature controller (Instec mk 1000). To apply voltage and to get the capacitance, the cell is connected through a Agilent E4980A LCR meter. To measure the voltage dependent birefringence, the temperature is kept constant and voltage varied with finite steps and at each step corresponding intensity is measured at the detector. Similarly, voltage kept fixed and the temperature is varied in discrete steps, to measure the temperature dependent birefringence. All the instruments are interfaced to the computer through the LabVIEW software.

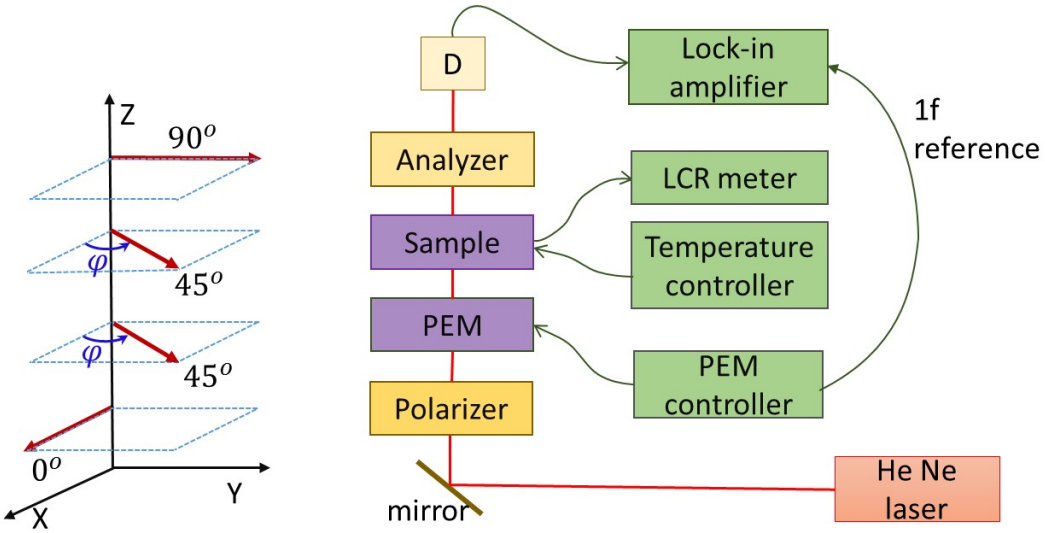

Figure 2.6: Experimental set-up to measure birefringence using PEM.

The expression for the transmitted electric field of the light is given by

$$E_{out} = P_{vertical} R(-\varphi) J_{lc} J_{PEM} R(\varphi) P_{horizontal} E_{in}, \tag{2.9}$$

where, $R(\varphi)$ rotation matrix about an angle φ, J_{lc} is the Jones matrix of the liquid crystal. If the PEM makes an oscillations with an amplitude A_o and with a frequency ω, then the retardation can be expressed as $A = A_o \cos(\omega t)$. The Jones matrix for

PEM is given by [4]

$$J_{PEM} = \begin{pmatrix} e^{\frac{2\pi i}{\lambda}\frac{A}{2}} & 0 \\ 0 & e^{\frac{-2\pi i}{\lambda}\frac{A}{2}} \end{pmatrix}. \tag{2.10}$$

By substituting the Jones matrix for each optical element, Eq.(2.9) can be written as

$$\begin{aligned} \begin{pmatrix} E_x^{out} \\ E_y^{out} \end{pmatrix} = \begin{pmatrix} 0 & 0 \\ 0 & 1 \end{pmatrix} \begin{pmatrix} \cos\varphi & -\sin\varphi \\ \sin\varphi & \cos\varphi \end{pmatrix} \begin{pmatrix} e^{\frac{-2\pi i}{\lambda}n_e d} & 0 \\ 0 & e^{\frac{-2\pi i}{\lambda}n_o d} \end{pmatrix} \begin{pmatrix} e^{\frac{2\pi i}{\lambda}\frac{A}{2}} & 0 \\ 0 & e^{\frac{-2\pi i}{\lambda}\frac{A}{2}} \end{pmatrix} \\ \times \begin{pmatrix} \cos\varphi & \sin\varphi \\ -\sin\varphi & \cos\varphi \end{pmatrix} \begin{pmatrix} 1 & 0 \\ 0 & 0 \end{pmatrix} \begin{pmatrix} E_x^{in} \\ E_y^{in} \end{pmatrix}. \end{aligned} \tag{2.11}$$

The intensity at the detector is given by

$$I = |E_x|^2 + |E_y|^2 = (E_x^{in})^2 sin^2(2\varphi) sin^2\left(\frac{\pi(\Delta n(\lambda)d + A)}{\lambda}\right). \tag{2.12}$$

In the setup, PEM and the rubbing direction makes an angle $\varphi = 45°$ with the polarizer, then the intensity is given by,

$$I_{mea} = I_o sin^2\left(\frac{\pi(\Delta n(\lambda)d + A)}{\lambda}\right). \tag{2.13}$$

By substituting $A = A_o \cos(\omega t)$ and by simplification

$$I = \frac{I_o}{2}\left(1 - \cos\left(\frac{2\pi}{\lambda}\Delta n d + \frac{2\pi}{\lambda}A_o\cos(\omega t)\right)\right). \tag{2.14}$$

Expressing retardation in terms of phase angle $\Delta\Phi = \frac{2\pi}{\lambda}(\Delta n)d$, it becomes

$$I = \frac{I_o}{2}\left[1 - \cos(\Delta\Phi)\cos(A_o\cos(\omega t)) + \sin(\Delta\Phi)\sin(A_o\cos(\omega t))\right]. \tag{2.15}$$

On simplification,

$$\begin{aligned} I = \frac{I_o}{2}[1 - \cos(\Delta\Phi) \times \{J_o(A_o) + 2(J_2(A_o)\cos(2\omega t)) + ...\} \\ + \sin(\Delta\Phi) \times \{2(J_1(A_o)\cos(\omega t)) + ...\}]. \end{aligned} \tag{2.16}$$

where J_o, J_1,& J_2 are various orders of Bessel's functions. The intensity can be written as

$$\begin{aligned} I = I_o[\frac{1 - J_o(A_o)\cos(\Delta\Phi)}{2} + J_1(A_o)\sin(\Delta\Phi)\cos(\omega t) \\ + J_2(A_o)\cos(\Delta\Phi)\cos(2\omega t) + ...], \end{aligned} \tag{2.17}$$

where the coefficients of the 1st and 2nd harmonics of the intensities are given by

$$\begin{aligned} I_{1f} &= I_o J_1(A_o)\sin(\Delta\Phi), \\ I_{2f} &= I_o J_2(A_o)\cos(\Delta\Phi). \end{aligned} \tag{2.18}$$

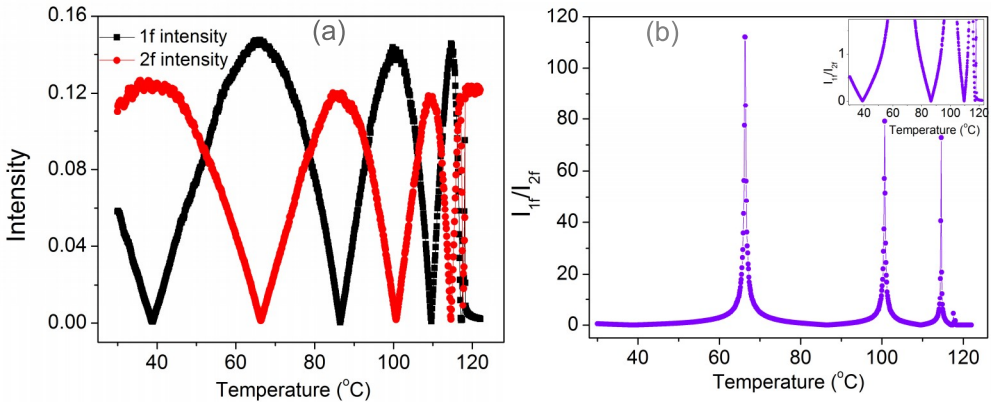

Figure 2.7: (a) A representative variation of 1st and 2nd harmonic intensities with temperature. (b) Ratio of 1st and 2nd harmonic intensities with temperature. (Inset) Enlarged image of minimum values of ratio of intensities in Mix-3 sample.

Here $A_o = 2.405$, then the values of $J_o(A_o) = 0$, $J_1(A_o) = 0.519$ and $J_2(A_o) = 0.4318$. A typical variation of 1st and 2nd harmonic intensities and the corresponding ratio of intensities with temperature (°C) are shown in Fig.2.7. By taking the ratio and simplifying the Eq.(2.18), the birefringence is given by

$$\Delta n = \frac{\lambda}{2\pi d}\Delta\Phi = \frac{\lambda}{2\pi d} arctan\left(\frac{I_{1f} \times J_2(A_o)}{I_{2f} \times J_1(A_o)}\right) \tag{2.19}$$

By using phase modulation technique, we can measure very small value of birefringence of order ($< 10^{-3}$) very accurately.

2.6 Measurement of elastic constants

Elastic constants can be measured by two indirect techniques namely electro-optic and dielectric technique. We can measure splay and bend elastic constants by measuring the voltage dependent retardation/dielectric values. Consider the nematic liquid crystal having positive dielectric anisotropy ($\Delta\varepsilon > 0$) in the cell of thickness d. The liquid crystal director ($\hat{n}$) is along the y-direction as shown in Fig.2.8. By applying the electric field E along the z-direction, the corresponding elastic energy can be minimized by tilting the director along the field direction. Above the Freedericksz threshold voltage, the director tend to align along the field direction and the director distortion is position dependent along the z-direction. So, we can write

$$\hat{n} = (0, \cos\theta(z), \sin\theta(z)), \tag{2.20}$$

$$\overrightarrow{E} = (0, 0, E_z), \tag{2.21}$$

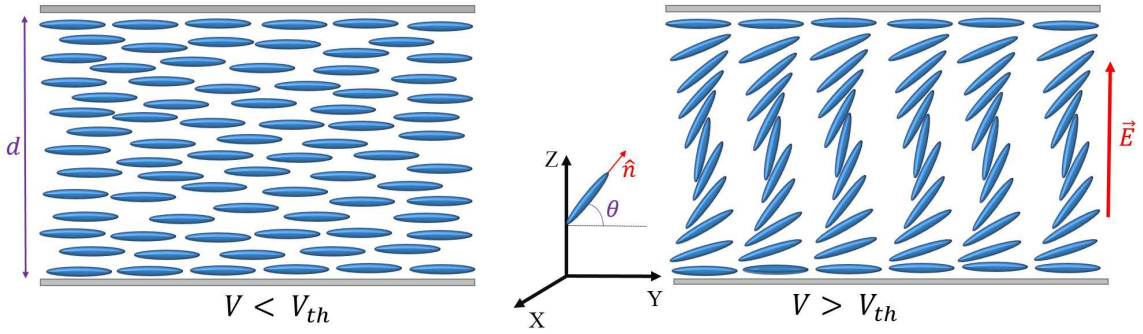

Figure 2.8: Schematic representation of director ($\hat{n}$) distribution below and above the threshold voltage (V_{th}).

with $\theta(0) = \theta(d) = 0$. $\theta(z)$ is a function of z and is maximum θ_m at the middle of the cell, $z = d/2$. The free energy per unit area is the sum of elastic energy, electric energy and the surface energy. The elastic free energy per unit volume is given by

$$F_v = \frac{1}{2}[K_{11}(\nabla.\hat{n})^2 + K_{22}(\hat{n}.\nabla \times \hat{n})^2 + K_{33}(\hat{n} \times \nabla \times \hat{n})^2]. \tag{2.22}$$

Since the distortion is along the z-axis, we can write

$$\nabla = \hat{k}\frac{\partial}{\partial z}. \tag{2.23}$$

The splay term can be written as

$$\nabla.\hat{n} = \cos\theta \frac{d\theta}{dz}. \tag{2.24}$$

The twist term can be written as

$$\begin{aligned} \nabla \times \hat{n} &= \begin{vmatrix} i & j & k \\ 0 & 0 & \frac{\partial}{\partial z} \\ 0 & \cos\theta & \sin\theta \end{vmatrix} = \hat{i}\sin\theta\frac{d\theta}{dz}, \\ \implies \quad & \hat{n}.\nabla \times \hat{n} = 0. \end{aligned} \tag{2.25}$$

So, in this configuration, the twist elastic energy is zero.
The bend term is given by

$$\begin{aligned} \hat{n} \times \nabla \times \hat{n} &= \begin{vmatrix} i & j & k \\ 0 & \cos\theta & \sin\theta \\ \sin\theta\frac{d\theta}{dz} & 0 & 0 \end{vmatrix} = \hat{j}\sin^2\theta\frac{d\theta}{dz} - \hat{k}\sin\theta\cos\theta\frac{d\theta}{dz}, \\ \implies (\hat{n} \times \nabla \times \hat{n})^2 &= \sin^2\theta\left(\frac{d\theta}{dz}\right)^2. \end{aligned} \tag{2.26}$$

The electrostatic energy per unit area is given by

$$F_{el} = -\frac{1}{2}\int_0^d \overrightarrow{D}.\overrightarrow{E}\,dz. \tag{2.27}$$

The total Frank free energy per unit area is the sum of elastic, electrostatic and surface free energy and is given by [5–8]

$$F = \frac{1}{2}\int_0^d \left[K_{11}\cos^2\theta + K_{33}\sin^2\theta\left(\frac{d\theta}{dz}\right)^2 - \overrightarrow{D}.\overrightarrow{E}\right] dz + 2f_s(\theta_0). \tag{2.28}$$

where $\overrightarrow{D}$ is the displacement vector, $f_s(\theta_0)$ is the surface free energy. Since, the liquid crystal medium is non-conducting, from the Maxwell's equations, we get

$$\nabla.\overrightarrow{D} = 0, \nabla\times\overrightarrow{E} = 0. \tag{2.29}$$

We have

$$\begin{aligned}
\overrightarrow{D} &= \varepsilon.\overrightarrow{E},\\
&= \varepsilon_o(\varepsilon_\perp\overrightarrow{E} + \Delta\varepsilon(\overrightarrow{E}.\hat{n})\hat{n}).\\
D_z &= \varepsilon_o\left\{\varepsilon_\perp E_z + (\varepsilon_{||}-\varepsilon_\perp)E_z\sin^2\theta\right\},\\
&= \varepsilon_o E_z\left\{\varepsilon_{||}\sin^2\theta + \varepsilon_\perp\cos^2\theta\right\}.
\end{aligned} \tag{2.30}$$

Now, the potential, V is given by

$$\begin{aligned}
V &= \int_0^d E_z dz\\
&= \int_0^d \frac{D_z}{\varepsilon_o(\varepsilon_{||}\sin^2\theta + \varepsilon_\perp\cos^2\theta)}dz\\
\Rightarrow D_z &= \varepsilon_o V\left\{\int_0^d(\varepsilon_{||}\sin^2\theta + \varepsilon_\perp\cos^2\theta)^{-1}dz\right\}^{-1}.
\end{aligned} \tag{2.31}$$

The electrostatic energy is given by

$$-\frac{1}{2}\int_0^d \overrightarrow{D}.\overrightarrow{E}\,dz = -\frac{1}{2}D_z V = -\frac{\varepsilon_o V^2}{2}\left\{\int_0^d(\varepsilon_{||}\sin^2\theta + \varepsilon_\perp\cos^2\theta)^{-1}dz\right\}^{-1}. \tag{2.32}$$

Total free energy density obtained from the Eq.(2.28) is given by

$$\begin{aligned}
F = \quad & \frac{1}{2}\int_0^d \left[K_{11}\cos^2\theta + K_{33}\sin^2\theta\left(\frac{d\theta}{dz}\right)^2\right] dz\\
& -\frac{\varepsilon_o V^2}{2}\left\{\int_0^d(\varepsilon_{||}\sin^2\theta + \varepsilon_\perp\cos^2\theta)^{-1}dz\right\}^{-1} + 2f_s(\theta_0).
\end{aligned} \tag{2.33}$$

By minimizing the free energy using the Euler-Lagrange equation[9], $\frac{d}{dz}\left(\frac{\partial F}{\partial\theta}\right) - \frac{\partial F}{\partial\theta} = 0$, we get

$$\begin{aligned}\frac{d}{dz}\left((K_{11}\cos^2\theta + K_{33}\sin^2\theta)\frac{d\theta}{dz}\right) =& (K_{33}-K_{11})\sin\theta\cos\theta\left(\frac{d\theta}{dz}\right)^2 \\ &- \frac{D_z^2}{\varepsilon_o}\frac{(\varepsilon_{||}-\varepsilon_\perp)\sin\theta\cos\theta}{\sqrt{\varepsilon_{||}\sin^2\theta+\varepsilon_\perp\cos^2\theta}} \\ \Rightarrow (K_{11}\cos^2\theta + K_{33}\sin^2\theta)\theta'' &+ (K_{33}-K_{11})\sin\theta\cos\theta(\theta')^2 \\ &= -\frac{D_z^2}{\varepsilon_o}\frac{(\varepsilon_{||}-\varepsilon_\perp)\sin\theta\cos\theta}{\sqrt{\varepsilon_{||}\sin^2\theta+\varepsilon_\perp\cos^2\theta}},\end{aligned} \tag{2.34}$$

where $\theta' = \frac{d\theta}{dz}$ and $\theta'' = \frac{d^2\theta}{dz^2}$.
Multiplying by $2\frac{d\theta}{dz}$ and integrating, we get

$$(K_{11}\cos^2\theta + K_{33}\sin^2\theta)(\theta')^2 = C + -\frac{D_z^2}{\varepsilon_o}\frac{1}{\varepsilon_{||}\sin^2\theta+\varepsilon_\perp\cos^2\theta}. \tag{2.35}$$

where C is the integration constant. By applying the boundary conditions, $\theta(0) = 0$, $\theta(d) = 0$ at $d/2$, $\theta(d/2) = \theta_m$, and $(\theta' = \frac{d\theta}{dz})_{d/2} = 0$, we get

$$C = -\frac{D_z^2}{\varepsilon_o}\frac{1}{\varepsilon_{||}\sin^2\theta_m+\varepsilon_\perp\cos^2\theta_m}. \tag{2.36}$$

By substituting $\gamma = \dfrac{\varepsilon_{||}}{\varepsilon_\perp} - 1, \kappa = \dfrac{K_{33}}{K_{11}} - 1$ and C in the Eq.(2.35), we get

$$K_{11}(\kappa\sin^2\theta+1)(\theta')^2 = \frac{D_z^2\gamma}{\varepsilon_o\varepsilon_\perp}\left(\frac{\sin^2\theta_m-\sin^2\theta}{(1+\gamma\sin^2\theta_m)(1+\gamma\sin^2\theta)}\right). \tag{2.37}$$

On simplification, we get

$$\frac{d\theta}{dz} = D_z\sqrt{\frac{\gamma}{\varepsilon_o\varepsilon_\perp K_{11}}}\left(\frac{\sin^2\theta_m-\sin^2\theta}{(1+\gamma\sin^2\theta_m)(1+\gamma\sin^2\theta)(1+\kappa\sin^2\theta)}\right)^{\frac{1}{2}}. \tag{2.38}$$

On integration, we get

$$D_z = \frac{2}{d}\sqrt{\frac{\varepsilon_o\varepsilon_\perp K_{11}}{\gamma}}\sqrt{(1+\gamma\sin^2\theta_m)}\int_\Theta^{\pi/2}\left(\frac{(1+\gamma\sin^2\theta)(1+\kappa\sin^2\theta)}{\sin^2\theta_m-\sin^2\theta}\right)^{\frac{1}{2}}d\theta. \tag{2.39}$$

From Eq.(2.31), the applied voltage is given by

$$\begin{aligned}V &= \frac{D_z}{\varepsilon_o}\int_0^d\frac{1}{(\varepsilon_{||}\sin^2\theta+\varepsilon_\perp\cos^2\theta)}dz \\ &= \frac{2D_z}{\varepsilon_o\varepsilon_\perp}\int_0^{d/2}\frac{1}{(1+\gamma\sin^2\theta)}.dz\end{aligned} \tag{2.40}$$

Using Eq.(2.38) and Eq.(2.39) and substituting $\sin\theta = \sin\theta_m\sin\psi$ in the above Equation, we get

$$\frac{V}{V_{th}} = \sqrt{1+\gamma\sin^2\theta_m}\int_{\Theta}^{\pi/2}\left(\frac{1+\kappa\sin^2\theta_m\sin^2\psi}{(1+\gamma\sin^2\theta_m\sin^2\psi)(1-\sin^2\theta_m\sin^2\psi)}\right)^{\frac{1}{2}}d\psi \tag{2.41}$$

where $\Theta = \sin^{-1}(\sin\theta_o/\sin\theta_m)$ and $V_{th} = \sqrt{\frac{K_{11}}{\varepsilon_0\varepsilon_\perp\gamma}}$ is the Freedericksz threshold voltage.

The Eq.(2.41), gives the relation between the director orientation (ψ) with respect to the applied voltage (V). There is no direct method by which we can measure variation of director $\hat{n}(\theta)$ in the cell. So we need to consider the effect of θ-variation in terms of the external measurable quantities. The two external quantities can be measured are the retardation and the dielectric constant. Here, we discuss two different techniques which are used in this thesis.

2.6.1 Electro-optic method

The optical retardation of the cell is given by

$$\delta\Phi = \frac{2\pi}{\lambda}\int_0^d \{n_{eff}(z) - n_o\}\,dz \tag{2.42}$$

where,

$$n_{eff} = \frac{n_e n_o}{\sqrt{n_e^2\sin^2\theta + n_o^2\cos^2\theta}}. \tag{2.43}$$

By substituting $\nu = \frac{n_e^2}{n_o^2} - 1$, Eq.(2.42) becomes,

$$\delta\Phi + \frac{2\pi}{\lambda}n_o d = \frac{2\pi}{\lambda}n_e\int_0^d \frac{1}{\sqrt{\nu\sin^2\theta+1}}dz \tag{2.44}$$

By substituting Eq.(2.38) and Eq.(2.39), in the above equation, we have

$$\delta\Phi + \frac{2\pi}{\lambda}n_o d = \frac{2\pi}{\lambda}n_e d\left(\frac{\int_\Theta^{\pi/2}\sqrt{\frac{(1+\kappa\sin^2\theta_m\sin^2\psi)(1+\gamma\sin^2\theta_m\sin^2\psi)}{(1-\sin^2\theta_m\sin^2\psi)(1+\nu\sin^2\theta_m\sin^2\psi)}}d\psi}{\int_\Theta^{\pi/2}\sqrt{\frac{(1+\kappa\sin^2\theta_m\sin^2\psi)(1+\gamma\sin^2\theta_m\sin^2\psi)}{(1-\sin^2\theta_m\sin^2\psi)}}d\psi}\right). \tag{2.45}$$

On rearranging the above equation, we have

$$\delta\Phi(V) = \frac{2\pi}{\lambda}n_e d\left[\frac{\int_\Theta^{\pi/2}\sqrt{\frac{(1+\kappa\sin^2\theta_m\sin^2\psi)(1+\gamma\sin^2\theta_m\sin^2\psi)}{(1-\sin^2\theta_m\sin^2\psi)(1+\nu\sin^2\theta_m\sin^2\psi)}}d\psi}{\int_\Theta^{\pi/2}\sqrt{\frac{(1+\kappa\sin^2\theta_m\sin^2\psi)(1+\gamma\sin^2\theta_m\sin^2\psi)}{(1-\sin^2\theta_m\sin^2\psi)}}d\psi} - \frac{n_o}{n_e}\right]. \tag{2.46}$$

The above Eq.(2.46) provides the value of retardation in terms of director distortion at a particular voltage. By using the parametric Eq.(2.41) and Eq.(2.46), we can calculate the splay and bend elastic constants simultaneously. The algorithm to calculate the elastic constants is given below.

Algorithm for calculating bend elastic constant (K_{33})

(i) Read experimental values Δn, n_o, $\varepsilon_{||}$, $\varepsilon_{\perp}$, and K_{11}
(ii) Choose appropriate value κ, θ_o and θ_m
(iii) Evaluate voltage (V) and retardation $\delta\Phi$
(iv) Interpolate the experimental data
(v) Measure the mean square deviation χ^2
(vi) Adjust κ and θ_o to get minimum χ^2
(vii) Measure K_{33} from κ and K_{11}

For measuring elastic constants, first we experimentally measure voltage dependent retardation. Bend elastic constant can be measured by using nonlinear least square fitting of the experimental data with theoratical Eq.(2.41) and Eq.(2.46). All the elliptical integrals are evaluated by using in-built packages in Mathematica software. For the fitting, we take experimental values of retardation ($\Delta\phi$), ordinary refractive index n_o, parallel and perpendicular components of dielectric constants ($\varepsilon_{||}$ and $\varepsilon_{\perp}$), voltage values above the Freedericksz threshold voltage. Initially, we choose approximate values of κ, tilt angle at the surface θ_o and maximum tilt angle at the middle of the cell θ_m to evaluate the theoretical equations. By using above values, theoretically we evaluated values of voltage and corresponding retardation. The experimentally measured voltages generally don't coincide with the theoretically evaluated voltages. So, we interpolate experimental voltage and retardation data to match with the theoretical values. At these voltages, we take mean square deviation (χ^2) of experimental and theoretical retardation values. For the minimum χ^2, the best fit parameters Θ and κ are noted. From the values, κ and K_{11}, bend elastic constant K_{33} is calculated. Experimental variation of retardation along with best fit with the parametric Eq.(2.41) and Eq.(2.46) is shown in Fig.2.9.

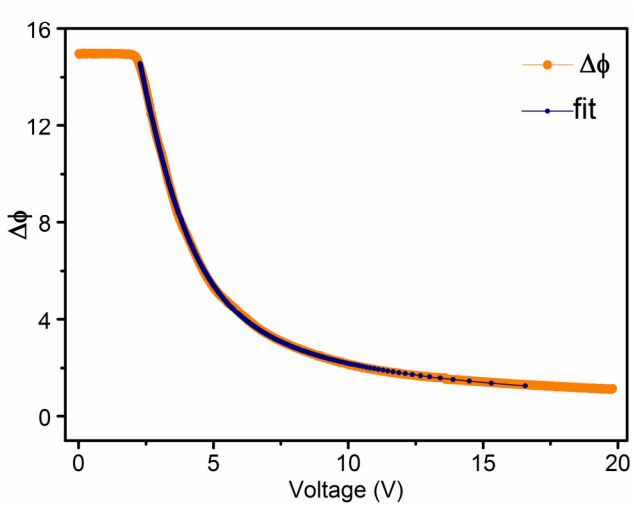

Figure 2.9: A representative experimental variation of retardation along with the best fit to the theoretical Eq.(2.41) and Eq.(2.46) as a function of voltage.

2.6.2 Dielectric method

In the dielectric technique, the capacitance of the small region of the sample is given by

$$dC = \varepsilon A/dz, \tag{2.47}$$

where dz is the small thickness along the cell seperation. By substituting ε from Eq.(2.30), the total capacitance is given by

$$\frac{1}{C} = \int_0^d \frac{dz}{A\varepsilon_o(\varepsilon_{||}\sin^2\theta + \varepsilon_\perp \cos^2\theta)} \tag{2.48}$$

By substituting the value $\gamma = \frac{\varepsilon_{||}}{\varepsilon_\perp} - 1$, we have

$$\frac{1}{C} = \frac{2}{A\varepsilon_o\varepsilon_\perp}\int_0^{d/2} \frac{dz}{1+\gamma\sin^2\theta} \tag{2.49}$$

From Eq.(2.38), we have

$$\frac{1}{C} = \frac{1}{D_z}\frac{2}{A\varepsilon_o\varepsilon_\perp}\sqrt{\frac{\varepsilon_o\varepsilon_\perp K_{11}}{\gamma}}\int_\Theta^{\pi/2}\left(\frac{(1+\gamma\sin^2\theta_m)(1+\kappa\sin^2\theta)}{(1+\gamma\sin^2\theta)(\sin^2\theta_m - \sin^2\theta)}\right)^{\frac{1}{2}} d\theta \tag{2.50}$$

By substituting D_z from Eq.(2.39), we get

$$\frac{1}{C} = \frac{d}{A\varepsilon_o\varepsilon_{||}}\left(\frac{\int_\Theta^{\pi/2}\sqrt{\left(\frac{(1+\kappa\sin^2\theta_m\sin^2\psi)}{(1+\gamma\sin^2\theta_m\sin^2\psi)(1-\sin^2\theta_m\sin^2\psi)}\right)}d\psi}{\int_\Theta^{\pi/2}\sqrt{\left(\frac{(1+\kappa\sin^2\theta_m\sin^2\psi)(1+\gamma\sin^2\theta_m\sin^2\psi)}{(1-\sin^2\theta_m\sin^2\psi)}\right)}d\psi}\right) \tag{2.51}$$

On rearranging,

$$\varepsilon(V) = \varepsilon_{||}\left(\frac{\int_\Theta^{\pi/2}\sqrt{\left(\frac{(1+\kappa\sin^2\theta_m\sin^2\psi)(1+\gamma\sin^2\theta_m\sin^2\psi)}{(1-\sin^2\theta_m\sin^2\psi)}\right)}d\psi}{\int_\Theta^{\pi/2}\sqrt{\left(\frac{(1+\kappa\sin^2\theta_m\sin^2\psi)}{(1+\gamma\sin^2\theta_m\sin^2\psi)(1-\sin^2\theta_m\sin^2\psi)}\right)}d\psi}\right) \tag{2.52}$$

The above equation gives relation between effective dielectric constant in terms of director orientation. Experimental variation of dielectric constant along with the best fit with the parametric Eq.(2.41) and Eq.(2.52) is shown in Fig.2.10. By using the parametric Eq. (2.41) and Eq.(2.52), following the similar algorithm used in the optical method, here also, we can calculate K_{11} and K_{33} values. We used the dielectric method for measuring K_{11} and K_{33} for negative dielectric materials in homeotropic cell.

2.7 Measurement of rotational viscosity (γ_1)

Rotational viscosity is measured by phase decay time measurement [10] of the homogeneously (parallel) aligned nematic LC cell under small excitation voltage. The

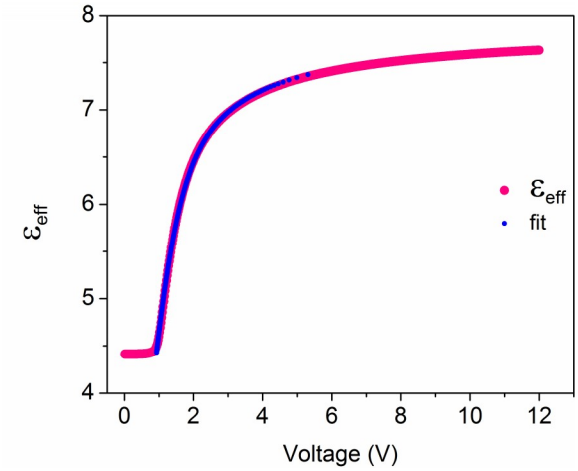

Figure 2.10: A representative experimental variation of effective dielectric constant along with the best fit to the theoretical relations Eq.(2.41) and Eq.(2.52) as a function of voltage.

setup for measurement of rotational viscosity is shown in Fig.2.11. The setup consists of two Glan-Thompson polarisers, a He-Ne laser, a photo-diode. Two polarisers are crossed and the rubbing direction of the cell makes an angle 45°, with the polarizer. A temperature controller, LCR meter, oscilloscope are used to vary temperature, to apply the voltage and to collect/see the intensity from the photo diode respectively.

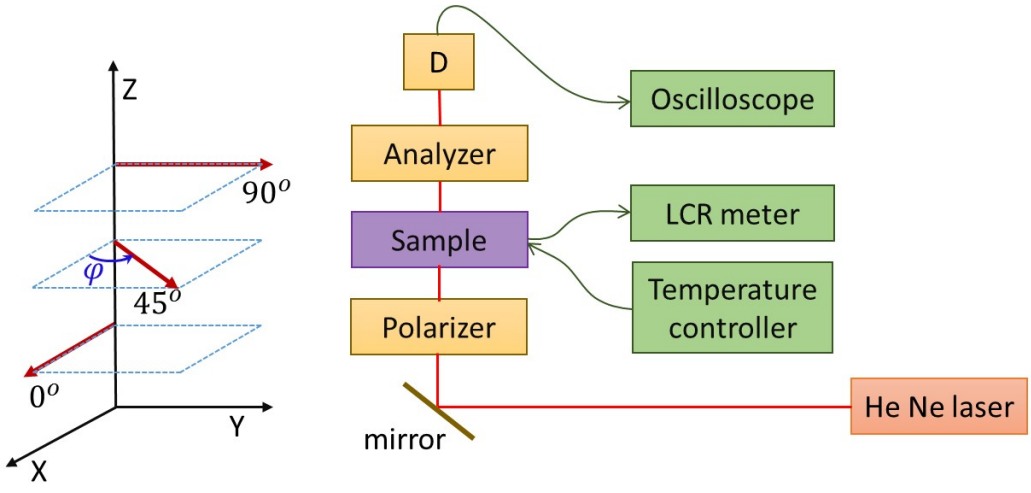

Figure 2.11: Experimental setup for measurement of rotational viscosity.

The equation of motion of the planar aligned cell under an electric field is given by [11, 12]

$$(K_{11}\cos^2\theta + K_{33}\sin^2\theta)\frac{d^2\theta}{dz^2} + (K_{33} - K_{11})\sin\theta\cos\theta\left(\frac{d\theta}{dz}\right)^2 + \varepsilon_o\Delta\varepsilon E^2\sin\theta\cos\theta = \gamma_1\frac{d\theta}{dt} + I\frac{d^2\theta}{dt^2}. \tag{2.53}$$

If the inertial effects and the back flow are ignored, for small angle approximation $\sin\theta \approx \theta$, $\cos\theta \approx 1$ and $K_{11} \approx K_{33}$. We can write

$$K_{11}\frac{d^2\theta}{dz^2} + +\varepsilon_o\Delta\varepsilon E^2\theta = \gamma_1\frac{d\theta}{dt}. \tag{2.54}$$

If the field is swiched off ($E = 0$), then

$$K_{11}\frac{d^2\theta}{dz^2} = \gamma_1\frac{d\theta}{dt}. \tag{2.55}$$

The solution of the above equation is given by

$$\theta(z,t) = \theta_m \sin\left(\frac{\pi z}{d}\right)\exp\left(\frac{-t}{\tau_o}\right). \tag{2.56}$$

where $\tau_o = \gamma_1 d^2/K_{11}\pi^2$ and θ_m is the tilt angle at the center of the cell gap.
The experimental procedure consists of two steps. First we measure voltage dependent transmitted intensity at a fixed temperature. Secondly, measurement of time dependent transmission intensity after the bias (V_b) voltage is switched off.

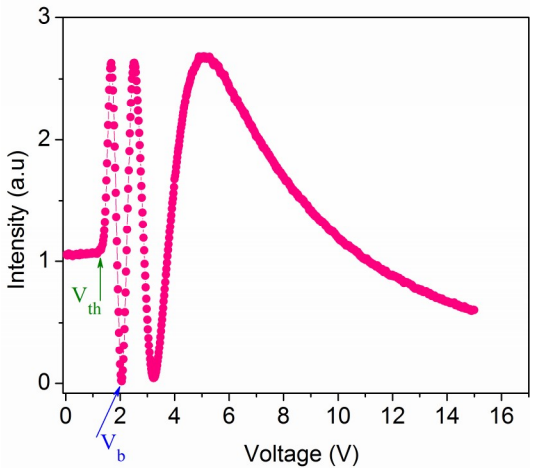

Figure 2.12: A representative voltage dependent transmitted intensity.

A representative variation of voltage dependent transmitted intensity is shown in Fig.2.12. The voltage dependent transmitted intensity has successive maxima and minima. It shows sharp transition at Freedericksz threshold voltage. A small bias voltage (V_b), corresponding to first maxima (minima) is applied and switched off at time $t = 0$. The time dependent transmitted intensity can be calculated using the relation

$$I(t) = I_o\sin^2\{[\Delta_{tot} - \delta(t)]/2\}, \tag{2.57}$$

where I_o is the maximum change in the intensity, Δ_{tot} is the total phase retardation of the LC cell and $\delta(t)$ is the time dependent phase change. The phase decay time of the liquid crystal cell is expressed as [13]

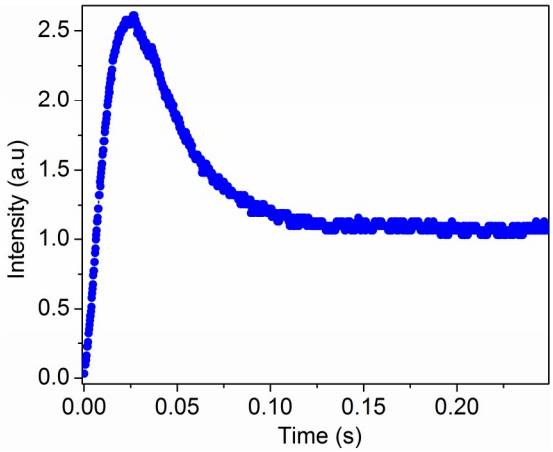

Figure 2.13: A representative time dependent transmitted intensity once the bias $V_b = 0$ voltage is switched off.

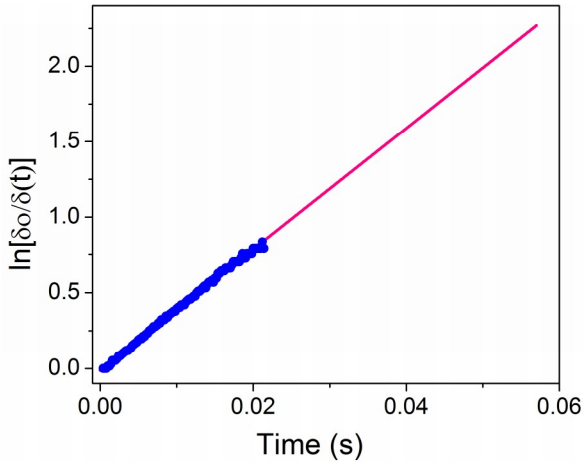

Figure 2.14: A representative linear variation of $ln[\delta_o/\delta(t)]$ with time.

$$\delta(t) = \delta_o \exp(-2t/\tau_o), \tag{2.58}$$

where δ_o is the phase change with and without bias voltage. τ_o is the relaxation time. Here δ_o is equal or close to $(N + 1/2)\pi$ and

$$\delta(t) = \delta_o \exp(-4t/\tau_o), \tag{2.59}$$

if δ_o is equal or close to $N\pi$. Once $\delta(t)$ is obtained, using the plot $ln[\delta_o/\delta(t)]$, relaxation time τ_o is estimated. The representative linear plot $ln[\delta_o/\delta(t)]$ is shown in Fig.2.14. and the rotational viscosity is calculated using the formula

$$\gamma_1 = \frac{\tau_o K_{11} \pi^2}{d^2}. \tag{2.60}$$

References

[1] K. Yang, "Measurements of empty cell gap for liquid-crystal displays using interferometric methods," *Journal of applied physics*, vol. 64, no. 9, pp. 4780–4781, 1988.

[2] T. Scharf, *Polarized light in liquid crystals and polymers*. John Wiley & Sons, 2007.

[3] T. C. Oakberg, "Measurement of low-level strain birefringence in optical elements using a photoelastic modulator," in *International Symposium on Polarization Analysis and Applications to Device Technology*, pp. 17–20, International Society for Optics and Photonics, 1996.

[4] J. C. Kemp, "Basic laboratory setup for various measurements possible with the photoelastic modulator," *Application note*, 1975.

[5] F. C. Frank, "I. liquid crystals. on the theory of liquid crystals," *Discussions of the Faraday Society*, vol. 25, pp. 19–28, 1958.

[6] H. Gruler, T. J. Scheffer, and G. Meier, "Elastic constants of nematic liquid crystals," *Zeitschrift für Naturforschung A*, vol. 27, no. 6, pp. 966–976, 1972.

[7] H. Gruler and G. Meier, "Electric field-induced deformations in oriented liquid crystals of the nematic type," *Molecular Crystals and Liquid Crystals*, vol. 16, no. 4, pp. 299–310, 1972.

[8] H. J. Deuling, "Deformation of nematic liquid crystals in an electric field," *Molecular Crystals and Liquid Crystals*, vol. 19, no. 2, pp. 123–131, 1972.

[9] Y. A. Nastishin, R. D. Polak, S. V. Shiyanovskii, V. H. Bodnar, and O. D. Lavrentovich, "Nematic polar anchoring strength measured by electric field techniques," *Journal of Applied Physics*, vol. 86, no. 8, 1999.

[10] S. T. Wu, "Phase retardation dependent optical response time of parallel-aligned liquid crystals," *Journal of applied physics*, vol. 60, no. 5, pp. 1836–1838, 1986.

[11] J. L. Ericksen, "Conservation laws for liquid crystals," *Transactions of The Society of Rheology (1957-1977)*, vol. 5, no. 1, pp. 23–34, 1961.

[12] F. M. Leslie, "Some constitutive equations for liquid crystals," *Archive for Rational Mechanics and Analysis*, vol. 28, no. 4, pp. 265–283, 1968.

[13] S. T. Wu and C. S. Wu, "Experimental confirmation of the osipov-terentjev theory on the viscosity of nematic liquid crystals," *Physical Review A*, vol. 42, no. 4, p. 2219, 1990.

3

Unusual temperature dependence of elastic constants of an ambient-temperature discotic nematic liquid crystal

3.1 Introduction

Discotic nematic LCs are very useful for wide and symmetrical viewing angle of LCDs and optical compensating film [1]. The physical studies on discotic nematic LCs are meagre compared to the number of compounds have synthesized. So far physical properties of a few discotic nematic liquid crystals have been reported. For example, Heppke *et al.* have measured the dielectric and elastic properties of hexakis ((4-alkylphenyl)ethynyl) benzene [2, 3]. Raghunathan *et al.* and Warmardam *et al.* measured the elastic properties of truxene ester compounds [4, 5]. Mourey *et al.* have reported various physical measurements on the triphenylene hexa (alkoxybenzoate) nematic discotic compounds [6]. In all these compounds the nematic phase appears at higher temperature and not useful for practical application. In 2000, Kumar *et al.* reported first synthesis of room temperature discotic nematic LCs [7, 8]. The range of nematic phase is very wide and the nematic to glass transition occurs much below the ambient temperature. However, so far there is no report on the viscoelastic properties of these compounds. In this chapter we report studies on the birefringence, dielectric

and viscoelastic properties of a discotic nematic LC.

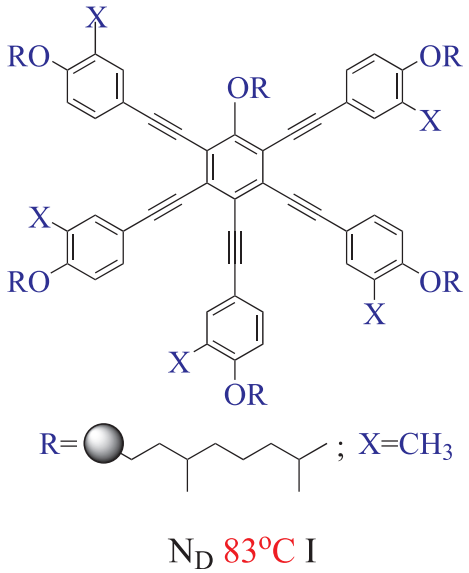

Figure 3.1: Chemical structure and phase transition temperatures of the discotic compound used in the experiment.

3.2 Results and discussions

3.2.1 Sample and alignment behavior

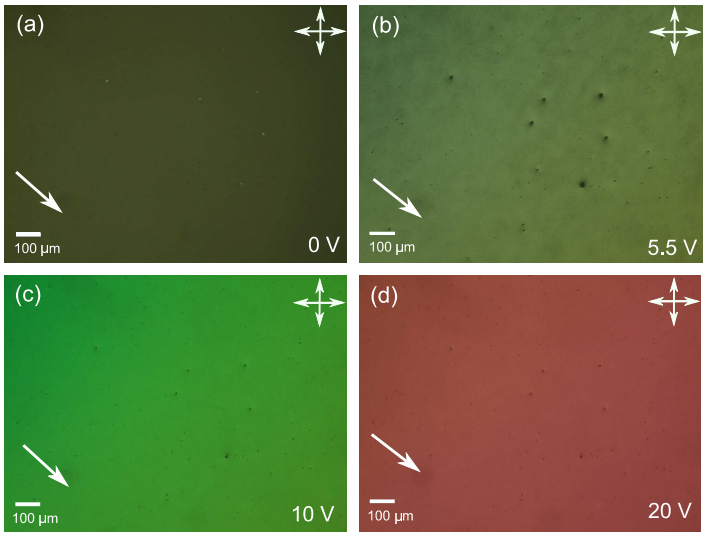

Figure 3.2: Photomicrographs obtained in the homeotropic cell at various voltages using polarising optical microscope. White arrows indicate the rubbing direction.

The chemical structure and the phase transition temperatures of the compound are shown in Fig.3.1. It is a pentaalkylnylbenzene derivative having a combination of

branched and alkoxy chains and exhibit wide temperature range of nematic phase. The compound was synthesized as per the reported procedure [7, 8].
The alignment of the sample was checked using a polarizing optical microscope at various applied voltages and temperatures. Fig.3.2(a) shows typical dark texture where the short axes of the discs are aligned perpendicular to the plane of the substrate. When the applied voltage is greater than Freedericksz threshold voltage, the field of view becomes brighter and the color change indicates increasing retardation with applied voltage (Fig.3.2(a) to Fig.3.2(d)). This suggests that the director is continuously tilting from homeotropic to planar state with increasing voltage. This is expected as the dielectric anisotropy of the material is negative (discussed in the later section).

3.2.2 Optical and dielectric properties

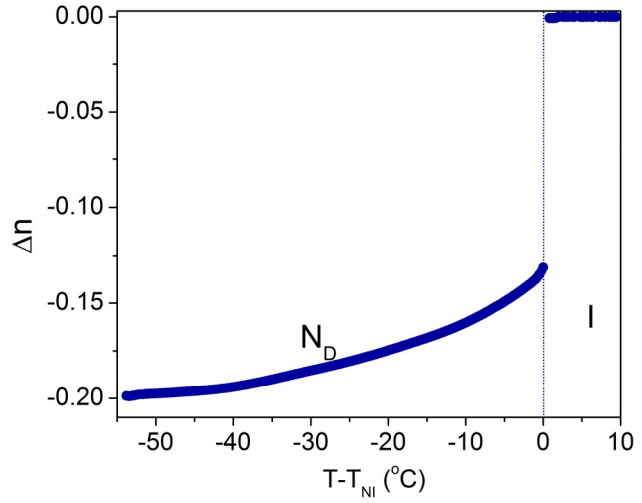

Figure 3.3: Variation of birefringence (Δn) as a function of shifted temperature.

To measure the birefringence (Δn) of the discotic nematic phase (N_D), we first measured the voltage dependent birefringence at room temperature. Beyond the Freedericksz threshold voltage, Δn increases and saturates above 20V. The saturation of Δn indicates planar state of the director. We applied 25V (higher than the saturation voltage) to measure the temperature dependent birefringence of the planar state. The temperature variation of Δn is shown in Fig.3.3. The birefringence is negative i.e., $(n_e - n_o) < 0$ and Δn jumps to ~ -0.13 from zero at the nematic-isotropic (NI) transition and gradually decreased as the temperature is lowered. At room temperature $(T - T_{NI} = -55°\text{C})$ it reaches to approximately -0.2. This is comparable to the other discotic nematic compounds having similar molecular structures [2].
We first studied the dielectric dispersion at various temperature and observed that the parallel component ($\varepsilon_{||}$) does not show any dielectric relaxation whereas the perpendicular component ($\varepsilon_{\perp}$) exhibits dielectric relaxation and the relaxation frequencies

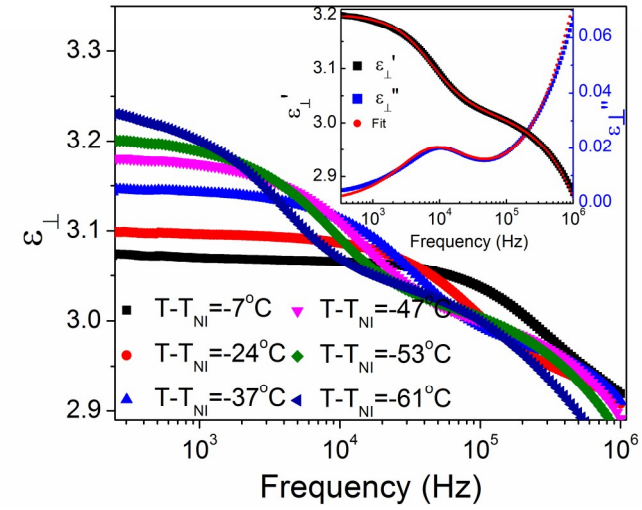

Figure 3.4: The frequency dispersion of real part of perpendicular component ($\varepsilon_\perp$) of dielectric constant at various temperatures. (Inset) Frequency dispersion of real ($\varepsilon'_\perp$) and imaginary ($\varepsilon''_\perp$) part of dielectric constant at $T - T_{NI} = -53$°C. Red colour dots are the theoretical fit to Eq.(3.1).

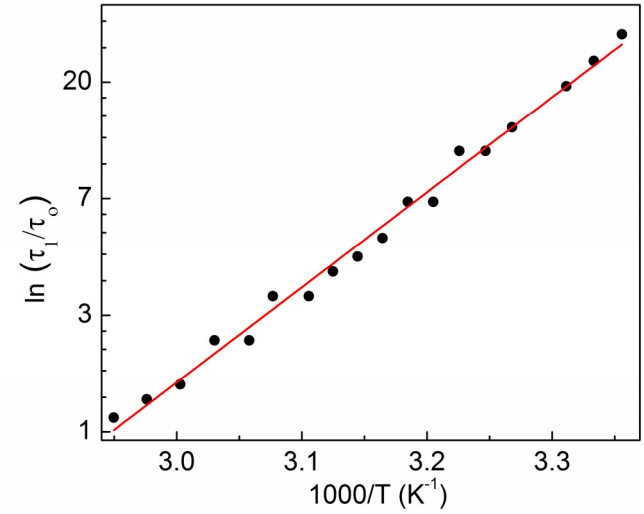

Figure 3.5: Variation of $ln(\tau_1/\tau_0)$ as a function of 1/T. The straight line is the theoretical fit to equation, $\tau_1 = \tau_0 exp(U/RT)$.

varies with temperature in the range 1kHz to 100kHz. The frequency dispersion of real part of perpendicular component ($\varepsilon_\perp$) of dielectric constant at various temperatures is shown in Fig.3.4. There are two dielectric relaxations in the perpendicular component of the dielectric constant with variation of temperature. One in common (above $\sim$ 1MHz frequency), even present in the empty cell and temperature independent, arises due to finite resistance of the ITO plates. Interstingly, another relaxation is temperature dependent (below $\sim$ 1MHz), where the relaxation frequency decreases with decreasing temperature. Red colour dots are the theoretical fit to Eq.(3.1) is shown in (inset) Fig.3.4. The dielectric relaxations present in the frequency dispersion of $\varepsilon_\perp(f)$ are fitted with complex dielectric constant ($\varepsilon(w)^* = \varepsilon'(w) - i\varepsilon''(w)$) and is given by the Eq.(3.1)

$$\varepsilon(w)^* = \varepsilon_2 + \frac{\varepsilon_0 - \varepsilon_1}{1 + (iw\tau_1)^{1-\alpha_1}} + \frac{\varepsilon_1 - \varepsilon_2}{1 + (iw\tau_2)^{1-\alpha_2}}, \tag{3.1}$$

Where ε_0 is the static dielectric permittivity, ε_i and τ_i are the dielectric limits and relaxation times of i^{th} mode. α_i is the cole cole distribution parameter of the respective mode. It is found that the parameters α_1 and α_2 having values between 0 and 0.2 at all temperatures and τ_2 is independent of temperature as expected. The temperature dependent relaxation time τ_1 varies linearly with the inverse temperature (Fig.3.5) and can be fitted well with the Arrhenius equation, $\tau_1 = \tau_0 exp(U/RT)$. The corresponding activation energy U = 57.78 kJmol^{-1}. Here, no electro convection is observed in the applied voltage and frequency range.

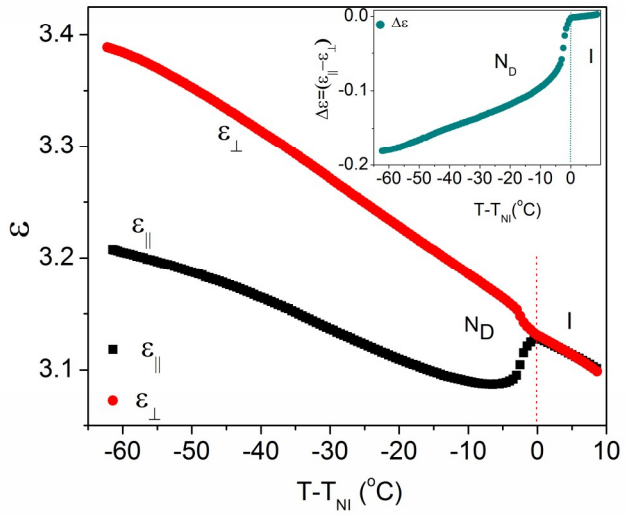

Figure 3.6: Variation of parallel ($\varepsilon_{||}$) and perpendicular ($\varepsilon_\perp$) component of dielectric constant as a function of shifted temperature. (Inset) Variation of dielectric anisotropy ($\Delta\varepsilon$) as a function of shifted temperature.

The dielectric constants were measured at a frequency, (411 Hz) away from the relaxation frequency. The variation of $\varepsilon_{||}$ and $\varepsilon_\perp$ as a function of temperature is shown

in Fig.3.6. Both the dielectric constants increase with decreasing temperature. In the N_D phase, the dielectric anisotropy ($\Delta\varepsilon = \varepsilon_{||} - \varepsilon_{\perp}$) is very small and negative ($\Delta\varepsilon \simeq -0.18$ at $T - T_{NI} = -60°$C). This is expected as the permanent dipoles are mostly confined in the plane of the disc molecules (see Fig.3.1).

3.2.3 Splay (K_{11}) and bend (K_{33}) elastic constants

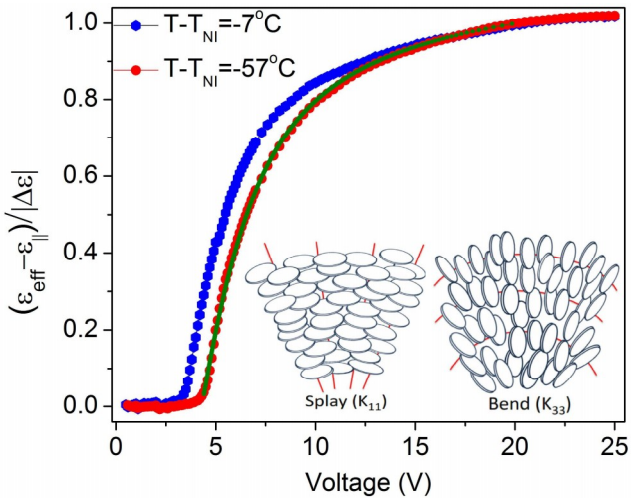

Figure 3.7: Variation of the normalised dielectric constant $(\varepsilon_{eff} - \varepsilon_{||})/\Delta\varepsilon$ at two representative temperatures. The continuous line is the best fit with the theoretical Eq.(2.41) and Eq.(2.52). (Inset) Schmatic representation of splay and bend distortions of the discotic nematic liquid crystal.

To obtain splay (K_{11}) and bend (K_{33}) elastic constants, we measured voltage dependent dielectric constant, $\varepsilon_{eff}(V)$ at various temperatures in the N_D phase. The variations of normalised dielectric constant at two representative temperatures are shown in Fig.3.7. It is clearly observed that the threshold voltage is increasing with decreasing temperature. The detailed procedure of measurement of K_{11} and K_{33} is discussed in chapter-2. The temperature variations of K_{11} and K_{33} are shown in Fig.3.8. They have the same order of magnitude as that of many calamitic liquid crystals but $K_{11} > K_{33}$ at all temperatures and they show very different temperature dependence. As the temperature is reduced from NI transition point, both the elastic constants increase but K_{11} increases more rapidly than K_{33}. Below $T - T_{NI} = -45°$C, K_{11} saturates whereas K_{33} shows rapid increase with decreasing temperature.
The temperature variation of K_{11}/K_{33} is also shown in the Fig.3.9. It is observed that the ratio increases as the temperature decreases and reaches a maximum around $T - T_{NI} = -40°$C. Below this, it reduces rapidly as the room temperature is approached. To gain more insight on the relationship between the order parameter and the elastic constants, we plotted variations of K_{33} and K_{11} with Δn (near NI transi-

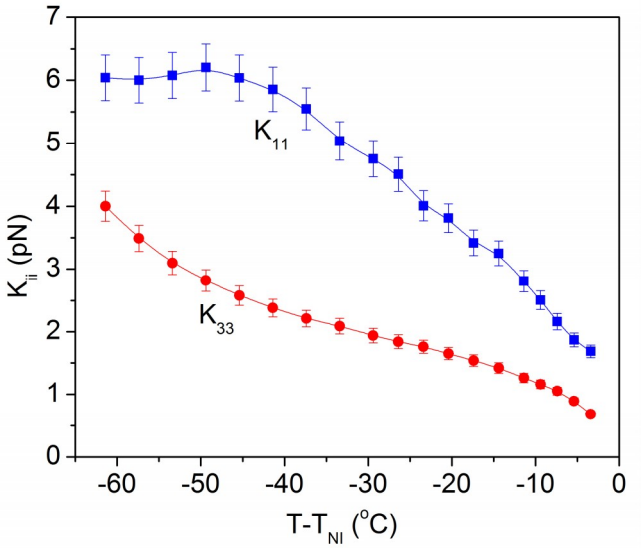

Figure 3.8: Variation of splay (K_{11}) and bend (K_{33}) elastic constants as a function of shifted temperature.

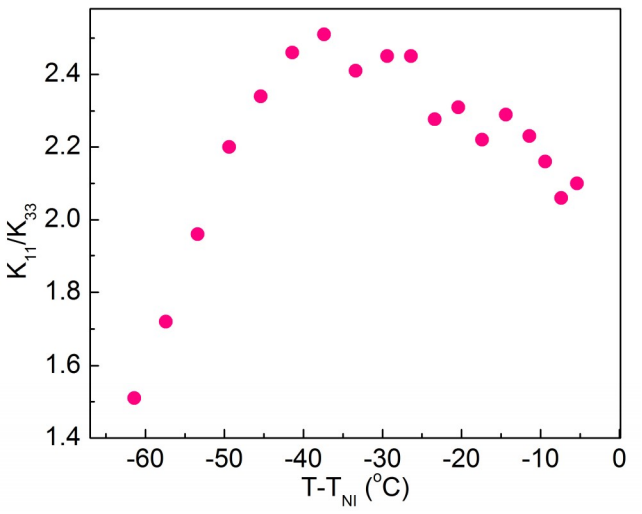

Figure 3.9: Variation of the ratio of K_{11}/K_{33} with temperature.

tion), according to the Mean field, $K_{ii} \propto S^2 \propto \Delta n^2$, where S is the order parameter [9]. The experimental data is fitted with $K_{ii} \propto \Delta n^x$, where x is the fit parameter (Fig.3.10). Interestingly, it is observed that for $K_{33} \propto \Delta n^{1.1}$, and $K_{11} \propto \Delta n^{4.1}$ respectively. Thus, both K_{11}, and K_{33} exhibit significant deviation from the mean field prediction.

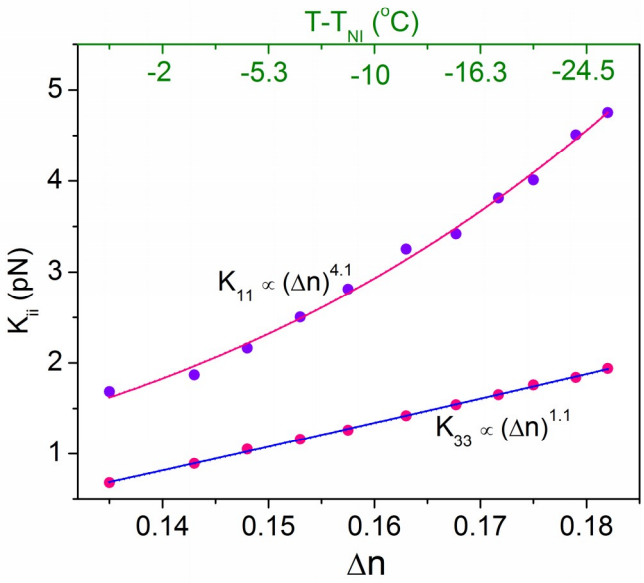

Figure 3.10: Variation of (K_{11}) and (K_{33}) with Δn. Corresponding temperature range is also shown in the upper abscissa. Continuous lines are the best fit to the equation $K_{ii} \propto \Delta n^x$.

There are a very few reports on the temperature dependence of splay and bend elastic constants of the N_D phase. Sokalski *et al.* theoretically predicted that for discotic nematic with long-range orientational order, $K_{11}/K_{33} > 1$ [10]. This has been experimentally verified by a couple of experiments. For example, Heppke *et al.* have measured both the splay and bend elastic constants of a homologous series of non-polar nematic discotic compounds showing I to N_D transition [2, 3]. They reported that in most of the compounds $K_{11}/K_{33} > 1$. Warmardam *et al.* measured the elastic constants of two discotic compounds with polar molecules [5]. In addition to N_D phase these compounds also exhibit two columnar phases. They reported that in the N_D phase, $K_{11}/K_{33} > 1$. Raghunathan *et al.* measured the elastic properties of truxene compounds and found that $K_{11}/K_{33} < 1$ [4]. In their compounds the nematic phase appeared between two discotic columnar phases and it was attributed to the short-rage columnar order. Phillips *et al.* studied the elastic properties of triphenylene discotic nematic liquid crystals [11]. These compounds exhibit I to N_D phase transition. They found that the ratio, K_{11}/K_{33} is very high ($\simeq 5$) and decreases ($\simeq 3$) as the temperature is decreased [11]. It has been reported that three types of discotic nematic can be envisaged based on the local organization of the disc-like molecules and they are

known as N_D, N_{col} and N_L. In the N_{col} and N_L phases there is a short-range columnar order and short-range 2D lattice respectively [12]. The effect of short-range columnar order in the discotic nematic has also been studied by computer simulation [13]. It was reported that the onset of growth in orientational order in the parent phase is found to induce translational order, arising from short-range columnar structures.

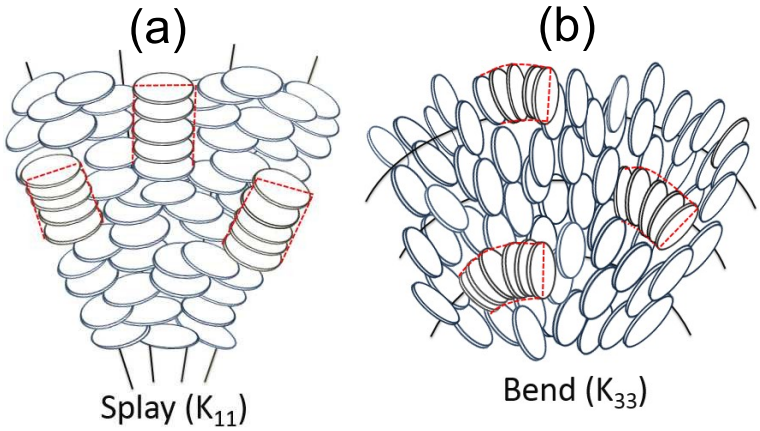

Figure 3.11: Splay (K_{11}) and bend (K_{33}) distortions in a discotic nematic liquid crystal. Columnar short range order of the disc molecules is shown using dotted red lines.

We gave simple explanation for the splay and bend elastic constants based on the short range columnar interaction. A short range columnar interaction does not prevent the splay distortion hence splay elastic constant does not changed significantly. On the other side short range columnar order increases the bend stress as it is energetically unfavorable to bend the columns. This leads to rapid increase in K_{33} over K_{11} and may lead to crossover at much lower temperature with the growth of orientational order. The elastic properties at higher temperature are due to the long-range orientational order. The short range columnar order increases as the temperature is decreased and the elastic constants show unusual temperature dependence.

3.2.4 Rotational viscosity

In this section we discuss the rotational viscosity of the discotic nematic LC. Rotational viscosity is measured by the phase decay time measurement technique. The detailed procedure is given in the experimental section (chapter-2). We measured the rotational viscosity (γ_1) of the N_D phase as a function of temperature. The normalized transmission intensity at various temperatures is shown in Fig.3.12. It is observed that at lower temperature (e.g., $T - T_{NI} = -57.4°C$) it (intensity) takes about 200s to decay to zero value. A representative variation of $ln[\delta_o/\delta(t)]$ with time (t) of experimental data at a shifted temperature together with the best fit is shown in (inset) Fig.3.12. Rotational viscosity γ_1 increases very rapidly with decreasing temperature Fig.3.13. For example, near the NI transition $\gamma_1 = 0.1$ Pa s and it increases to about

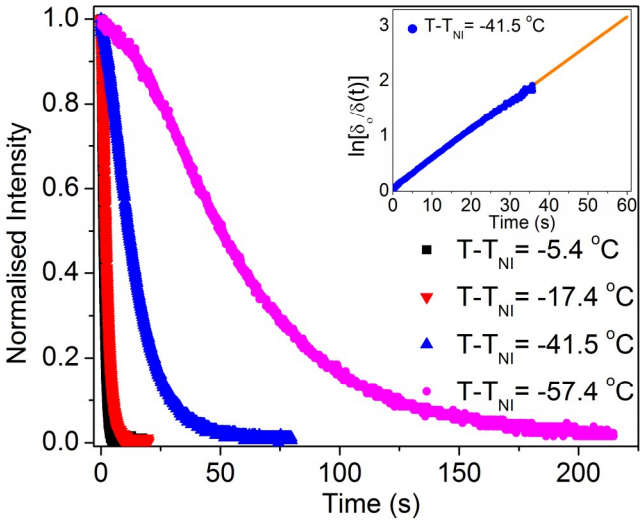

Figure 3.12: Time dependent normalized transmitted intensity after the removal of bias voltage (V_b) for various temperatures. (Inset) Variation of $ln[\delta_o/\delta(t)]$ with time at $T - T_{NI} = -41.5$°C.

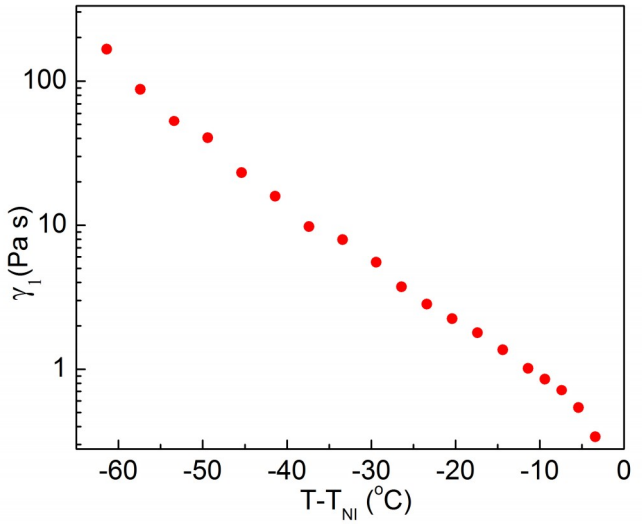

Figure 3.13: Variation of rotational viscosity (γ_1) as a function of temperature.

200 Pa s at room temperature. The direct value of γ_1 of discotic nematic has not been reported before us. Warmerdam *et al.* directly measured the temperature dependence of $\gamma_1/\Delta\chi$, where $\Delta\chi$ is the diamagnetic susceptibility anisotropy [14]. By taking a typical value of $\Delta\chi$, they estimated that γ_1 for discotic nematic is about 10 to 100 times larger compared to the rod-like mesogens. In the present compound it is about three orders of magnitude larger than conventional calamitic liquid crystals. It could be due to short range columnar order and due to the effect of glass transition below the room temperature. In this sample glass transition was reported much below the room temperature [7].

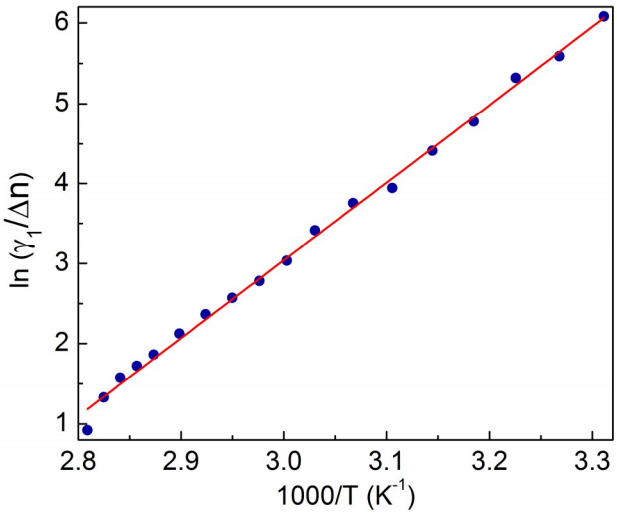

Figure 3.14: A linear variation of $ln(\gamma_1/\Delta n)$ with $1/T$

The rotational viscosity can be written as $\gamma_1 \propto Sexp(W/k_BT)$, where S is the order parameter and k_B is the Boltzmann constant [15]. Since $S \propto \Delta n$, we show variation of the $ln(\gamma_1/\Delta n)$ with $1/T$ in the inset of Fig.3.14. The estimated activation energy is about 837 meV, which is about double compared to the values known in conventional calamitic liquid crystals [16].

3.3 Conclusions

In conclusion, we measured birefringence, dielectric, curvature elastic constants and rotational viscosity of a discotic nematic liquid crystal with wide nematic temperature range. Both the birefringence and the dielectric anisotropy are negative. Near the NI transition, K_{11} and K_{33} exhibit quartic and linear variation with temperature respectively. This is not in accordance with the Mean field prediction. As the ambient temperature is approached the elastic constants show unusual temperature dependence. The rotational viscosity is three orders of magnitude high at the room temperature and the corresponding activation energy is more than double compared to conventional calamitic mesogens. These results suggest that viscoelastic properties

at the ambient temperature are influenced by the short-range columnar order.

References

[1] H. Mori, "Novel optical compensators of negative birefringence for wide-viewing-angle twisted-nematic liquid-crystal displays," *Japanese journal of applied physics*, vol. 36, no. 3R, p. 1068, 1997.

[2] G. Heppke, H. Kitzerow, F. Oestreicher, S. Quentel, and A. Ranft, "Electrooptic effect in a non-polar nematic discotic liquid crystal," *Molecular Crystals and Liquid Crystals Letters*, vol. 6, no. 3, pp. 71–79, 1988.

[3] G. Heppke, A. Ranft, and B. Sabaschus, "Bend and splay elastic constants of some discotic nematic compounds," *Molecular Crystals and Liquid Crystals Letters*, vol. 8, no. 1, pp. 17–25, 1991.

[4] V. Raghunathan, N. Madhusudana, S. Chandrasekhar, and C. Destrade, "Bend and splay elastic constants of a discotic nematic," *Molecular Crystals and Liquid Crystals*, vol. 148, no. 1, pp. 77–83, 1987.

[5] T. Warmerdam, D. Frenkel, and R. Zijlstra, "Measurements of the ratio of the frank constants for splay and bend in nematics of disc-like molecules," *Journal de physique*, vol. 48, no. 2, pp. 319–324, 1987.

[6] B. Mourey, J. Perbet, M. Hareng, and S. L. Berre, "Physical parameters of a fluid discotic mesophase," *Molecular Crystals and Liquid Crystals*, vol. 84, no. 1, pp. 193–199, 1982.

[7] S. Kumar and S. K. Varshney, "A room-temperature discotic nematic liquid crystal," *Angewandte Chemie*, vol. 112, no. 17, pp. 3270–3272, 2000.

[8] S. Kumar, S. K. Varshney, and D. Chauhan, "Room-temperature discotic nematic liquid crystals," *Molecular Crystals and Liquid Crystals*, vol. 396, no. 1, pp. 241–250, 2003.

[9] P. G. de Gennes and J. Prost, *The Physics of Liquid Crystals*. International Series of Monographs on Physics, Clarendon Press, 1995.

[10] K. Sokalski and T. W. Ruijgrok, "Elastic constants for liquid crystals of disc-like molecules," *Physica A: Statistical Mechanics and its Applications*, vol. 113, no. 1, pp. 126–132, 1982.

[11] T. Phillips, J. Jones, and D. McDonnell, "On the influence of short range order upon the physical properties of triphenylene nematic discogens," *Liquid Crystals*, vol. 15, no. 2, pp. 203–215, 1993.

[12] P. H. Kouwer, W. F. Jager, W. J. Mijs, and S. J. Picken, "The nematic lateral phase: A novel phase in discotic supramolecular assemblies," *Macromolecules*, vol. 34, no. 22, pp. 7582–7584, 2001.

[13] D. Chakrabarti and D. J. Wales, "Energy landscape of a model discotic liquid crystal," *Physical Review E*, vol. 77, no. 5, p. 051709, 2008.

[14] T. Warmerdam, R. Zijlstra, and D. Frenkel, "Dynamics of the frederiks transition in nematics consisting of disc-like molecules thermal dependence of a bend viscosity coefficient," *Liquid crystals*, vol. 3, no. 8, pp. 1105–1114, 1988.

[15] D. V. Sai, K. Zuhail, R. Sarkar, and S. Dhara, "Structure–property correlation of bicyclohexane nematic liquid crystals," *Liquid Crystals*, vol. 42, no. 3, pp. 328–333, 2015.

[16] M. Dark, M. Moore, D. Shenoy, and R. Shashidhar, "Rotational viscosity and molecular structure of nematic liquid crystals," *Liquid crystals*, vol. 33, no. 1, pp. 67–73, 2006.

4

Experimental studies on the phase diagram and physical properties of mixture of calamitic and discotic nematic liquid crystals

4.1 Introduction

In the previous chapter we studied various physical properties of a room temperature discotic LC. This discotic LC showed unusual temperature dependence of physical properties in comparision to calamitic LCs. Liquid crystals (LCs) used in display devices are mostly the calamitic nematic, which are composed of rod-shaped molecules. For a desired electro-optic response, the physical properties are required to be optimised, and that is usually achieved in the mixture of several single component liquid crystals. Here we concentrate on the studies of mixture of a calamitic and a discotic nematic liquid crystals, which are interesting from several aspects. First, they have the opposite sign of the birefringence and dielectric anisotropy, which makes it possible to tune the electro-optic response and elasticity. Second, there may be a region of immiscibility of rod-like and disk-like nematics, resulting in a liquid dispersion of one phase in another. This should result in a dispersion of microdroplets of one liquid crystal phase in another liquid crystal phase, which could be of great interest for applications in topological microphotonics [1] and for the fundamental studies of topology in liquid

crystals. In such a liquid crystal-liquid crystal dispersion, individual nematic droplets might function as tunable optical microcavities [2, 3] and microlasers [4], which could be elastically bound by topological defects [5, 6] of the other nematic carrier fluid (continuous phase). Third, immiscible liquid crystalline phases could provide a novel testbed for studying topological defects in both phases, as well as their interrelation across the interfaces. Understanding and tailoring of mixtures of rod-like and disc-like nematic materials is therefore not only of high interest, but could also lead to new research directions. There are a very few reports on the phase diagram and physical properties of mixture of calamitic and discotic nematic liquid crystals. For example, Pratibha *et al.* experimentally studied the phase diagram and defect structure in the binary mixture of a calamitic and a discotic nematic LCs [7, 8]. Apreutesei *et al.* experimentally showed a complete miscibility of disc-like and rod-like compounds [9]. Andrzej *et al.* theoretically studied the elastic constants in the binary mixture and reported a discontinuous change of elastic anisotropy from disc-like to rod-like properties [10]. A possibility of getting biaxial nematic and smectic phases in such binary systems was discussed by G J Vroege [11]. Recently, Parthasarathi *et al.* measured several physical properties of binary mixtures of a calamitic and a columnar discotic liquid crystals [12]. They also observed an anchoring transition driven by short-range ordering in the calamitic-discotic composites. In the above mentioned reports (experimental), the compounds studied exhibit nematic phase above the ambient temperature. To the best of our knowledge, there are no reports on the phase behaviour and physical studies on the mixture of ambient temperature discotic and calamitic nematic LCs. In this chapter, we report experimental studies on the phase diagram, and physical properties such as birefringence, dielectric anisotropy, curvature elastic constants and rotational viscosity of the mixture of a calamitic and a room temperature discotic nematic liquid crystals.

4.2 Results and discussions

4.2.1 Samples and phase behavior

The sample E-18 (a room temperature calamitic nematic mixture) exhibits the following phase transitions: Cr. 10°C N 60°C I. The discotic nematic was synthesised in our laboratory (Fig.4.1(a)) and it has the following phase transitions: N 83°C I. It also exhibits a glass transition much below the room temperature [13, 14]. We prepared three different mixtures with increasing concentration of discotic compound, namely; E-18+disc(2.5 wt%), E-18+disc(5 wt%), E-18+disc(7.5 wt%). Physical appearance of the mixtures is shown in Fig.4.1(b) and the phase diagram is shown in Fig.4.2. From turbid and white, it becomes brownish in colour with increasing wt% of discotic compound. In pure E-18, there exists an isotropic-nematic coexistence (I+N) range

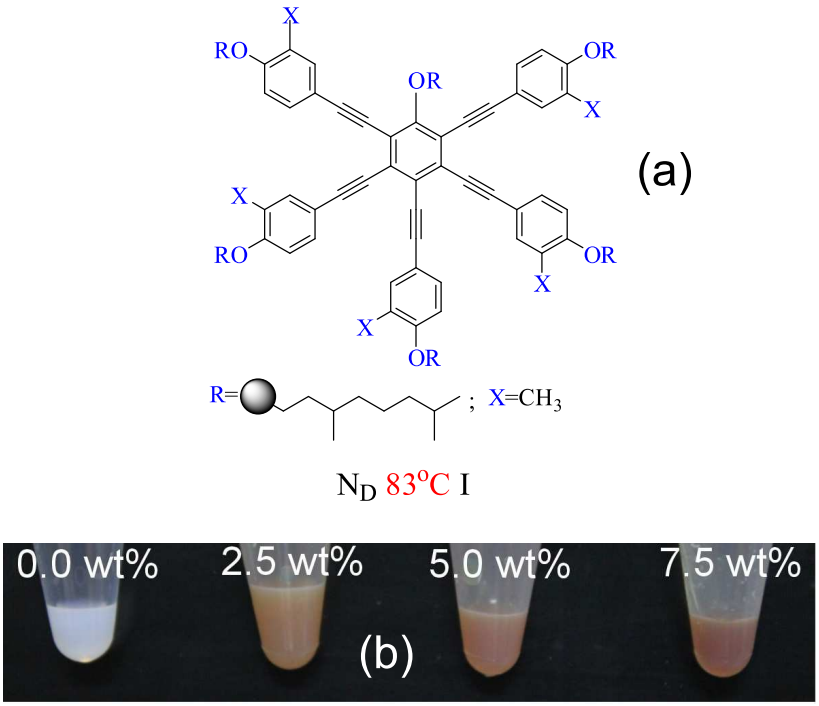

Figure 4.1: (a) Chemical structure of the discotic molecule. (b) Physical appearance of the samples with increasing wt% of the discotic compound in E-18.

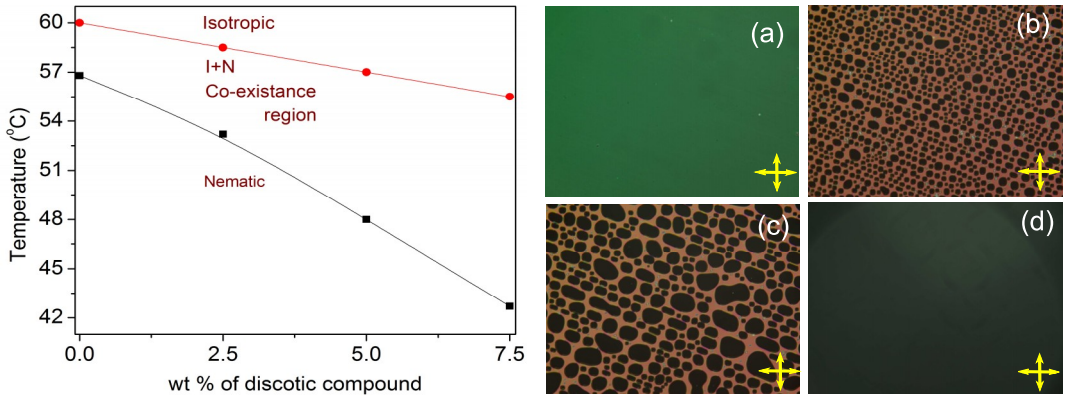

Figure 4.2: Phase diagram of the E18 + discotic mixtures with increaing wt% of discotic compound. The transition temperatures are measured while heating the samples from the room temperature. Few representative photomicographs at temperatures (a) 30°C, (b) 47°C, (c) 50°C and (d) 60°C of E18 + 7.5 wt% sample.

of approximately 3°C and this range increases with increasing wt% of discotic compound. In case of mixture with 7.5 wt% discotic compound, while cooling, the I+N coexistence range exists nearly up to 30°C. Below this temperature, it exhibits a monodomain (no coexistence) nematic sample. During heating, the coexistence reappears at 43°C. Thus, larger temperature range of monodomain nematic is obtained during heating. Hence we performed all the measurements while heating and the physical measurements in the I+N coexistence region are excluded.

4.2.2 Optical and dielectric properties

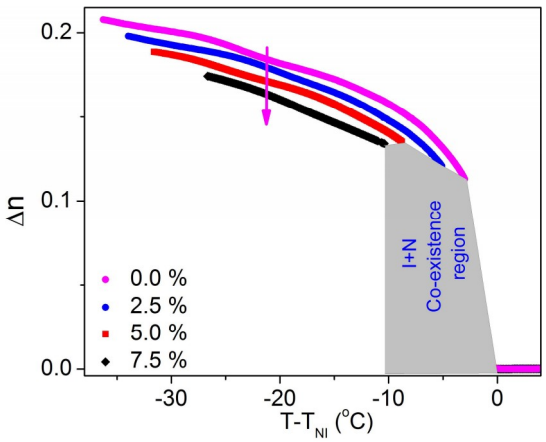

Figure 4.3: Variation of birefringence (Δn) as a function of shifted temperature. The shaded region indicates the nematic-isotropic (N+I) coexistence range. The downward arrow indicates the decrease of Δn with increasing wt% of the discotic compound.

The temperature variation of birefringence (Δn) of E-18 and various mixtures is shown in Fig.4.3. The birefringence of E-18 is large and positive whereas in discotic nematic it is large but negative. For example, at room temperature, in E-18, $\Delta n \sim 0.21$ and this is consistent with the previous measurements [15]. In pure discotic nematic, at room temperature, Δn is negative and large ($\Delta n \sim -0.2$) [16]. In the mixtures, Δn decreases with increasing wt% of discotic compound. For example, at a fixed temperature (e.g., $T - T_{NI} = -26$°C), Δn of the mixture (E-18 + 7.5 wt%) decreases by 13% compared to the pure E-18. This suggests that the mutual orientation of the rod and disc-like molecules is such that the polarisability anisotropies are antithetically related.

The variation of dielectric anisotropy ($\Delta\varepsilon$) of various mixtures as a function of shifted temperature is shown in Fig.4.4. In pure E-18, $\Delta\varepsilon$ is positive and relatively large whereas in discotic nematic it is small and negative [16]. For example, at room temperature in E-18, $\Delta\varepsilon = 13.5$ and in pure discotic nematic, $\Delta\varepsilon = -0.18$ [16]. It is observed that $\Delta\varepsilon$ decreases with increasing wt% of discotic compound. For example, at a fixed temperature ($T - T_{NI} = -30.5$°C), $\Delta\varepsilon$ of the mixture, E-18 + 7.5 wt%

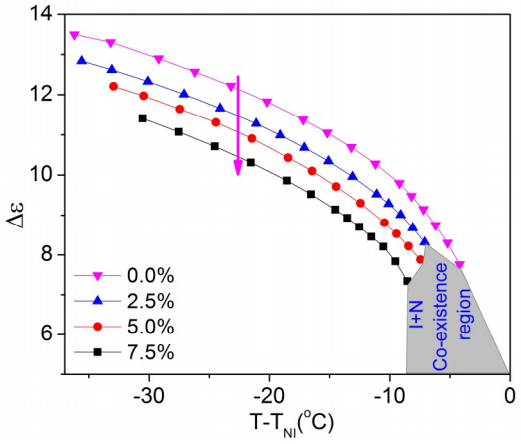

Figure 4.4: Variation of dielectric anisotropy ($\Delta\varepsilon$) as a function of shifted temperature. Continuous lines are drawn as a guide to the eye. The shaded region indicates the nematic-isotropic (N+I) coexistence range. The downward arrow indicates the decrease of $\Delta\varepsilon$ with increasing wt% of the discotic compound.

decreases by 12% compared to the pure E-18. Though $\Delta\varepsilon$ of pure discotic compound is very small and negative, it has a significant contribution in reducing the dielectric anisotropy of the mixtures.

4.2.3 Splay (K_{11}) and bend (K_{33}) elastic constants

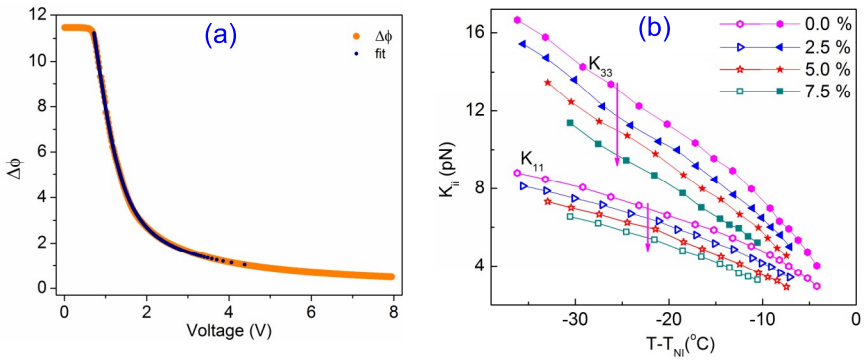

Figure 4.5: (a) Experimental variation of retardation along with the best fit to the theoretical Eq.(2.41) and Eq.(2.46) as a function of voltage of E18 + 5wt% mixture at $T - T_{NI} = -14.5$°C. (b) Variation of splay (K_{11}) and bend (K_{33}) elastic constants of the mixtures as a function of shifted temperature. Continuous lines are drawn as a guide to the eye. The downward arrows indicate the decrease of the respective quantities with increasing wt% of the discotic compound.

The optical phase difference ($\Delta\Phi$) of the samples was measured as a function of applied

voltage to measure splay (K_{11}) and bend elastic constants (K_{33}) simultaneously. The temperature variation of K_{11} and K_{33} is shown in Fig.4.5(b). K_{33} is always greater than K_{11} and both the elastic constants decrease with increasing wt% of discotic compound. At room temperature, ($T - T_{NI} = -30°C$), K_{11} and K_{33} decreases by 25% and 30%, respectively. According to the mean-field theory, $K_{ii} \propto S^2 \propto \Delta n^2$. Since Δn decreases by about 13% (see Fig.4.2), the decrease of the elastic constants is consistent with the prediction of the mean-field theory. However, it may be noted that the relative decrease of K_{33} is slightly larger (about 5%) than K_{11}. This is due to the fact, that in pure discotic nematic, the elastic anisotropy is negative i.e., K_{33} is less than K_{11} [16], and this is opposite to the behaviour observed in pure E-18.

4.2.4 Rotational viscosity and proposed orientation

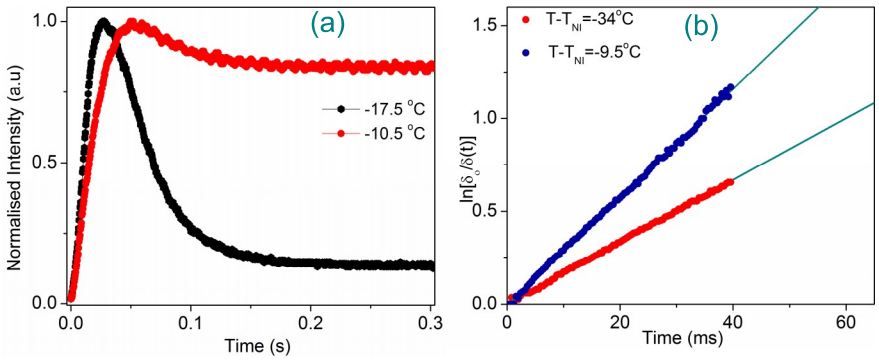

Figure 4.6: (a) Time dependent normalised intensity at two representative temperatures after removal of bias voltage (V_b) of E18 + 5 wt% mixture. (b) Linear variation of $ln[\delta_o/\delta(t)]$ with time at two representative temperatures of E18 + 5 wt% mixture.

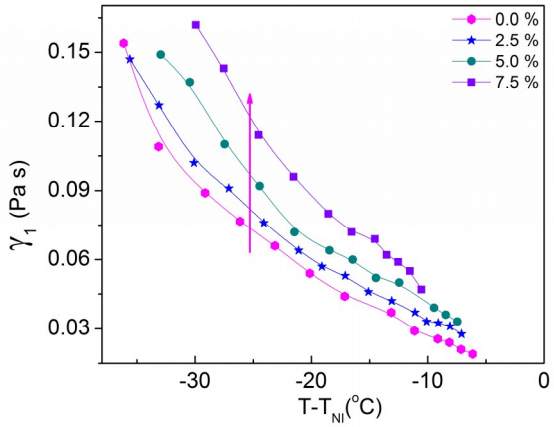

Figure 4.7: Variation of rotational viscosity (γ_1) of the mixtures as a function of temperature. The upward arrow indicates the increase of γ_1 with increasing wt% of the discotic compound.

We also measured the rotational viscosity (γ_1) of the mixtures with temperature (see Fig.4.7). γ_1 increases with increasing wt% of the discotic compound. For example, near the room temperature ($T - T_{NI} = -30°C$), γ_1 of the mixture, E-18 + 7.5 wt% is 73% larger than that of the pure E-18. The rotational viscosity is given by: $\gamma_1 = \tau_o K_{11}\pi^2/d^2$, where d is the sample thickness and τ_o is the relaxation time. In the mixtures, γ_1 increases significantly in spite of the decrease of K_{11}. So the increase of γ_1 is mainly due to the increase of relaxation time of the system. This is expected as the relaxation time of the pure discotic nematic is very large [16]. The birefringence, dielectric anisotropy and the elastic properties clearly suggest that the plane of the disc molecules is parallel to the director as shown schematically in Fig.4.8.

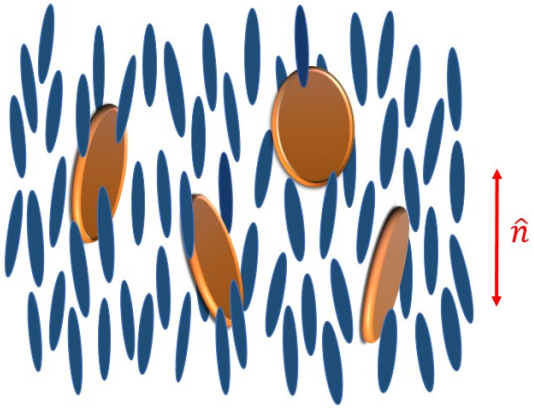

Figure 4.8: Schematic representation of mutual orientation of rod-like and disc-like molecules in the nematic phase.

4.3 Conclusions

In conclusion, we have determined the phase diagram, and measured several physical properties such as birefringence, dielectric anisotropy, curvature elastic constants and the rotational viscosity of mixture of E-18 and a discotic nematic liquid crystals. We find rather broad temperature range of coexistence of the isotropic and nematic phases. The temperature range of nematic-isotropic coexistence increases with increasing wt% of discotic nematic compound. At room temperature, with a small (7.5 wt%) addition of discotic compound, the birefringence and dielectric anisotropy decreases by about 13%. The splay and bend elastic constants decrease by 25% and 30% respectively. On the other hand rotational viscosity increases by about 73%. We have shown that the physical properties of the calamitic nematic liquid crystals can be changed significantly by adding a small amount of discotic nematic compound. This is therefore a very efficient method of tuning the electro-optic parameters of nematic mixtures. The experimental results suggest that the planes of the disc-like molecules are oriented parallel to the nematic director. Future studies should focus on the high concentration

range of discotic component in the phase diagram (Fig.4.2), where a coexistence region of two immiscible nematic phases was observed in preliminary experiments above 10 wt% of discotic component.

References

[1] I. Muševič, "Liquid-crystal micro-photonics," *Liquid Crystals Reviews*, vol. 4, no. 1, pp. 1–34, 2016.

[2] M. Humar, M. Ravnik, S. Pajk, and I. Muševič, "Electrically tunable liquid crystal optical microresonators," *Nature Photonics*, vol. 3, no. 10, pp. 595–600, 2009.

[3] M. Humar and I. Muševič, "Surfactant sensing based on whispering-gallery-mode lasing in liquid-crystal microdroplets," *Optics express*, vol. 19, no. 21, pp. 19836–19844, 2011.

[4] M. Humar and I. Muševič, "3d microlasers from self-assembled cholesteric liquid-crystal microdroplets," *Optics express*, vol. 18, no. 26, pp. 26995–27003, 2010.

[5] I. Muševič, M. Škarabot, U. Tkalec, M. Ravnik, and S. Žumer, "Two-dimensional nematic colloidal crystals self-assembled by topological defects," *Science*, vol. 313, no. 5789, pp. 954–958, 2006.

[6] A. Nych, U. Ognysta, M. Škarabot, M. Ravnik, S. Žumer, and I. Muševič, "Assembly and control of 3d nematic dipolar colloidal crystals," *Nature communications*, vol. 4, p. 1489, 2013.

[7] R. Pratibha and N. V. Madhusudana, "Evidence for two coexisting nematic phases in mixtures of rod-like and disc-like nematogens," *Molecular Crystals and Liquid Crystals Letters*, vol. 1, no. 3-4, pp. 111–116, 1985.

[8] R. Pratibha and N. V. Madhusudana, "On the occurrence of point and ring defects in the nematic-nematic coexistence range of a binary mixture of rod-like and disc-like mesogens," *Molecular crystals and liquid crystals*, vol. 178, no. 1, pp. 167–178, 1990.

[9] D. Apreutesei and G. H. Mehl, "Completely miscible disc and rod shaped molecules in the nematic phase," *Chemical communications*, no. 6, pp. 609–611, 2006.

[10] A. Kapanowski and K. Sokalski, "Elastic constants of binary mixtures of uniaxial nematic liquid crystals," *Molecular Crystals and Liquid Crystals*, vol. 301, no. 1, pp. 431–436, 1997.

[11] G. J. Vroege, "Biaxial phases in mineral liquid crystals," *Liquid Crystals*, vol. 41, no. 3, pp. 342–352, 2014.

[12] S. Parthasarathi, D. S. S. Rao, H. K. Singh, B. Singh, and S. K. Prasad, "Anchoring transition driven by short range ordering in calamitic-discotic composites," *Thermochimica Acta*, vol. 616, pp. 61–68, 2015.

[13] S. Kumar and S. K. Varshney, "A room-temperature discotic nematic liquid crystal," *Angewandte Chemie*, vol. 112, no. 17, pp. 3270–3272, 2000.

[14] S. Kumar, S. K. Varshney, and D. Chauhan, "Room-temperature discotic nematic liquid crystals," *Molecular Crystals and Liquid Crystals*, vol. 396, no. 1, pp. 241–250, 2003.

[15] A. Miyaji, H. Mada, and S. Kobyashi, "Optical properties of 90 twisted nematic liquid crystal displays; estimation by colorimetry," *Molecular Crystals and Liquid Crystals*, vol. 74, no. 1, pp. 121–135, 1981.

[16] D. V. Sai, G. Mirri, P. H. J. Kouwer, R. Sahoo, I. Musevic, and S. Dhara, "Unusual temperature dependence of elastic constants of an ambient-temperature discotic nematic liquid crystal," *Soft matter*, vol. 12, no. 11, pp. 2960–2964, 2016.

5

Effect of smectic short-range order on the discontinuous anchoring transition in nematic liquid crystals

5.1 Introduction

In the previous chapters we have studied the physical properties of ambient temperature discotic and mixtures of discotic and calamitic LCs. In this chapter, we study the anchoring transition in a bicyclohexane based LCs. The alignment of liquid crystal depends upon physical condition of the surfaces, aligning agents, rubbing strengths, chemistry of the liquid crystals, and curing temperatures [1–7]. There are some reports on the change of orientation of the director $\hat{n}$ from planar to homeotropic and vice versa continuously or discontinuously with temperature [8–20]. Several theories have evolved to explain various interactions such as van der Waals interaction [21–23], long range electrostatic interaction [24], short range dipolar and quadrapolar interaction, and smectic short range order effect. In the recent past, Dhara *et al.* observed discontinuous anchoring transition of a liquid crystal CCN-47, from planar to homeotropic with a large thermal hysteresis on perfluoropolymer treated cells [25]. There are some interesting applications reported such as re-writable memory device [26–28], optical wave guiding [29], photo thermal switching [30]. In the above applications director

orientation changes from planar to homeotropic and vice versa with variation of temperature. However, the reason for discontinuous anchoring transition in the CCNs LC system remained unexplored. In this chapter, we present a detailed study of the alignment properties of homologous series of CCNs liquid crystals, anchoring transition temperatures and present a simple theory for the observed discontinuous anchoring transition.

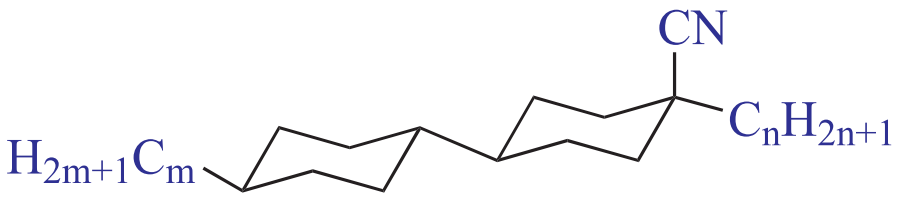

Figure 5.1: Chemical structure of the CCN-mn compound.

5.2 Results and discussion

5.2.1 Liquid crystal samples and phase transitions

Table 5.1: Phase transition temperatures, and nematic range of the compounds. K → Crystal, SmB → Smectic-B, SmA → Smectic-A, N → Nematic, I → Isotropic.

Sample	Phase transition (°C)	nematic range (°C)
CCN-35	K 38.4 N 49.3 I	10.9
CCN-38	K 41 SmA (23) N 49.5 I	26.5
CCN-46	K 30 SmB (26) N 54.7 I	28.7
CCN-47	K 25.6 SmA 28.2 N 57.3 I	29.1
CCN-55	K 25 SmB 30 N 66.4 I	30.4
CCN-73	K 38.6 SmB (38) N 50.2 I	12.2

In this chapter, we studied six compounds of a homologous series of trans trans-4,4′-dialkyl-(1α, 1′α-bicyclohexyl-4β-carbonitrile (CCNs) liquid crystals. The generic molecular structure of the compound is shown in Fig.5.1. These compounds formed by bicyclohexyl core group with transverse dipolemoment (cyano group -CN) and different alkyl chains at the two ends. The homologous series of the compounds, and transition temperatures are shown in Table.5.1. The six compounds are CCN-35, CCN-38, CCN-46, CCN-47, CCN-55, and CCN-73. Among them, CCN-35 has only nematic phase, CCN-38 and CCN-47 have both nematic and smectic-A phases CCN-46, CCN-55, and CCN-73 have both nematic and smectic-B phases. Physical characterizations such as X-ray, NMR and dielectric relaxation studies have already been reported [31–34].

5.2.2 Alignment layer

Here amorphous perfluoropolymer, perfluoro(4-vinyloxy-1-butene) also known as CYTOP was used as alignment layer. The chemical structure is shown in Fig.5.2. It was prepared by adding 1 part of CTX-809A to 2 parts of CT-Sol.180 by weight. These two were obtained from Asahi Glass Co., Ltd. Japan. It has various advantages such as, it can act as anti reflective coating and high transmittance over a wide wave length range [35]. It has high thermal and chemical stability. CYTOP was spin coated at 3500 rpm over glass slides and then cured at 100°C for 30 min. It gives the homogeneous (planar) orientation to most of the nematic liquid crystal. The experimental cell used in the experiment having typical thickness 8μm.

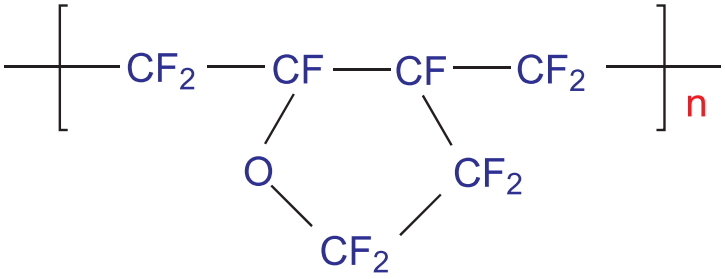

Figure 5.2: Chemical structure of the alignment layer CYTOP.

5.2.3 Optical polarising microscope (OPM) observations:

In this section, we studied temperature dependent textures of the compounds (CCN-35, CCN-38, CCN-55, CCN-73) in an unrubbed CYTOP coated cell. In CCN-35, after isotropic-nematic phase transition, a schliren texture with half and integer strength disclinations are observed (Fig.5.3(a)-Fig.5.3(c)). This implies that the director is in the plane and any tilt of the director is not allowed topologically [36, 37]. It shows crystallisation at 38.4°C without any smectic phase. The texture remains the same in the entire nematic phase indicating no anchoring transition. In CCN-38, similar kind of texture was observed in the nematic phase (Fig.5.3(d)). On further cooling in the nematic phase, at a paricular temperature, small dark spots appeared spontaneously and randomly (Fig.5.3(e)). These dark spots grow in size and the total region becomes complete dark within temperature range of 1°C (Fig.5.3(f)). This indicates that on cooling, director orientation spontaneously changes from planar to homeotropic. In case of sample CCN-55, the texture in the nematic phase (Fig.5.3(g)) is similar to the nematic texture of CCN-38 (Fig.5.3(d)). The sample on further cooling in the nematic phase, dark spots along with the typical SmB textures (Fig.5.3(h)) were observed. Finally, dark regions along with SmB textures (Fig.5.3(i)) were remained in the field of view. In case of CCN-73, the nematic texture (Fig.5.3(j)) is similar to the nematic textures (Fig.5.3(a), Fig.5.3(d), Fig.5.3(g)) of the above mentioned

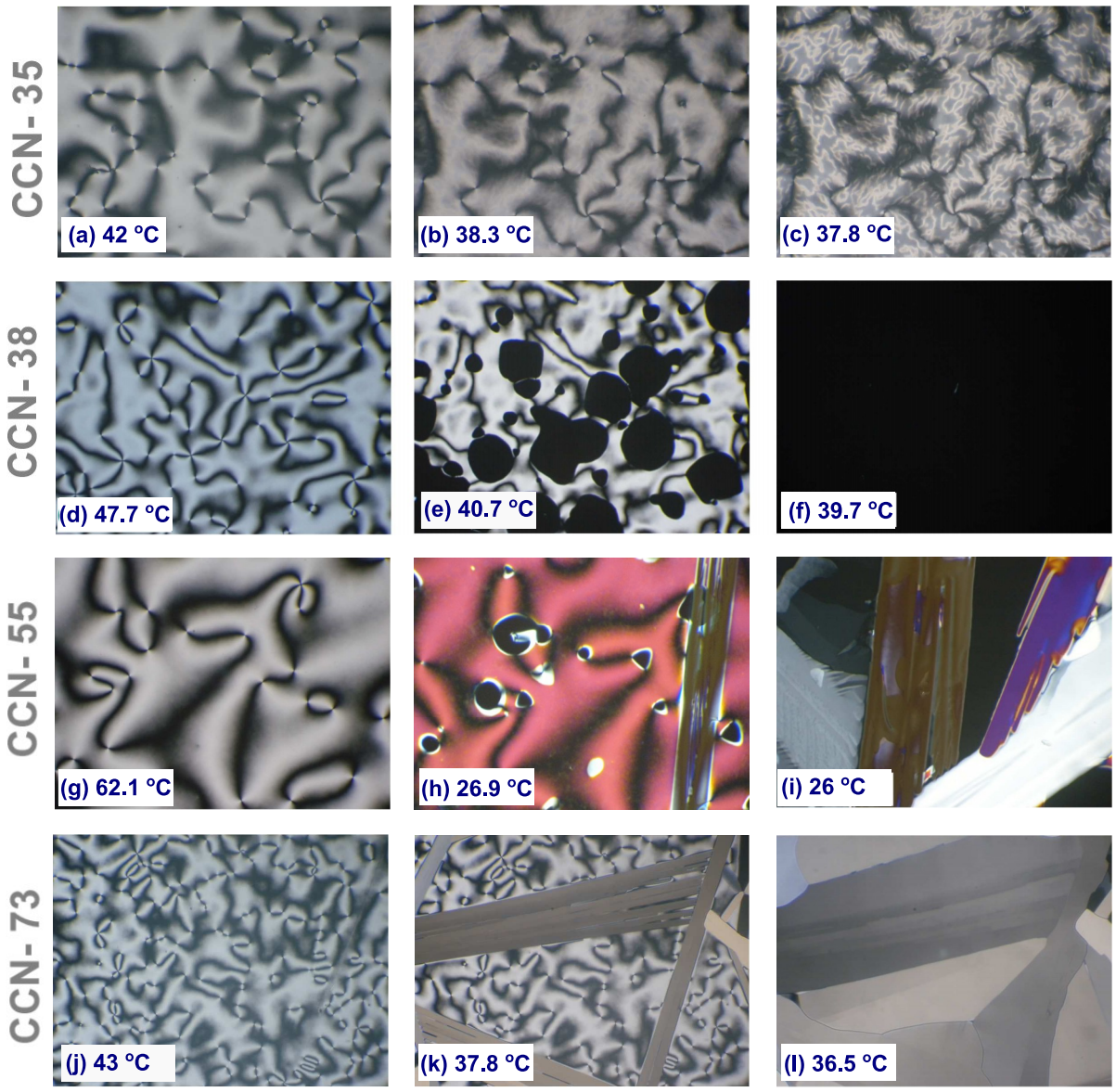

Figure 5.3: (colour online) Typical photomicrographs of four compounds at various temperatures while anchoring transition from planar to homeotropic during cooling. (a) CCN-35 at 42°C (b) CCN-35 at 38.3°C (c) CCN-35 at 37.8°C (d) CCN-38 at 47.7°C (e) CCN-38 at 40.7°C (f) CCN-38 at 38.7°C (g) CCN-55 at 62.1°C (h)CCN-55 at 26.9°C (i) CCN-55 at 26°C (j) CCN-73 at 43°C (k) CCN-73 at 37.8°C (l) CCN-73 at 36.5°C.

compounds. The nematic to SmB phase transition (Fig.5.3(k)) was observed around 37.8°C and it forms SmB phase (Fig.5.3(l)) without any anchoring transition. When the samples (the samples which exhibited anchoring transition) were heated up, the dark texture goes to planar texture with characteristic nematic umbilic defects beyond a certain temperature. This homeotropic to planar transition temperature occurs at a higher temperature than the temperature observed during cooling. Thus, the anchoring transition exhibits thermal hysteresis in the nematic phase.

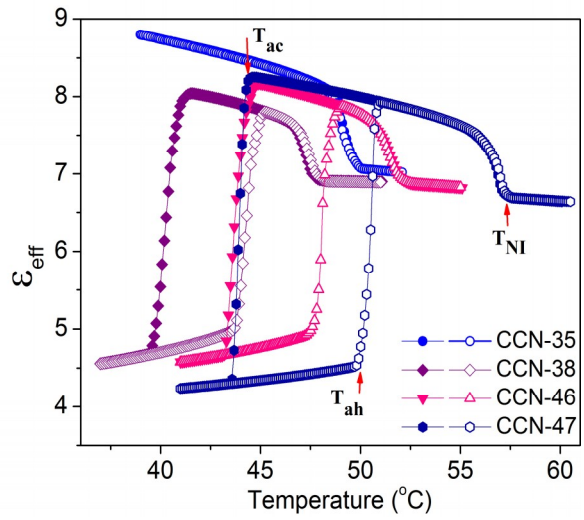

Figure 5.4: Temperature variation of effective dielectric constant (ε_{eff}) of CCN-35, CCN-38, CCN-46, and CCN-47. The solid and open symbols correspond to the data while cooling and heating, respectively. The phase transition and anchoring transition temperatures during cooling and heating are indicated with arrows. Nematic-isotropic phase transition: T_{NI}; Planar to homeotropic transition in cooling: T_{ac}; Homeotropic to planar transition in heating: T_{ah}.

In order to get more insight, we measured anchoring transition temperatures and the range of thermal hysteresis. For this, we performed the effective dielectric constant (ε_{eff}) measurements with variation of temperature in all the samples. The dielectric measurements were preferred over optical measurements since they does not need rubbing which may alter the surface properties and can change the anchoring transition temperatures. The dielectric constant was measured by using LCR meter (Agilent E4980A). A sinusoidal frequency 1kHz at an amplitude 0.2V is applied and temperature is varied step of 0.1°C/min during the experiment. The temperature variation of dielectric constant as a function of temperature is shown in Fig.5.4 and Fig.5.5. The effective dielectric constant (ε_{eff}) in nematic phase is greater than the isotropic phase in all the compounds. This indicates that the all the compounds have negative dielectric anisotropy $\Delta\varepsilon = (\varepsilon_{||} - \varepsilon_{\perp}) < 0$, where the subscripts refer to the direction in relation to the director $\hat{n}$. So, the dielectric constant in the planar state is $\varepsilon_{\perp}$ and

in the homeotropic state $\varepsilon_{eff} = \varepsilon_{||}$. This was confirmed by measuring the dielectric constants in the independent planar and homeotropic cells (coated with AL-1254 and JALS-204) respectively [38]. It is observed that in compound CCN-35, there is no observable change in dielectric constant while heating and cooling cycles in the nematic phase. For the samples CCN-38, CCN-46, and CCN-47, we observe an abrupt decrease of ε_{eff} in the nematic phase at a certain temperature (T_{ac}) (Fig.5.4). Similarly, again an abrupt increase in ε_{eff} is noticed during heating at higher temperature (T_{ah}). For example, in case of CCN-38, we notice ε_{eff} decreases abruptly during cooling at about 41.4°C (=T_{ac}).

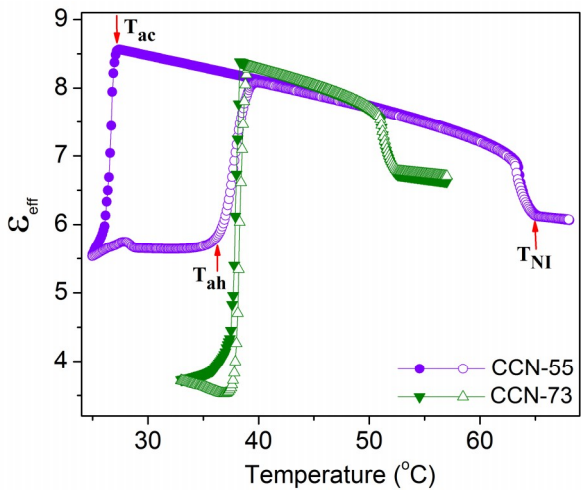

Figure 5.5: Temperature variation of effective dielectric constant (ε_{eff}) of CCN-55 and CCN-73. The solid and open symbols correspond to the data while cooling and heating, respectively. The phase transition and anchoring transition temperatures during cooling and heating are indicated with arrows. Nematic-isotropic phase transition: T_{NI}; Planar to homeotropic transition in cooling: T_{ac}; Homeotropic to planar transition in heating: T_{ah}.

Similarly again an abrupt increase in ε_{eff} is noticed during heating at about 43.7°C (=T_{ah}). So the temperature range of thermal hysteresis ($\Delta T_h = T_{ah} - T_{ac}$) is 2.3 °C. The temperature variation of ε_{eff} for both CCN-55 and CCN-73 is shown in Fig.5.5. In case of CCN-55, the planar to homeotropic transition occurs while cooling just before the SmB phase transition as discussed previously (Fig.5.3(h)). Interestingly, there is no anchoring transition noticed in CCN-73. The abrupt decrease of the dielectric constant in CCN-73 at 37.8°C is due to the N-SmB phase transition (Fig.5.3(k)). The anchoring transition temperatures (T_{ah} and T_{ac}) and the thermal widths (ΔT_h) of the hysteresis are listed in Table-5.2. It is observed that CCN-35 does not show any anchoring transition, CCN-38, CCN-46, CCN-47, and CCN-55 shows discontinuous anchoring transition in the nematic phase with increasing thermal hysteresis. The largest thermal hysteresis is observed in CCN-55 (ΔT_h=9.5°C).

Table 5.2: Anchoring transition temperatures and thermal hysteresis of the compounds. $T_{ac} \longrightarrow$ anchoring transition temperature while cooling, $T_{ah} \longrightarrow$ anchoring transition temperature while heating, thermal hysteresis, ΔT_h=T_{ah}-T_{ac}

Sample	T_{ac}(°C)	T_{ah}(°C)	ΔT_h(°C)
CCN-35	No anchoring transition		0
CCN-38	41.4	43.7	2.3
CCN-46	44.7	47.8	3.1
CCN-47	44.5	49.8	5.3
CCN-55	27.3	36.8	9.5
CCN-73	No anchoring transition		0

There are some experimental studies reported on the anchoring transition in nematic liquid crystals. In these studies, various types of molecules such as polar, nonpolar, symmetry such as centrosymmetric with liquid crystalline phases such as nematic and nematic in combination of smectic-A have choosen in various substrate conditions. Various theoretical aspects were discussed to understand the experimental observations. For example, Parsons *et al.* have shown that the competition between dipolar and quadrupolar interactions can lead to the anchoring transition [14]. From the pseudo-molecular model, Barbero *et al.* have shown that the competition between nematic-nematic and nematic-substrate interactions based on the angular and temperature dependence can lead to the anchoring transition [17]. Alexe-Ionescu *et al.* showed that besides dielectric coupling, the quadrupolar flexoelectric coupling between nematic liquid crystal-substrate interaction can decrease the anchoring energy and further can lead the anchoring transition [12]. By considering the ionic impurities in a nematic liquid crystal made up of centrosymmetric molecules, Nazarenko and Lavantovich proposed balance between direct molecular interaction and the orientational tendencies of electric double layer at the surface is responsible for the observed second order anchoring transition [13]. Komitov *et al.* reported on the anchoring transition in hybrid aligned cell and gave a model that accounts for the dependence of the elastic constants on the scalar order parameter [16]. Zhang *et al.* had shown anchoring transition on micro-structured surface and suggested that it is due to frustrated boundary condition in which the elastic energy due to spacial variation of molecular orientation compromises an increase in the surface anchoring energy [15]. From the above discussions, several interactions in different experimental conditions give various types of anchoring transitions. In the present system, based on the high polarity of CCN molecules Parsons model is more appropriate compared to other models discussed. Missing of anchoring transition in CCN-35 ruled out the Parsons model, since it is due

to competetion between dipole and quadrapolar interactions. From the Table-5.2, it appear that the presence of smectic phase and relatively wide temperature range of nematic is important for the occurrence of discontinuous anchoring transition in the CCNs homologue. Chakrabarti and Bagchi *et al.* have shown that onset growth of the orientational order in the nematic phase induces translational order, producing a smectic kind of layer in the underlying inherent structures. Interestingly, they observed that these inherent structures maintain orientational order alone if the initial nematic phase placed between the high temperature isotropic and low temperature smectic phases [39]. Based on the surface treatment and associated induced smectic order Shioda *et al.* observed continuous anchoring transition from tilted to homeotropic in the nematic phase while cooling towards the smectic-A phase transition temperature [5]. However, discontinuous anchoring transition from planar to homeotropic with large thermal hysteresis so far has not been explained theoretically.

5.2.4 Theory

We developed a theoretical model for the observed discontinuous anchoring transition in the nematic phase. We assume that the nematic liquid crystal exist in a cell of thickness (d) having identical surfaces. The surfaces are in the xy-plane and the normal to the surface is along the z-axis. The orientational order is same across the cell. The Landau form of free energy of the sample per unit area can be written as [11, 40]

$$\begin{aligned} F &= F_o + 2[\gamma_{11}\nu_i Q_{ij}\nu_j + \gamma_{20}Q_{ij}Q_{ji} + \gamma_{21}\nu_i Q_{ij}Q_{jl}\nu_l + \gamma_{22}(\nu_i Q_{ij}\nu_j)^2] \\ &\quad -D\int_0^d \Psi(z)q^2(\nu_i Q_{ij}\nu_j)dz \end{aligned} \tag{5.1}$$

where F_o is the free energy in the isotropic phase, ν is the outward normal at the interface, the nematic tensor order parameter, $Q_{ij} = \frac{3}{2}S(n_i n_j - \frac{1}{3}\delta_{ij})$, where S the scalar order parameter and n being director in the nematic phase respectively. The anchoring transition was not observed by the lower homologue in the series CCN-35, which does not have any smectic phase. So, it is reasonable to assume smectic-like order developed in the nematic phase itself and is important for the observed discontinuous anchoring transition. However, the effect of smectic short range order on the anchoring transition was discussed previously [5, 7]. The constant in each term (γ_{ij}) is related to intermolecular forces in the NLC and NLC-surface interaction. The second, third, fourth and fifth terms related to various interactions in the nematic liquid crystal and NLC to the surface field. The last term related to coupling of surface induced smectic order and orientational order parameter Q_{ij}.
We have

$$Q_{ij} = \frac{3}{2}S(n_i n_j - \frac{1}{3}\delta_{ij}), \tag{5.2}$$
$$\Psi = \psi_o e^{iqr}; q = 2\pi/\lambda; \tag{5.3}$$

where λ = smectic layer thickness,
By substituting Eq.(5.2) and Eq.(5.3); we have

$$\begin{aligned}
\nu_i Q_{ij}\nu_j &= \nu_i \left(\frac{3}{2}S(n_i n_j - \frac{1}{3}\delta_{ij})\right)\nu_j, \\
&= \frac{3}{2}S\left(\nu_i n_i n_j \nu_j - \frac{1}{3}\nu_i\delta_{ij}\nu_j\right), \\
&= \frac{3}{2}S\left((\nu_i.n_i)^2 - \frac{1}{3}\right).
\end{aligned}$$

$$\begin{aligned}
Q_{ij}Q_{ji} &= \left(\frac{3}{2}S\right)^2\left[(n_i n_j - \frac{1}{3}\delta_{ij})(n_j n_i - \frac{1}{3}\delta_{ji})\right], \\
&= \frac{9}{4}S^2\left[(n_i n_j n_j n_i - \frac{1}{3}n_i n_j\delta_{ji} - \frac{1}{3}\delta_{ij}n_j n_i + \frac{1}{9}\delta_{ij}\delta_{ji})\right], \\
&= \frac{9}{4}S^2\left[(n_i^2 n_j^2 - \frac{1}{3}n_i^2 - \frac{1}{3}n_i^2 + \frac{1}{9}\delta_{ii})\right], \\
&= \frac{9}{4}S^2\left[1 - \frac{1}{3} - \frac{1}{3} + \frac{1}{3}\right], \\
&= \frac{9}{4}S^2\left[\frac{2}{3}\right], \\
&= \frac{3}{2}S^2.
\end{aligned}$$

$$\begin{aligned}
\nu_i Q_{ij}Q_{jl}\nu_l &= \left(\frac{3}{2}S\right)^2\nu_i\left[(n_i n_j - \frac{1}{3}\delta_{ij})(n_j n_l - \frac{1}{3}\delta_{jl})\right]\nu_l, \\
&= \frac{9}{4}S^2\nu_i\left[n_i n_j n_j n_l - \frac{1}{3}n_i n_j\delta_{jl} - \frac{1}{3}\delta_{ij}n_j n_l + \frac{1}{9}\delta_{ij}\delta_{jl}\right]\nu_l, \\
&= \frac{9}{4}S^2\left[\nu_i n_i n_j^2 n_l\nu_l - \frac{1}{3}\nu_i n_i n_l\nu_l - \frac{1}{3}\nu_i n_i\nu_l n_l + \frac{1}{9}\nu_i\delta_{il}\nu_l\right], \\
&= \frac{9}{4}S^2\left[(\nu.n).1.(\nu.n) - \frac{1}{3}(\nu.n)^2 - \frac{1}{3}(\nu.n)^2 + \frac{1}{9}.1\right], \\
&= \frac{9}{4}S^2\left[\frac{1}{3}(\nu.n)^2 + \frac{1}{9}\right], \\
&= \frac{3}{4}S^2\left[(\nu.n)^2 + \frac{1}{3}\right].
\end{aligned}$$

$$\begin{aligned}(\nu_i Q_{ij}\nu_j)^2 &= (\nu_i Q_{ij}\nu_j)(\nu_i Q_{ij}\nu_j),\\ &= \frac{3}{2}S\left\{(\nu_i.n_i)^2-\frac{1}{3}\right\}\frac{3}{2}S\left\{(\nu_i.n_i)^2-\frac{1}{3}\right\},\\ &= \frac{9}{4}S^2\left((\nu_i.n_i)^2-\frac{1}{3}\right)^2,\\ &= \frac{9}{4}S^2\left((\nu_i.n_i)^4-\frac{2}{3}(\nu_i.n_i)^2+\frac{1}{9}\right).\end{aligned}$$

Eq.(5.1) becomes,

$$\begin{aligned}F &= F_o+2\left\{\gamma_{11}\frac{3}{2}S[(\nu_i.n_i)^2-\frac{1}{3}\right\}+\gamma_{20}\frac{3}{2}S^2+\gamma_{21}\frac{3}{4}S^2\left\{(\nu.n)^2+\frac{1}{3}\right\}\\ &\quad+\gamma_{22}\frac{9}{4}S^2\left\{(\nu_i.n_i)^4-\frac{2}{3}(\nu_i.n_i)^2+\frac{1}{9}\right\}-D\int_0^d\Psi(z)q^2(\nu_i Q_{ij}\nu_j)dz,\\ &= F_o+\beta_{11}S\left\{(\nu_i.n_i)^2-\frac{1}{3}\right\}+\beta_{20}S^2+\beta_{21}S^2[(\nu.n)^2+\frac{1}{3}]\\ &\quad\beta_{22}S^2\left\{(\nu_i.n_i)^4+\frac{1}{9}\right\}-\frac{3}{2}Dq^2\int_0^d\Psi(z)\left\{(\nu.n)^2-\frac{1}{3}\right\}dz,\end{aligned}\tag{5.4}$$

Here, $\beta_{11}=3\gamma_{11}$, $\beta_{20}=3\gamma_{20}$, $\beta_{21}=\frac{3}{2}\gamma_{21}$, $\beta_{22}=\frac{9}{2}\gamma_{22}$,
and,
$3Dq^2\int_0^d\Psi(z)\{(\nu.n)^2-\frac{1}{3}\}dz=-6Dq^2S\xi\psi_o\{(\nu.n)^2-\frac{1}{3}\}$.
Now the free energy can be written as,

$$F[S,\xi,(n.\nu)]=F_o+F_1[S,\xi]+F_2[S,\xi,(n.\nu)],\tag{5.5}$$

where, $F_1[S,\xi]$ is the isotropic part of the free energy and is given by

$$F_1[S,\xi]=\left[\left\{2Dq^2\xi\psi_o-\frac{\beta_{11}}{3}\right\}S+\left\{\beta_{20}+\frac{\beta_{21}}{3}+\frac{\beta_{22}}{9}\right\}S^2\right],\tag{5.6}$$

and $F_2[S,\xi,(n.\nu)]$ is the anisotropic part of the free energy and is given by

$$F_2[S,\xi,(n.\nu)]=A(S,\xi)(n.\nu)^2+B(S)(n.\nu)^4,\tag{5.7}$$

where,

$$A(S,\xi)=(\beta_{11}-6Dq^2\psi_o\xi)S+\left\{\beta_{21}-\frac{2\beta_{22}}{3}\right\}S^2,\tag{5.8}$$

and

$$B(S)=\beta_{22}S^2.\tag{5.9}$$

The surface orientation ϕ is given by, $\phi=\cos^{-1}(n.\nu)$. Now minimization of Eq.(5.7), gives

$$F_2[S,\xi,(n.\nu)]=A(S,\xi)(n.\nu)^2+B(S)(n.\nu)^4,\tag{5.10}$$

$$\begin{aligned} F_2 &= A(S,\xi)cos^2\phi + B(S)cos^4\phi, \\ F_2^{'} = \frac{dF_2}{d\phi} &= -A(S)2cos\phi sin\phi - B(S)4cos^3\phi sin\phi, \\ &= -A(S)sin2\phi - B(S)2cos^2\phi sin2\phi, \\ &= -sin2\phi[A(S) + 2B(S)cos^2\phi]. \end{aligned} \tag{5.11}$$

Now,

$$\begin{aligned} F_2^{''} = \frac{d^2F_2}{d\phi^2} &= \frac{dF_2^{'}}{d\phi}, \\ &= -2cos2\phi[A(S) + 2B(S)cos^2\phi] \\ &\quad -sin2\phi[2B(S).2cos\phi(-sin\phi)], \\ &= -2.cos2\phi[A(S) + 2B(S)cos^2\phi] \\ &\quad +2B(S)sin^2 2\phi. \end{aligned}$$

The stable orientation ϕ, which satisfy both $F_2^{'} = 0$ and $F_2^{''} > 0$ relations.
The condition $F_2^{'} = 0$, gives

$$\Rightarrow F_2^{'} = -sin2\phi.[A(S) + 2B(S).cos^2\phi] = 0, \tag{5.12}$$

either $sin2\phi = 0$ or $A(S) + 2B(S).cos^2\phi = 0$.
So, it leads to $\phi = 0, \pi/2$, and $cos^2\phi = -\frac{A(S)}{2B(S)}$.
Now,

$$\begin{aligned} \phi = 0, F_2^{''} > 0 &\Rightarrow -2[A(S) + 2B(S).1] > 0, \\ &\Rightarrow [A(S) + 2B(S)] < 0. \end{aligned} \tag{5.13}$$

$$\begin{aligned} \phi = \pi/2, F_2^{''} > 0 &\Rightarrow -2(-1)[A(S)] > 0, \\ &\Rightarrow A(S) > 0. \end{aligned} \tag{5.14}$$

$$\begin{aligned} cos^2\phi = \frac{-A(S)}{2B(S)}, F_2^{''} > 0 &\Rightarrow 2B(S)sin^2 2\phi > 0, \\ &\Rightarrow 2B(S)4sin^2\phi cos^2\phi > 0, \\ &\Rightarrow B(S)sin^2\phi cos^2\phi > 0, \\ &\Rightarrow B(S)[1 - cos^2\phi]cos^2\phi > 0, \end{aligned} \tag{5.15}$$

$$\begin{aligned}
\Rightarrow \quad & B(S)\left\{-\frac{A(S)}{2B(S)}\right\}.\left\{1+\frac{A(S)}{2B(S)}\right\}>0, \\
\Rightarrow \quad & B(S)\left\{\frac{A(S)}{2B(S)}\right\}\left\{\frac{2B(S)+A(S)}{2B(S)}\right\}<0, \\
\Rightarrow \quad & \left\{\frac{A(S)}{B(S)}\right\}[2B(S)+A(S)]<0.
\end{aligned} \tag{5.16}$$

Minimization gives the following conditions,

$$\begin{aligned}
\phi=0 \quad &\Rightarrow \quad [A(S,\xi)+2B(S)]<0, \\
\phi=\pi/2 \quad &\Rightarrow \quad A(S,\xi)>0, \\
cos^2\phi=\frac{-A(S,\xi)}{2B(S)} \quad &\Rightarrow \quad \left\{\frac{A(S,\xi)}{B(S)}\right\}[2B(S)+A(S,\xi)]<0.
\end{aligned} \tag{5.17}$$

From the mean field theory, smectic correlation length,

$$\xi=\xi_o[(T-T_{NA})/T_{NA}]^{-1/2}.$$

As the anchoring transition in our samples occur at temperature far below the IN transition temperature (T_{NI}), we assume that the orientational order parameter S saturates to a constant value and independent of temperature during the anchoring transition. This is one of the reason, the four compounds which showed anchoring transition have comparatively large nematic range. The minimization of Eq.(5.7) and the stability conditions Eq.(5.17) predict a first order transition from $\phi=\pi/2$ at temperature $T>T_{ah}$ to $\phi=0$ at temperature $T<T_{ac}$ with thermal hysteresis between T_{ah} and T_{ac} as observed experimentally.
Hence we have,

$$\begin{aligned}
T_{ah} &= T_{NA}+T_{NA}\frac{36D^2q^4\psi_o^2\xi_o^2}{[\beta_{11}+(\beta_{21}-4|\beta_{22}|/3)S]^2}, \\
T_{ac} &= T_{NA}+T_{NA}\frac{36D^2q^4\psi_o^2\xi_o^2}{[\beta_{11}+(\beta_{21}+2|\beta_{22}|/3)S]^2}, \\
\Delta T_h &= T_{ah}-T_{ac}.
\end{aligned} \tag{5.18}$$

Here, ΔT_h is the thermal hysteresis. We now estimate T_{ah}, T_{ac}, and ΔT_h from Eq.(5.18). By considering the compound CCN-47, the value of smectic layer spacing $\lambda=20\times10^{-8}$cm, gives $q\sim3\times10^{7}$cm^{-1}. By assuming the bare smectic correlation length $\xi_0\sim5\times10^{-8}$cm and $D\sim3.9\times10^{-8}$erg/cm [5]. The anchoring coefficients β_{11}, β_{21} are expected to be of similar magnitudes. The magnitude of the higher

order anchoring coefficient β_{22} is expected to be relatively smaller than β_{11} and we assume that $|\beta_{22}| \sim 0.15\beta_{11}$. At temperatures corresponding to anchoring transition in our samples, we assume that the nematic order parameter $S \sim 0.6$ and the surface induced smectic order parameter $\psi_0^2 \sim 0.005$. Using the above parameters, T_{ah}, T_{ac}, and ΔT_h are estimated to be 323°K, 318°K, and 5°K, respectively, which agrees very well with our experimental observations. As reported earlier by Shioda *et al.* [5] the surface induced smectic order in the nematic phase can drive an anchoring transition from the planar to homeotropic orientation which is continuous in nature. Here, we demonstrated both experimentally and theoretically that such transition can be of first order with the discontinuous jump in the surface orientation from planar to homeotropic orientation with a thermal hysteresis.

5.3 Conclusion

We studied anchoring transition in the homologous series of liquid crystals (CCN-mn) on perfluoropolymer treated cells. The compounds CCN-38, CCN-46, CCN-47 and CCN-55 exhibit discontinuous anchoring transition and increasing thermal hysteresis. We observed the compound CCN-35, which has no Smectic A or Smectic B phase does not show any anchoring transition. In case of compound CCN-73, has smectic B phase, but short range of nematic phase and does not show anchoring transition. The observed experimental results show that smectic phase and wide range of nematic phase are important for the discontinuous anchoring transition. We developed a simple theory considering the experimental observations and showed the discontinuous anchoring transition with a finite thermal hysteresis.

References

[1] K. Takatoh, M. Sakamoto, R. Hasegawa, M. Koden, N. Itoh, and M. Hasegawa, *Alignment technology and applications of liquid crystal devices*. CRC Press, 2005.

[2] T. Arun Kumar, K. V. Le, J. K. Kim, H. Takezoe, and S. Dhara, "Alignment of unconventional nematic liquid crystals," *Liquid Crystals*, vol. 38, no. 7, pp. 917–924, 2011.

[3] Y. Galerne and P. Hubert, "Anchoring transitions with polar and non-polar nematic liquid crystals on incompletely oxidized silane substrates," *The European Physical Journal B-Condensed Matter and Complex Systems*, vol. 8, no. 2, pp. 245–249, 1999.

[4] S. Faetti, M. Gatti, V. Palleschi, and T. J. Sluckin, "Almost critical behavior of

the anchoring energy at the interface between a nematic liquid crystal and a sio substrate," *Physical review letters*, vol. 55, no. 16, p. 1681, 1985.

[5] T. Shioda, B. Wen, and C. Rosenblatt, "Continuous nematic anchoring transition due to surface-induced smectic order," *Physical Review E*, vol. 67, no. 4, p. 041706, 2003.

[6] G. P. Sinha, B. Wen, and C. Rosenblatt, "Large, continuously controllable nematic pretilt from vertical orientation," *Applied Physics Letters*, vol. 79, no. 16, pp. 2543–2545, 2001.

[7] H. V. Känel, J. D. Litster, J. Melngailis, and H. I. Smith, "Alignment of nematic butoxybenzilidene octylaniline by surface-relief gratings," *Physical Review A*, vol. 24, no. 5, p. 2713, 1981.

[8] J. Goodby, T. Leslie, P. Cladis, and P. Finn, "Liquid crystals and ordered fluids," *by A C Griffin and J F Johnson, Plenum Press, New York*, vol. 4, p. 89, 1984.

[9] Y. Aoki, T. Watabe, T. Hirose, and K. Ishikawa, "Noble orientation change with temperature in nematic liquid crystalline mixtures," *Chemistry Letters*, vol. 36, no. 3, pp. 380–381, 2007.

[10] J. S. Patel and H. Yokoyama, "Continuous anchoring transition in liquid crystals," *Nature*, vol. 362, pp. 525–527, 1993.

[11] A. Poniewierski and A. Samborski, "Anchoring transitions in the nematic-substrate system: Study of the landau–de gennes model," *The Journal of chemical physics*, vol. 105, no. 17, pp. 7632–7640, 1996.

[12] A. L. Alexe-Ionescu, G. Barbero, and A. G. Petrov, "Gradient flexoelectric effect and thickness dependence of anchoring energy," *Physical Review E*, vol. 48, no. 3, p. R1631, 1993.

[13] V. G. Nazarenko and O. D. Lavrentovich, "Anchoring transition in a nematic liquid crystal composed of centrosymmetric molecules," *Physical Review E*, vol. 49, no. 2, p. R990, 1994.

[14] J. D. Parsons, "Structural critical point at the free surface of a nematic liquid crystal," *Physical Review Letters*, vol. 41, no. 13, p. 877, 1978.

[15] B. Zhang, F. K. Lee, O. K. C. Tsui, and P. Sheng, "Liquid crystal orientation transition on microtextured substrates," *Physical review letters*, vol. 91, no. 21, p. 215501, 2003.

[16] L. Komitov, P. Rudquist, A. Strigazzi, and M. Warenghem, "Anomalous anchoring transition in hybrid aligned nematics," *Molecular Crystals and Liquid Crystals*, vol. 282, no. 1, pp. 259–268, 1996.

[17] G. Barbero, Z. Gabbasova, and M. A. Osipov, "Surface order transition in nematic liquid crystals," *Journal de Physique II*, vol. 1, no. 6, pp. 691–705, 1991.

[18] Y. Kurioz, D. Kurysh, V. Y. Reshetnyak, and Y. Reznikov, "Temperature induced anchoring transition in nematic liquid crystal cell," in *Ninth International Conference on Nonlinear Optics of Liquid and Photorefractive Crystals*, pp. 128–131, International Society for Optics and Photonics, 2003.

[19] J. Bechhoefer, J. Duvail, L. Masson, B. Jérme, R. M. Hornreich, and P. Pieranski, "Critical behavior in anchoring transitions of nematic liquid crystals," *Physical review letters*, vol. 64, no. 16, p. 1911, 1990.

[20] K. R. Amundson and M. Srinivasarao, "Liquid-crystal-anchoring transitions at surfaces created by polymerization-induced phase separation," *Physical Review E*, vol. 58, no. 2, p. R1211, 1998.

[21] H. Kimura, "Statistical theory of surface tension and molecular orientations in nematic liquid crystals. iii. on hard flat walls," *Journal of the Physical Society of Japan*, vol. 62, no. 8, pp. 2725–2733, 1993.

[22] E. Dubois-Violette and P. G. De Gennes, "Local frederiks transitions near a solid/nematic interface," *Journal de Physique Lettres*, vol. 36, no. 10, pp. 255–258, 1975.

[23] E. Dubois-Violette and P. G. De Gennes, "Effects of long range van der waals forces on the anchoring of a nematic fluid at an interface," *Journal of Colloid and Interface Science*, vol. 57, no. 3, pp. 403–410, 1976.

[24] K. Okano, N. Matsuura, and S. Kobayashi, "Alignment of a liquid crystal on an anisotropic substrate," *Japanese Journal of Applied Physics*, vol. 21, no. 2A, p. L109, 1982.

[25] S. Dhara, J. K. Kim, S. M. Jeong, R. Kogo, F. Araoka, K. Ishikawa, and H. Takezoe, "Anchoring transitions of transversely polar liquid-crystal molecules on perfluoropolymer surfaces," *Physical Review E*, vol. 79, no. 6, p. 060701, 2009.

[26] J. K. Kim, F. Araoka, S. M. Jeong, S. Dhara, K. Ishikawa, and H. Takezoe, "Bistable device using anchoring transition of nematic liquid crystals," *Applied Physics Letters*, vol. 95, no. 6, p. 063505, 2009.

[27] J. K. Kim, K. Van Le, S. Dhara, F. Araoka, K. Ishikawa, and H. Takezoe, "Heat-driven and electric-field-driven bistable devices using dye-doped nematic liquid crystals," *Journal of Applied Physics*, vol. 107, no. 12, p. 123108, 2010.

[28] T. A. Kumar, K. V. Le, S. Aya, S. Kang, F. Araoka, K. Ishikawa, S. Dhara, and H. Takezoe, "Anchoring transition in a nematic liquid crystal doped with chiral agents," *Phase Transitions*, vol. 85, no. 10, pp. 888–899, 2012.

[29] V. S. R. Jampani, M. Skarabot, H. Takezoe, I. Muševič, and S. Dhara, "Laser-driven microflow-induced bistable orientation of a nematic liquid crystal in perfluoropolymer-treated unrubbed cells," *Optics express*, vol. 21, no. 1, pp. 724–729, 2013.

[30] M. V. Rasna, K. P. Zuhail, R. Manda, P. Paik, W. Haase, and S. Dhara, "Discontinuous anchoring transition and photothermal switching in composites of liquid crystals and conducting polymer nanofibers," *Physical Review E*, vol. 89, no. 5, p. 052503, 2014.

[31] L. Walz, W. Haase, and R. Eidenschink, "The crystal and molecular structures of four homologous, mesogenic trans, trans-4, 4'-dialkyl-(1 α, 1'-bicyclohexyl)-4ß-carbonitril (ccn's)," *Molecular Crystals and Liquid Crystals*, vol. 168, no. 1, pp. 169–182, 1989.

[32] R. Eidenschink, G. Haas, M. Römer, and B. S. Scheuble, "Flüssigkristalline 4-bicyclohexylcarbonitrile mit außergewöhnlichen physikalischen eigenschaften," *Angewandte Chemie*, vol. 96, no. 2, pp. 151–151, 1984.

[33] D. Ganzke, S. Wrobel, and W. Haase, "Dielectric studies of bicyclohexylcarbonitrile nematogens with large negative dielectric anisotropy," *Molecular Crystals and Liquid Crystals*, vol. 409, no. 1, pp. 323–333, 2004.

[34] S. Dhara and N. V. Madhusudana, "Physical characterisation of 4'-butyl-4-heptyl-bicyclohexyl-4-carbonitrile," *Phase Transitions*, vol. 81, no. 6, pp. 561–569, 2008.

[35] S. M. Jeong, J. K. Kim, Y. Shimbo, F. Araoka, S. Dhara, N. Y. Ha, K. Ishikawa, and H. Takezoe, "Perfluoropolymer surface for shock-free homeotropic alignment of smectic liquid crystals," *Advanced Materials*, vol. 22, no. 1, pp. 34–38, 2010.

[36] T. A. Kumar, P. Sathyanarayana, V. S. S. Sastry, H. Takezoe, N. V. Madhusudana, and S. Dhara, "Temperature-and electric-field-induced inverse freedericksz transition in a nematogen with weak surface anchoring," *Physical Review E*, vol. 82, no. 1, p. 011701, 2010.

[37] T. Arun Kumar, V. S. S. Sastry, K. Ishikawa, H. Takezoe, N. V. Madhusudana, and S. Dhara, "Effect of an electric field on defects in a nematic liquid crystal with variable surface anchoring," *Liquid Crystals*, vol. 38, no. 8, pp. 971–979, 2011.

[38] D. V. Sai, K. P. Zuhail, R. Sarkar, and S. Dhara, "Structure–property correlation of bicyclohexane nematic liquid crystals," *Liquid Crystals*, vol. 42, no. 3, pp. 328–333, 2015.

[39] D. Chakrabarti and B. Bagchi, "Energy landscape view of phase transitions and slow dynamics in thermotropic liquid crystals," *Proceedings of the National Academy of Sciences*, vol. 103, no. 19, pp. 7217–7221, 2006.

[40] T. J. Sluckin, A. Poniewierski, and C. A. Croxton, "Fluid interfacial phenomena," *Wiley, Chichester*, p. 215, 1986.

6

Structure property correlation of bicyclohexane nematic liquid crystals

6.1 Introduction

In the previous chapter we have studied the anchoring transition in a homologous series of CCN-mn compounds. In this chapter, we study the physical properties of these compounds. Here, we report on the measurements of physical properties such as birefringence, dielectric anisotropy, splay and bend elastic constants with temperature. The results are discussed based on the optimized molecular structure obtained from the density functional theory (DFT).

6.2 Results and discussions

6.2.1 Samples and phase transitions

The phase transition temperatures of the compounds $4,4^{'}$-dialkyl-(1α,$1^{'}$ α-bicyclohexyl)-4β-carbonitrile (CCN-mn) are shown in the Table-6.1. All the compounds have the same bicyclohexane core with varying alkyl chain length on both sides shown in Fig.6.6. The compound CCN-35 exhibits only nematic (N) phase. CCN-38 and CCN-47 exhibit nematic and smectic-A (SmA) phases. The remain-

Sample	Phase transition ($^{\circ}C$)
CCN-35	K 38.4 N 49.3 I
CCN-38	K 41 SmA (23) N 49.5 I
CCN-46	K 30 SmB (26) N 54.7 I
CCN-47	K 25.6 SmA 28.2 N 57.3 I
CCN-55	K 25 SmB 30 N 66.4 I
CCN-73	K 38.6 SmB (38) N 50.2 I

Table 6.1: Homologous series of the bicyclohexane compounds and corresponding phase transition temperatures (°C). K→ crystal, SmB→ Smectic-B, SmA→ Smectic-A, I→ Isotropic.

ing compounds CCN-46, CCN-55 and CCN-73 exhibit nematic and smectic-B (SmB) phases. Some physical characterisations such as X-ray, NMR and dielectric relaxation studies on some of these compounds have been reported [1–7].

6.2.2 Optical and dielectric properties

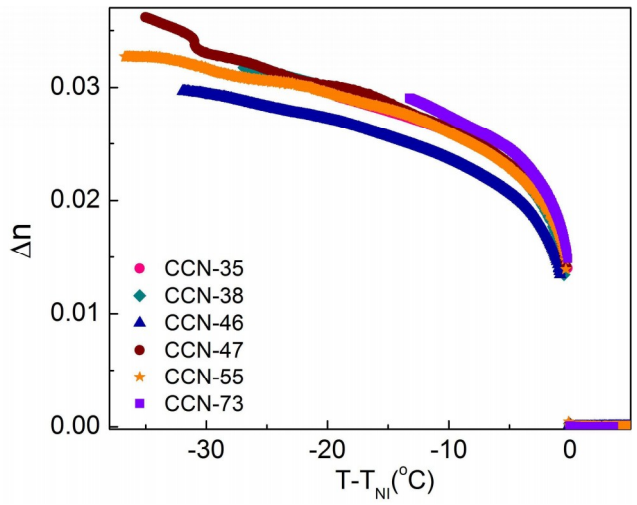

Figure 6.1: Temperature variation of birefringence (Δn) measured at λ=632.8 nm.

The birefringence of the LCs is measured by phase modulation technique. The detailed experimental procedure is given in chapter-2. The variation of birefringence (Δn) of the compounds with shifted temperature is shown in the Fig.6.1. The birefringence is very low in all the compounds ($\Delta n \sim 0.03$ near the room temperature). It may be mentioned that Δn is more than five times lower than some common liquid crystals, for example, 5CB (pentyl cyanobiphenyl). The birefringence of bicyclohexane compounds

with longitudinal cyano group such as nCCH (trans, trans-4′-n-alkylbicyclohexyl-4-carbonitriles) has been reported by several authors [8]. It appears that the birefringence of CCN-mn homologues is about 25% lower than that of nCCH compounds.

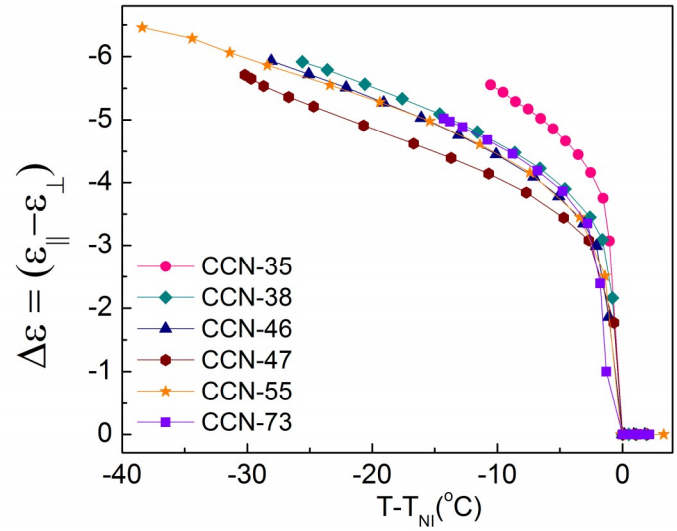

Figure 6.2: Variation of dielectric anisotropy $\Delta\varepsilon$ of the compounds as a function of shifted temperature. Frequency for the dielectric measurement is 4111 Hz.

The variation of dielectric anisotropy ($\Delta\varepsilon$) with shifted temperature is shown in Fig.6.2. The dielectric anisotropy is negative ($\Delta\varepsilon < 0$) in all the compounds and exhibits a typical behaviour, i.e., $\Delta\varepsilon$ increases with decreasing temperature. At relative temperature (below $T - T_{NI} \approx -10°$C), the dielectric anisotropy is largest for CCN-35 and lowest for CCN-47.

6.2.3 Splay (K_{11}) and bend (K_{33}) elastic constants

The splay and bend elastic constants (K_{11} and K_{33}) were measured from the voltage-dependent dielectric constant data obtained from the homeotropic cell following the dielectric method described in the experimental chapter-2. The variation of ε_{eff} together with the best fit with the theoretical Eq.(2.41) and Eq.(2.52) is shown in the inset of Fig.6.3. The variation of splay (K_{11}) and bend (K_{33}) elastic constants as a function of temperature is shown in Fig.6.3 and Fig.6.4. Both K_{11} and K_{33} of all the compounds in the nematic phase increase with decreasing temperature. Both the elastic constants of CCN-47 show presmectic divergence. The presmectic divergence of K_{11} is rare as the splay distortion is permitted even in the smectic-A phase. However, there are a few reports showing presmectic divergence of both K_{11} and K_{33} [9, 10]. Similar behaviour may also be expected in CCN-38 but the N-SmA transition temperature is below the ambient and beyond accessible temperature range of our temperature controller. The ratio of K_{33}/K_{11} is shown in the Fig.6.5. Interestingly, it is observed that K_{33} is lower than K_{11}, i.e., $K_{33}/K_{11} = 0.7$, except very close to the SmA phase

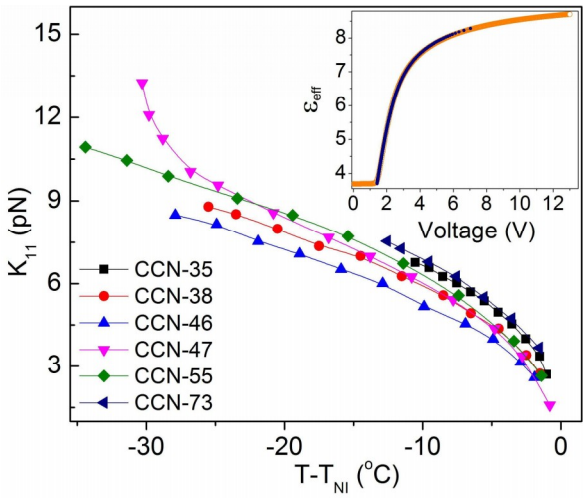

Figure 6.3: Variation of splay elastic constant (K_{11}) as a function of shifted temperature. (Inset) Effective dielectric constant as a function of applied voltage. Solid black line is a theoretical fit to the experimental data.

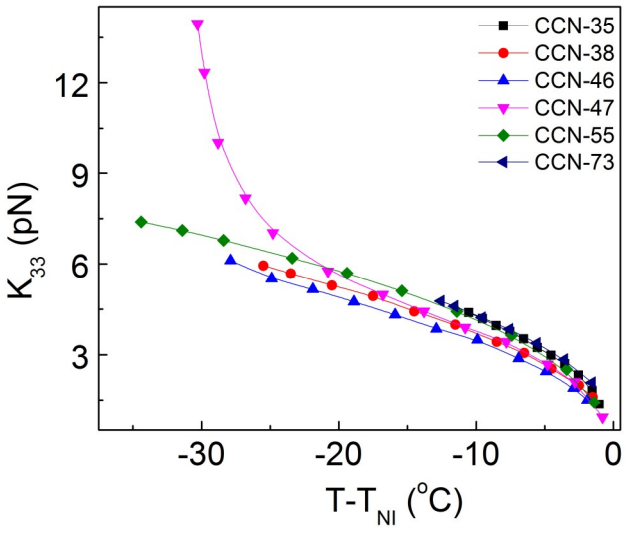

Figure 6.4: Temperature variation of bend elastic constant (K_{33}).

transition of CCN-47. This is opposite to the behaviour observed in the calmitic liquid crystals.

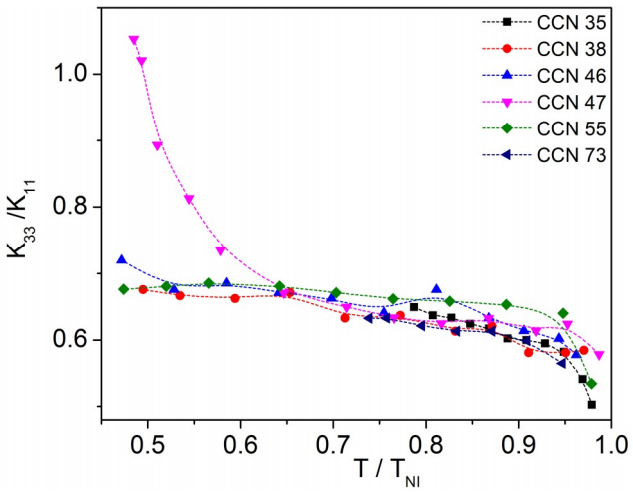

Figure 6.5: Temperature variation of the ratio, K_{33}/K_{11}

6.2.4 Optimized molecular structure from DFT calculations

In order to understand the structure- property correlation, we performed ground state electronic structure calculations of all the molecules with the help of the density functional theory (DFT) by using GAUSSIAN-09 suite programming package. All the calculations are performed in the gas phase and optimisation of the structures is done by B3LYP level of theory using cc-pVDZ basis set [11]. Fig.6.6 shows the two-dimensional (2D) projection of optimised structures of the molecules. It is observed that the molecules are not linear and their 2D projections (keeping the cyano group along the y-axis and bicyclohexane along the x-axis) are bent-shaped.

The principal components of the dipole moments and polarisabilities are listed in Table-6.2. The transverse components of dipole moments (μ_y or μ_z) are much larger in magnitude than that of the longitudinal components (μ_x). For example, in CCN-35, $\mu_x = 0.276D, \mu_y = 3.818D$ and $\mu_z = 0.438D$ respectively. This explains the origin of large negative dielectric anisotropy in all the compounds.

The polarisabilities of all the compounds are larger along the long molecular axis (x-axis) compared to the components in the y and z directions. The birefringence of the compounds is proportional to the polarisability anisotropy ($\Delta\alpha$). The polarisability anisotropy can be defined as $\Delta\alpha \approx \alpha_{xx} - (\alpha_{yy} + \alpha_{zz})/2$. The average $\Delta\alpha$ of all the compounds is about 50 (a.u.) and it is about five times lower than that of 5CB [12] and consistent with five times lower birefringence of CCN-mn compounds. In case of bent-core nematic liquid crystals, it has been reported that $K_{33} < K_{11}$ and occasionally they exhibit unusual temperature dependence [13, 14]. It was suggested that the strain in the bend distortion is partly relieved if the molecules are curved or bent shaped

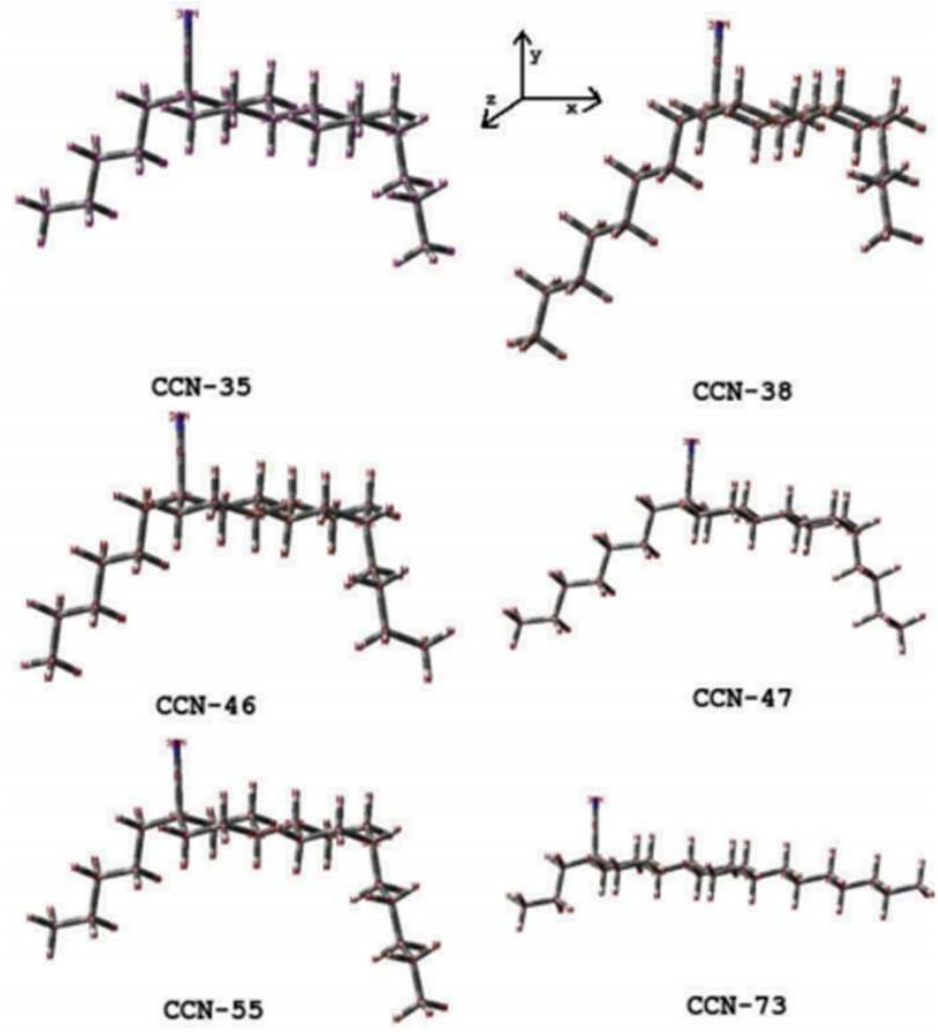

Figure 6.6: Two-dimensional projection of the energy-minimised molecular structures obtained by DFT calculations in the gas phase.

	Dipolemoment (D)			Polarisability (a.u.)		
Compounds	μ_x	μ_y	μ_z	α_{xx}	α_{yy}	α_{zz}
CCN-35	0.276	3.818	0.438	262.56	225.34	216.53
CCN-38	0.726	3.757	0.314	308.70	259.53	244.50
CCN-46	0.138	3.864	0.159	286.48	248.99	239.52
CCN-47	0.165	3.903	0.186	304.48	257.39	249.64
CCN-55	0.910	3.639	0.932	283.67	256.86	235.70
CCN-73	0.482	2.199	3.158	295.61	224.72	262.47

Table 6.2: Components of dipole moment and principal polarisabilities obtained from DFT calculations.

and consequently K_{33} is expected to be lower than K_{11} [15]. The energy-minimised shapes of the present calamitic molecules are bent type (Fig.6.6) and expected to be responsible for the similar results ($K_{33}/K_{11} = 0.7 < 1$) as that of bent-core nematic liquid crystals.

It may be useful to discuss and compare the elastic constant ratio with bicyclohexane nematic compounds such as nCCH with longitudinal cyano groups. It was reported that the elastic constant ratio of nCCH is always greater than 1 (i.e.$K_{33}/K_{11} > 1$) [16]. This is in contrast to the observed effect in the present compounds. The important structural difference between the two homologous series of nCCH and CCN-mn is the position of the cyano group (-CN). In case of nCCH, the cyano group is at the longitudinal position, whereas in CCN-mn, it is in the lateral position. In addition, the alkyl chains are present on both sides of bicyclohexane. The side chains of CCN-mn increase the flexibility of the molecules. Apart from the enhanced flexibility, the transverse dipole moment of CCN-mn molecules can have a significant role on the ratio of the curvature elastic constants. It was proposed that the effect of dipole moment on the elastic constants is connected to the local ordering of the dipoles in nCCH compounds [17]. The effective molecular length could be greater in nCCH compounds because of the antiparallel local ordering of the molecules with the overlapped group. It has been shown both experimentally and theoretically that in nematic liquid crystals, $K_{33}/K_{11} \propto (L/W)^2$, where L is the length and W is the width of the mesogenic molecule, respectively [15]. Thus, the lower ratio of K_{33}/K_{11} of CCN-mn compounds than nCCH compounds partially could be due to the absence of local ordering, apart from the effect of molecular shape

6.3 Conclusions

In conclusion, in this chapter we have reported the measurement of birefringence, dielectric anisotropy, splay and bend elastic constants of homologous series of bicyclohexane nematic liquid crystals. All the compounds exhibit small birefringence and negative dielectric anisotropy. The ratio of elastic constants, i.e., $K_{33}/K_{11} < 1$. The optimized molecular structure obtained from the calculations of DFT shows that the molecules are bend shaped with large transverse dipole moments and low polarisability anisotropy. The low birefringence, high negative dielectric anisotropy and low elastic constant ratio of the compounds are explained based on the optimised molecular properties.

References

[1] L. Walz, W. Haase, and R. Eidenschink, “The crystal and molecular structures of four homologous, mesogenic trans, trans-4, 4’-dialkyl-(1 α, 1’-bicyclohexyl)-

4ß-carbonitril (ccn's)," *Molecular Crystals and Liquid Crystals*, vol. 168, no. 1, pp. 169–182, 1989.

[2] R. Eidenschink, G. Haas, M. Römer, and B. S. Scheuble, "Liquid-crystalline 4-bicyclohexylcarbonitriles with extraordinary physical properties," *Angewandte Chemie International Edition in English*, vol. 23, no. 2, pp. 147–147, 1984.

[3] D. Ganzke, S. Wrobel, and W. Haase, "Dielectric studies of bicyclohexylcarbonitrile nematogens with large negative dielectric anisotropy," *Molecular Crystals and Liquid Crystals*, vol. 409, no. 1, pp. 323–333, 2004.

[4] S. Dhara and N. V. Madhusudana, "Physical characterisation of 4'-butyl-4-heptyl-bicyclohexyl-4-carbonitrile," *Phase Transitions*, vol. 81, no. 6, pp. 561–569, 2008.

[5] S. Dhara and N. V. Madhusudana, "Enhancement of the orientational order parameter of nematic liquid crystals in thin cells," *The European Physical Journal E: Soft Matter and Biological Physics*, vol. 13, no. 4, pp. 401–408, 2004.

[6] S. Dhara and N. V. Madhusudana, "Influence of director fluctuations on the electric-field phase diagrams of nematic liquid crystals," *EPL (Europhysics Letters)*, vol. 67, no. 3, p. 411, 2004.

[7] A. Zawadzki and H. G. Walton, "Measurements of the splay and bend elastic constants of 4'-butyl-4-heptyl-bicyclohexyl-4-carbononitrile, ccn47," *Molecular Crystals and Liquid Crystals*, vol. 569, no. 1, pp. 10–14, 2012.

[8] I. H. Ibrahim and W. Haase, "On the molecular polarizability of nematic liquid crystals," *Molecular Crystals and Liquid Crystals*, vol. 66, no. 1, pp. 189–198, 1981.

[9] P. Sathyanarayana, M. C. Varia, A. K. Prajapati, B. Kundu, V. S. S. Sastry, and S. Dhara, "Splay-bend elasticity of a nematic liquid crystal with t-shaped molecules," *Physical Review E*, vol. 82, no. 5, p. 050701, 2010.

[10] S. W. Morris, P. Palffy Muhoray, and D. Balzarini, "Measurements of the bend and splay elastic constants of octyl-cyanobiphenyl," *Molecular Crystals and Liquid Crystals*, vol. 139, no. 3-4, pp. 263–280, 1986.

[11] T. H. Dunning Jr, "Gaussian basis sets for use in correlated molecular calculations. i. the atoms boron through neon and hydrogen," *The Journal of chemical physics*, vol. 90, no. 2, pp. 1007–1023, 1989.

[12] D. Demus and T. Inukai, "Calculation of molecular, dielectric and optical properties of 4'-n-pentyl-4-cyano-biphenyl (5cb)," *Liquid crystals*, vol. 26, no. 9, pp. 1257–1266, 1999.

[13] P. Sathyanarayana, M. Mathew, Q. Li, V. S. S. Sastry, B. Kundu, K. V. Le, H. Takezoe, and S. Dhara, "Splay bend elasticity of a bent-core nematic liquid crystal," *Physical Review E*, vol. 81, no. 1, p. 010702, 2010.

[14] P. Sathyanarayana, S. Radhika, B. K. Sadashiva, and S. Dhara, "Structure–property correlation of a hockey stick-shaped compound exhibiting n-sma-smc a phase transitions," *Soft Matter*, vol. 8, no. 7, pp. 2322–2327, 2012.

[15] W. H. Jeu, *Physical properties of liquid crystalline materials*, vol. 1. CRC Press, 1980.

[16] M. J. Bradshaw and E. P. Raynes, "Electric permittivities and elastic constants of the cyano bi-cyclohexanes (cch)," *Molecular Crystals and Liquid Crystals*, vol. 72, no. 2-3, pp. 35–42, 1981.

[17] G. J. Brownsey and A. J. Leadbetter, "Novel liquid crystal structures in cyano bi-cyclohexanes," *Journal de Physique Lettres*, vol. 42, no. 6, pp. 135–139, 1981.

7

Birefringence, permittivity, elasticity and rotational viscosity of ambient temperature, high birefringent nematic liquid crystal mixtures

7.1 Introduction

In the previous chapter, we studied various physical properties of a homologous series of CCNs LCs and its co-relation to the structure. They exhibit very low birefringence. In the recent times, high birefringent LCs have been synthesized and they have drawn a lot of attention due to its various applications. For example, they are crucial for laser beam steering [1], directional reflectors [2], infrared special light modulators [3], tunable focus lenses [4], optical switches for telecommunication etc. They also have significant importance for radio frequency applications in the GHz and THz frequency range [5, 6], holographic devices, and broad range filters. Moreover high birefringence enriches the display brightness and contrast ratio of liquid crystal displays such as polymer dispersed liquid crystals (PDLC), holographic PDLC, cholesteric LCD, and liquid crystal gels [7–9]. The birefringence of a liquid crystal strongly depends on the

structure of the molecule and π-electron conjugation [10, 11]. Generally more linearly conjugated liquid crystal exhibits higher birefringence [12]. The increase of conjugation length leads to high melting temperature, decrease of nematic range, enhanced viscosity, and decrease of solubility to form eutectic mixtures. The nematic range can be increased by preparing eutectic mixture of high birefringent liquid crystals. There are some reports on the synthesis and optical measurement of high birefringent nematic liquid crystals [13–23]. Recently, J. Herman *et al.* synthesized novel high birefringent nematic liquid crystals containing quarterphenyl and phenylethynyltolane cores with isothiocyanate terminal group [11]. In these liquid crystals nematic phase exists much above the ambient temperature. For ambient temperature applications, we prepared some binary mixtures. In this chapter, we report detailed study on physical properties of a few high birefringent mixtures containing quarterphenyl and phenylethnyltolane cores.

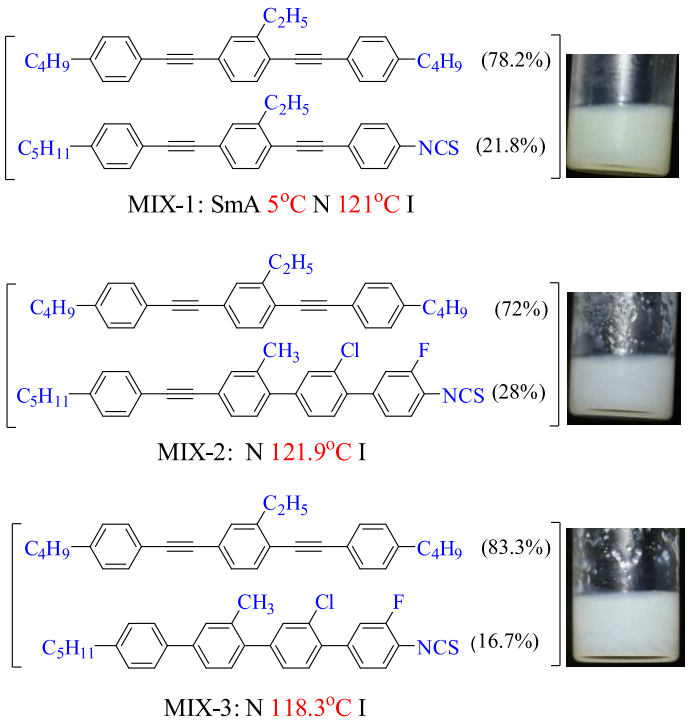

Figure 7.1: Molecular structure and wt% of the individual compounds and the phase transition temperature of the mixtures. The physical appearance of the samples in the bottles at room temperature are also shown.

7.2 Results and discussion

7.2.1 Samples and phase transitions

We studied three different mixtures using four different nematic liquid crystals. The chemical structure of the individual compounds and the phase transition temperatures of the mixtures are shown in Fig.7.1. At room temperature they are nematic and highly turbid. In each mixture, one compound is common and non polar with larger wt%. The second compound is polar with isothiocyanate terminal group containing laterally alkyl, fluorine, and chlorine substituted and less in wt%. The polar compounds are mixed with the non polar host with maximum solubility. The four compounds containing quarterphenyl and phenylethynyltolane cores. All the mixtures have high clearing point and wide nematic range. The synthesis and phase transition temperatures of the individual compounds have already been reported [11].

7.2.2 Birefringence and orientational order parameter

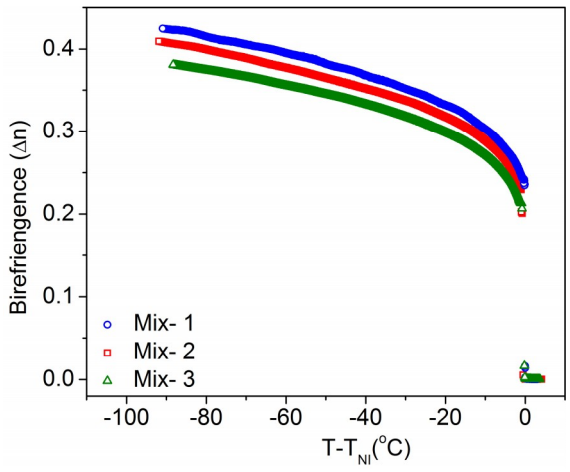

Figure 7.2: Variation of birefringence (Δn) of the mixtures as a function of shifted temperature.

The temperature dependent variation of birefringence (Δn) of the mixtures are shown in Fig.7.2. Δn jumps to about $\simeq 0.22$ from 0 at the nematic-isotropic (NI) transition in all the mixtures and reaches to a high value $\Delta n \simeq 0.4$ at room temperature. The birefringence of the mixtures increases as follows: $\Delta n_{Mix-1} > \Delta n_{Mix-2} > \Delta n_{Mix-3}$. This can be understood based on the molecular structure of the individual components in the mixture. In all the compounds, a significant contribution to the Δn is due to the presence of -C≡C- group and phenyl rings. Usually -C≡C- group contributes more to Δn than phenyl rings [11]. As we proceed from Mix-3 to Mix-1 we notice that apart from a small variation in the lateral groups, the number of phenyl rings decreases and -C≡C- groups increases. Thus the effective conjugation length and hence Δn in the

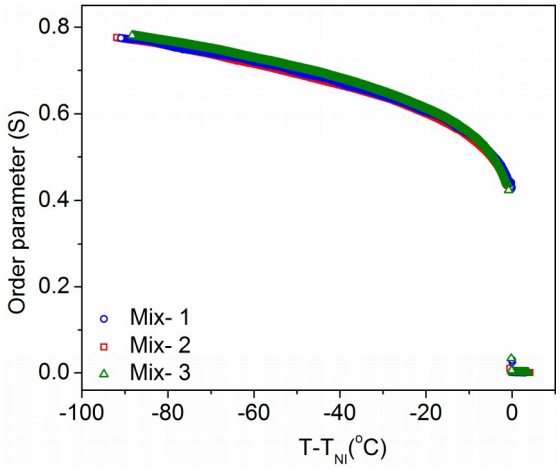

Figure 7.3: Variation of orientational order parameter (S) of the mixtures as a function of shifted temperature.

Table 7.1: Fit parameters of the mixtures.

Mixtures	Δn_o	T_1	T_{NI}	β
Mix-1	0.55	125	121	0.18
Mix-2	0.53	125.4	121.9	0.18
Mix-3	0.49	120	118.3	0.17

mixtures increases.

To estimate the order parameter the temperature variation of Δn can be approximated by the Hallar extrapolation formula [24], $\Delta n = \Delta n_0(1 - T/T_1)^\beta$, where β, T_1 are the adjustable parameters, and Δn_0 is the birefringence of the perfectly aligned sample. The fit parameters are listed in Table-7.1. T_1 is slightly higher than T_{NI}, and β is about $\simeq$0.18. Similar value of β was also reported in many other liquid crystals [25]. The order parameter S of the long molecular axis was estimated using the relation $S \approx \Delta n/\Delta n_o$. The temperature variation of S is shown in Fig.7.3. The value of S increases with decreasing temperature and at room temperature it is quite high (about $S \simeq$0.8) and larger than that of many common liquid crystals. Similar large order parameter in high birefringent nematic liquid crystals were also reported by Sekine *et al.* [26].

7.2.3 Dielectric constants

The variation of parallel ($\varepsilon_{||}$) and perpendicular ($\varepsilon_\perp$) components of dielectric constants and the average value of dielectric constant, $\overline{\varepsilon}$ $(= (\varepsilon_{||} + 2\varepsilon_\perp)/3)$ as a function of temperature is shown in Fig.7.4. The dielectric anisotropy is positive i.e., $\Delta\varepsilon(=$

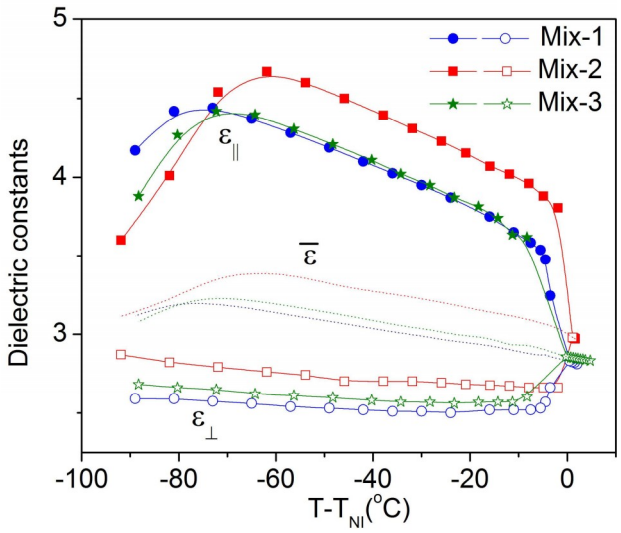

Figure 7.4: Variation of parallel ($\varepsilon_{||}$), perpendicular ($\varepsilon_{\perp}$) components of dielectric constants and $\overline{\varepsilon} = (\varepsilon_{||} + 2\varepsilon_{\perp})/3$ as a function of temperature. Solid lines are drawn as guides to the eye.

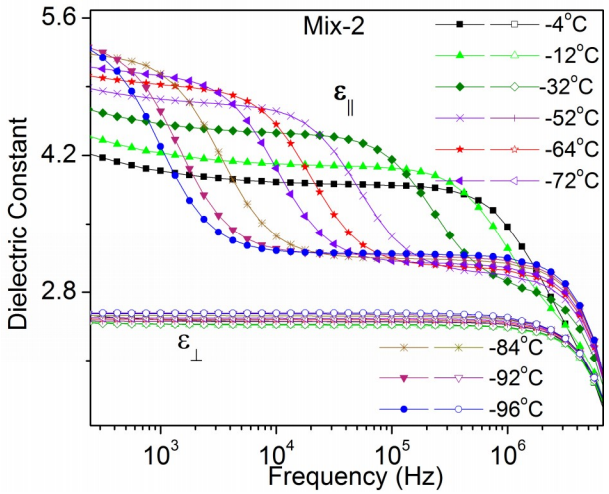

Figure 7.5: The frequency dispersion of real part of the dielectric constants, i.e., $\varepsilon_{||}$ and $\varepsilon_{\perp}$ at various temperatures of Mix-2. Solid lines are drawn as guides to the eye.

$\varepsilon_{||} - \varepsilon_{\perp}) > 0$ and almost the same in all the mixtures. $\varepsilon_{||}$ increases up to a certain value and then decreases significantly near the room temperature. Similar unusual behavior of $\varepsilon_{||}$ was observed in many compounds showing nematic to smectic phase transition [27, 28]. In addition, in those compounds, it was found that $\varepsilon_{\perp}$ also tend to increase at the same temperature and eventually $\Delta\varepsilon$ can change sign. It was shown that due to the presmectic order, the antiparallel correlation of the dipoles parallel to the director increases as a result the effective dipole moment reduces in the nematic phase leading to the decrease of $\varepsilon_{||}$. Similar argument was given for increase of $\varepsilon_{\perp}$. However in the present mixtures only Mix-1 exhibits N to SmA transition around 5°C and Mix-2 and Mix-3 does not show any smectic phase but some kind of solidification was noted around this temperature. In addition, $\varepsilon_{\perp}$ does not show any increasing tendency at the same temperature. Thus, the the unusual temperature dependence of $\varepsilon_{||}$ for Mix-1 is not due to the antiparallel correlation of dipoles.
To understood this, we measured the frequency dispersion of both $\varepsilon_{||}(f)$ and $\varepsilon_{\perp}(f)$ of one sample (for e.g., Mix-2) in the frequency range of 100 Hz - 10 MHz (Fig.7.5). We note that in both the components one relaxation is common beyond 1 MHz which comes from the finite resistance of the ITO electrodes. $\varepsilon_{\perp}(f)$ is almost independent of temperature and does not show any other dielectric relaxation. On the other hand $\varepsilon_{||}(f)$ exhibits another dielectric relaxation below 1MHz and the relaxation frequency decreases rapidly with decreasing temperature. For example, relaxation frequency at 90°C is about 237 kHz and reduces to 1 kHz at room temperature (26°C). The temperature dependent dielectric constant was measured at a fixed frequency of 4.11 kHz. But the relaxation frequency decreases below this value around 50°C. Hence the decreases of $\varepsilon_{||}$ is due to the decreases of relaxation frequency below the measuring frequency.

7.2.4 Splay (K_{11}) and bend (K_{33}) elastic constants

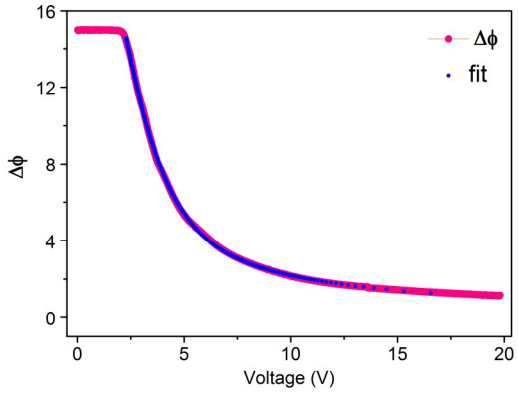

Figure 7.6: Experimental variation of retardation as a function of applied voltage. Blue points are the theoretical fit to the experimental data.

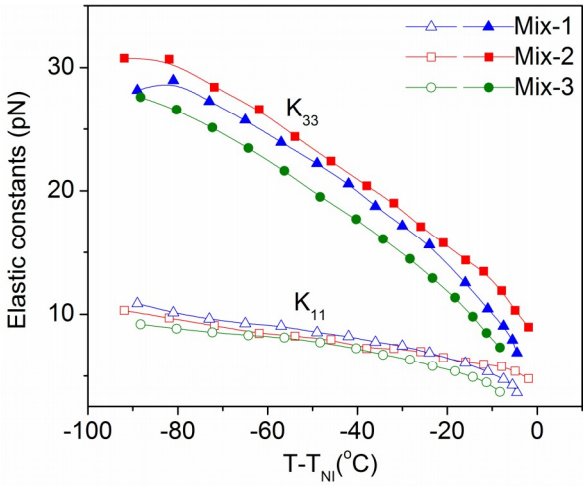

Figure 7.7: Variation of splay (K_{11}) and bend (K_{33}) elastic elastic constants as a function of shifted temperature. Solid lines are drawn as guides to the eye.

The splay and bend elastic constants (K_{11} and K_{33}) were measured from the voltage dependent retardation data as described in Chapter-2. The variation of retardation together with best fit of theoretical Eq.(2.41) and Eq.(2.46) is shown in Fig.7.6. The temperature variation of splay (K_{11}) and bend (K_{33}) elastic constants is shown in Fig.7.7. Though K_{11} is almost the same within the experimental accuracy, K_{33} appears to be slightly different in the three mixtures. Both K_{11} and K_{33} increase with decrease of temperature and these values are comparatively larger than that of many common (lower birefringent) nematic liquid crystals. For instance, in 5CB, $K_{11} = 5$ pN and $K_{33} = 9$ pN whereas in the present mixture (Mix-1) these numbers are 10 pN and 30 pN respectively at room temperature. Since $K_{ii} \propto S^2$, [29] the large elastic constant could be due to the large orientational order of the mixtures.

7.2.5 Rotational viscosity (γ_1) and figure-of-merit(FOM)

Here, we discuss the rotational viscosity (γ_1) of the mixtures in the nematic phase. The experimental technique was discussed in chapter 2. The normalized intensities of the transient response of Mix-I at two temperatures after removal of bias $V_b = 0$ field is shown in Fig.7.8(a). A representative variation of $\ln[\delta_o/\delta(t)]$ with time(t) is shown in Fig. 7.8(b). γ_1 was calculated by measuring the relaxation time τ_o and K_{11} of the mixtures. The variation of γ_1 as a function of temperature is shown in Fig.7.9. γ_1 increases vary rapidly with decrease of temperature. For instance, at room temperature this is $\simeq$1 Pa s (Mix-2) which is about two orders of magnitude larger than conventional (low birefringent) nematic liquid crystals.
The rotational viscosity can be written as $\gamma_1 \sim S\exp(W/k_BT)$, W being the activation energy, S the order parameter and k the Boltzmann constant [27]. Since $S \propto \Delta n$, we plotted $\ln(\gamma_1/\Delta n)$ with $1/T$ in Fig.7.10. The estimated activation energy for the three

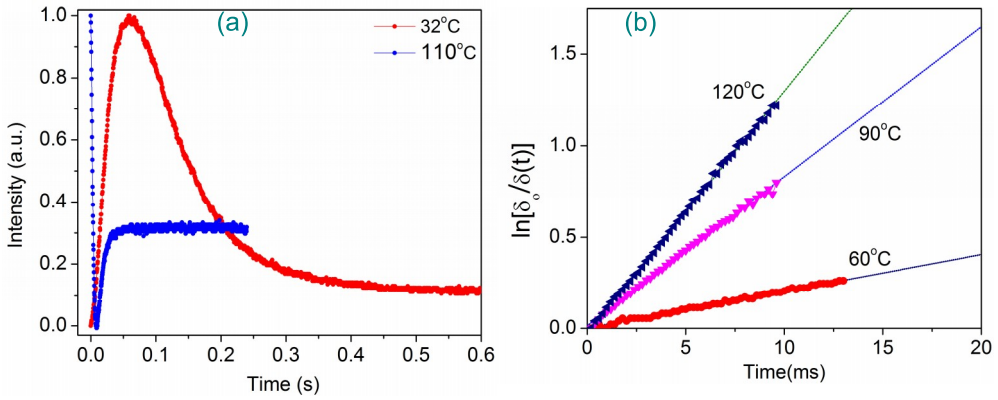

Figure 7.8: (a) Time dependent normalised transmitted intensity after the removal of bias voltage (V_b) for two temperatures of Mix-1. (b) Linear variation of $\ln[\delta_o/\delta(t)]$ with time(t) at various temperatures of Mix-1. Solid lines are theoretical fits to the experimental data.

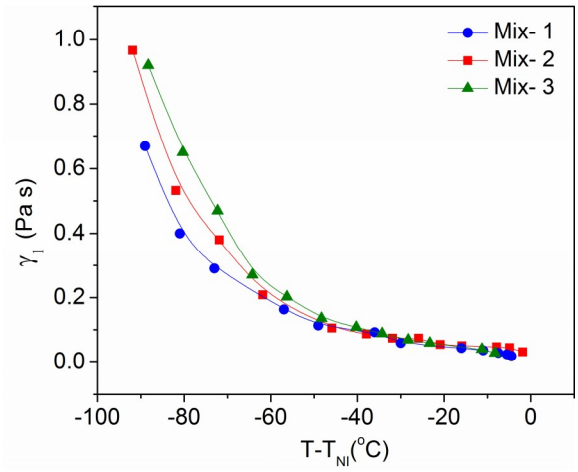

Figure 7.9: Variation of rotational viscosity (γ_1) of different mixtures as a function of shifted temperature.

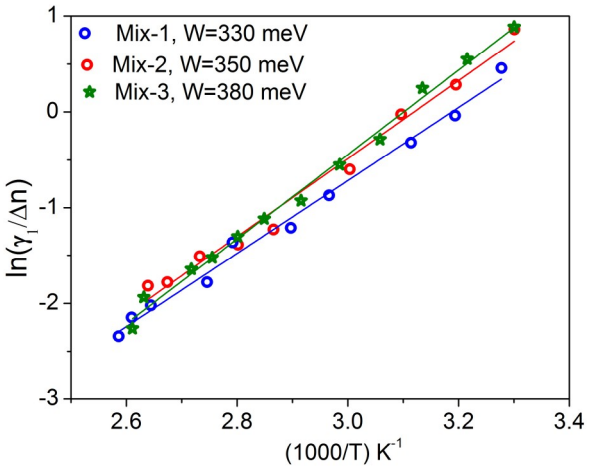

Figure 7.10: Linear variation of $\ln(\gamma_1/\Delta n)$ with 1/T. Solid lines are theoretical fits to the corresponding equations as described in the text.

mixtures are 330 meV, 350 meV and 380 meV respectively and these are comparable to the values reported for many low birefringent nematic liquid crystals [30].
To characterize the performance of the liquid crystal materials, we estimated figure-of-merit (FoM) using the formula, FoM= $K_{11}\Delta n^2/\gamma_1$ as a function of temperature. Fig.7.11 shows the temperature variation of the FoM. Since, $K_{11} \propto S^2 \propto \Delta n^2$, the temperature dependence of FoM can be written as

$$\text{FoM} = A(1 - T/T_1)^{3\beta}\exp(-W/kT). \tag{7.1}$$

FoM is largest for Mix-1 and reduced in Mix-2 and Mix-3. At higher temperature the FoM of all the mixtures are reasonably larger than conventional low birefringence nematic liquid crystals but it decreases at room temperature. For instance, for Mix-1, at 95°C, FoM is 15 $\mu m^2/s$ and decreases to 1.5 $\mu m^2/s$ near room temperature. The reports on FoM at room temperature, high birefringent nematic liquid crystal is rare hence not available for comparative discussion. In case of standard liquid crystal sample like 5CB, by taking K_{11}, Δn and γ_1 values from the literature [31, 32] and calculating the FoM from the Eq.(7.1), FOM obtained 2.32 $\mu m^2/s$ at room temperature $T - T_{NI} = -10$°C. In our mixtures, their high value of FoM exist around 95°C. It will be advantages if it would exist at room temperature. Though the birefringence is large at room temperature, high viscosity is disadvantageous specially where fast switching is needed.

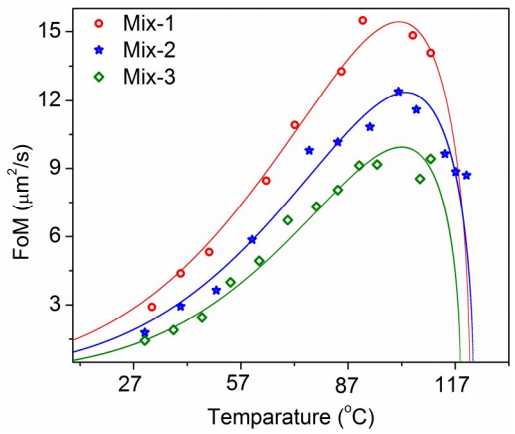

Figure 7.11: Temperature variation of the figure of merit (FoM). Solid lines are theoretical fits of the experimental data to Eq.(7.1).

7.3 Conclusion

In conclusion, we measured various physical properties of three high birefringent room temperature nematic liquid crystal mixtures. The orientational order parameter, both splay and bent elastic constants are comparatively larger than that of many common liquid crystal mixtures. The unusual temperature dependence of parallel component of dielectric constant ($\varepsilon_{||}$) near the room temperature is due to the rapid decrease of dielectric relaxation frequency with decreasing temperature. The figure of merit at higher temperature is reasonably larger but reduces at room temperature due to the very high viscosity. Thus elastic and dielectric properties of high birefringence materials are suitable but high viscosity is a matter of concern for application.

References

[1] P. F. McManamon, T. A. Dorschner, D. L. Corkum, L. J. Friedman, D. S. Hobbs, M. Holz, S. Liberman, H. Q. Nguyen, D. P. Resler, R. C. Sharp, *et al.*, "Optical phased array technology," *Proceedings of the IEEE*, vol. 84, no. 2, pp. 268–298, 1996.

[2] C. C. Bowley, H. Yuan, and G. P. Crawford, "Morphology of holographically-formed polymer dispersed liquid crystals (h-pdlc)," *Molecular Crystals and Liquid Crystals*, vol. 331, no. 1, pp. 209–216, 1999.

[3] S. T. Wu and D. K. Yang, *Reflective liquid crystal displays*. Wiley, 2001.

[4] H. Ren, Y. H. Fan, S. Gauza, and S. T. Wu, "Tunable-focus flat liquid crystal spherical lens," *Applied Physics Letters*, vol. 84, no. 23, 2004.

[5] N. Vieweg, C. Jansen, M. K. Shakfa, M. Scheller, N. Krumbholz, R. Wilk, M. Mikulics, and M. Koch, "Molecular properties of liquid crystals in the terahertz frequency range," *Optics express*, vol. 18, no. 6, pp. 6097–6107, 2010.

[6] N. Vieweg and M. Koch, "Terahertz properties of liquid crystals with negative dielectric anisotropy," *Applied optics*, vol. 49, no. 30, pp. 5764–5767, 2010.

[7] R. L. Sutherland, V. P. Tondiglia, L. V. Natarajan, T. J. Bunning, and W. W. Adams, "Electrically switchable volume gratings in polymer-dispersed liquid crystals," *Applied Physics Letters*, vol. 64, no. 9, pp. 1074–1076, 1994.

[8] N. Mizoshita, K. Hanabusa, and T. Kato, "Fast and high-contrast electro-optical switching of liquid-crystalline physical gels: Formation of oriented microphase-separated structures," *Advanced Functional Materials*, vol. 13, no. 4, pp. 313–317, 2003.

[9] Y. H. Fan, H. Ren, and S. T. Wu, "Normal-mode anisotropic liquid-crystal gels," *Applied physics letters*, vol. 82, no. 18, pp. 2945–2947, 2003.

[10] A. Spadlo, R. Dabrowski, M. Filipowicz, Z. Stolarz, J. Przedmojski, S. Gauza, C. Y. Fan, and S. T. Wu, "Synthesis, mesomorphic and optical properties of isothiocyanatotolanes," *Liquid crystals*, vol. 30, no. 2, pp. 191–198, 2003.

[11] J. Herman, J. Dziaduszek, R. Dbrowski, J. Kdzierski, K. Kowiorski, V. S. Dasari, S. Dhara, and P. Kula, "Novel high birefringent isothiocyanates based on quaterphenyl and phenylethynyltolane molecular cores," *Liquid Crystals*, vol. 40, no. 9, pp. 1174–1182, 2013.

[12] R. Dabrowski, P. Kula, and J. Herman, "High birefringence liquid crystals," *Crystals*, vol. 3, no. 3, pp. 443–482, 2013.

[13] R. Dbrowski, J. Dziaduszek, A. Ziolek, Z. Stolarz, G. Sasnouski, V. Bezborodov, W. Lapanik, S. Gauza, S. T. Wu, *et al.*, "Low viscosity, high birefringence liquid crystalline compounds and mixtures," *Opto-Electronics Review*, vol. 15, no. 1, pp. 47–51, 2007.

[14] S. Gauza, H. Wang, C. H. Wen, S. T. Wu, A. J. Seed, and R. Dabrowski, "High birefringence isothiocyanato tolane liquid crystals," *Japanese journal of applied physics*, vol. 42, no. 6R, p. 3463, 2003.

[15] S. T. Wu, M. E. Neubert, S. S. Keast, D. G. Abdallah, S. N. Lee, M. E. Walsh, and T. A. Dorschner, "Wide nematic range alkenyl diphenyldiacetylene liquid crystals," *Applied Physics Letters*, vol. 77, no. 7, pp. 957–959, 2000.

[16] S. Gauza, A. Parish, S. T. Wu, A. Spadlo, and R. Dabrowski, "Physical properties of laterally fluorinated isothiocyanato phenyl-tolane single liquid crystals components and mixtures," *Molecular Crystals and Liquid Crystals*, vol. 489, no. 1, pp. 135–461, 2008.

[17] C. Sekine, K. Iwakura, N. Konya, M. Minai, and K. Fujisawa, "Synthesis and properties of some novel high birefringence phenylacetylene liquid crystal materials with lateral substituents," *Liquid Crystals*, vol. 28, no. 9, pp. 1375–1387, 2001.

[18] S. Gauza, J. Li, S. T. Wu, A. Spadlo, R. Dabrowski, Y. N. Tzeng, and K. L. Cheng, "High birefringence and high resistivity isothiocyanate-based nematic liquid crystal mixtures," *Liquid crystals*, vol. 32, no. 8, pp. 1077–1085, 2005.

[19] S. Gauza, C. H. Wen, S. T. Wu, N. Janarthanan, and C. S. Hsu, "Super high birefringence isothiocyanato biphenyl-bistolane liquid crystals," *Japanese journal of applied physics*, vol. 43, no. 11R, p. 7634, 2004.

[20] J. Dziaduszek, P. Kula, R. Dabrowski, W. Drzewiski, K. Garbat, S. Urban, and S. Gauza, "General synthesis method of alkyl–alkoxy multi-fluorotolanes for negative high birefringence nematic mixtures," *Liquid Crystals*, vol. 39, no. 2, pp. 239–247, 2012.

[21] P. Kula, A. Aptacy, J. Herman, W. Wojciak, and S. Urban, "The synthesis and properties of fluoro-substituted analogues of 4-butyl-4'-[(4-butylphenyl) ethynyl] biphenyls," *Liquid Crystals*, vol. 40, no. 4, pp. 482–491, 2013.

[22] Y. M. Zhang, D. Wang, Z. C. Miao, S. K. Jin, and H. Yang, "Novel high birefringence bistolane liquid crystals with lateral fluorosubstituent," *Liquid Crystals*, vol. 39, no. 11, pp. 1330–1339, 2012.

[23] Y. Arakawa, S. Nakajima, S. Kang, M. Shigeta, G. Konishi, and J. Watanabe, "Synthesis and evaluation of dinaphthylacetylene nematic liquid crystals for high-birefringence materials," *Liquid Crystals*, vol. 39, no. 9, pp. 1063–1069, 2012.

[24] I. Haller, "Thermodynamic and static properties of liquid crystals," *Progress in solid state chemistry*, vol. 10, pp. 103–118, 1975.

[25] S. Dhara and N. V. Madhusudana, "Enhancement of the orientational order parameter of nematic liquid crystals in thin cells," *The European Physical Journal E*, vol. 13, no. 4, pp. 401–408, 2004.

[26] C. Sekine, K. Iwakura, N. Konya, M. Minai, and K. Fujisawa, "Synthesis and properties of some novel high birefringence phenylacetylene liquid crystal mate-

rials with lateral substituents," *Liquid Crystals*, vol. 28, no. 9, pp. 1375–1387, 2001.

[27] W. H. De Jeu, T. W. Lathouwers, and P. Bordewijk, "Dielectric properties of di-n-heptyl azoxybenzene in the nematic and in the smectic-a phases," *Physical Review Letters*, vol. 32, no. 2, p. 40, 1974.

[28] P. Sathyanarayana, M. Mathew, Q. Li, V. S. S. Sastry, B. Kundu, K. V. Le, H. Takezoe, and S. Dhara, "Splay bend elasticity of a bent-core nematic liquid crystal," *Physical Review E*, vol. 81, no. 1, p. 010702, 2010.

[29] J. Prost, *The physics of liquid crystals*. No. 83, Oxford university press, 1995.

[30] S. T. Wu and C. S. Wu, "Experimental confirmation of the osipov-terentjev theory on the viscosity of nematic liquid crystals," *Physical Review A*, vol. 42, no. 4, p. 2219, 1990.

[31] P. Sathyanarayana, V. S. R. Jampani, M. Skarabot, I. Musevic, K. V. Le, H. Takezoe, and S. Dhara, "Viscoelasticity of ambient-temperature nematic binary mixtures of bent-core and rodlike molecules," *Physical Review E*, vol. 85, no. 1, p. 011702, 2012.

[32] A. Bogi and S. Faetti, "Elastic, dielectric and optical constants of 4'-pentyl-4-cyanobiphenyl," *Liquid Crystals*, vol. 28, no. 5, pp. 729–739, 2001.

List of Publications

Publications

Publications related to thesis

1. Experimental studies on the phase diagram and physical properties of mixture of calamitic and discotic nematic liquid crystals
   D. Venkata Sai, G. Mirri, P. Kouwer, I. Musevic and Surajit Dhara.
   Liq. Cryst., **1-5**, (2016).

2. Unusual temperature dependence of splay and bend elastic constants of a discotic nematic liquid crystals
   D. Venkata Sai, G. Mirri, P. Kouwer, R. Sahoo, I. Musevic and Surajit Dhara.
   Soft matter, **12**, 2960 (2016).

3. Structure-property correlation of bicyclohexane nematic liquid crystals
   D. Venkata Sai, K. P. Zuhail, Rudraditya Sarkar and Surajit Dhara
   Liq. Cryst., **42**, 3 (2015).

4. Effect of smectic short-range order on the discontinuous anchoring transition in nematic liquid crystals
   D. Venkata Sai, T. Arun Kumar, W. Haase, Arun Roy and Surajit Dhara
   J. Chem. Phys., **141**, 044706 (2014).

5. Birefringence, permittivity, elasticity and rotational viscosity of ambient temperature, high birefringent nematic liquid crystal mixtures
   D. Venkata Sai, P. Sathyanarayana, V.S.S. Sastry, J. Herman, P. Kula, R. Dabrowski, and Surajit Dhara.
   Liq. Cryst., **41**,591 (2013).

Other publications

6. Possible enhancement of physical properties of nematic liquid crystals doping of conducting polymer nanofibres
   R. Manda,**V. Dasari**, P. Sathyanarayana, M. V. Rasna, P. Paik, and Surajit Dhara
   Appl. Phys. Lett., **103**, 141910 (2013).

7. Novel high birefringent isothiocyanates based on quaterphenyl and phenylethynyltolane molecular cores
   Jakub Herman, Jerzy Dziaduszek, Roman Dabrowski, Jerzy Kedzierski, Krystian Kowiorski, **Venkata Sai Dasari**, Surajit Dhara And Przemyslaw Kula.
   Liq. Cryst., **40**, 1174 (2013).